

AMERICAN UNIVERSITY OF BEIRUT

QUANTIFYING THE EFFECT OF RETROFITTING ON THE
SEISMIC COLLAPSE PERFORMANCE OF A
REPRESENTATIVE MID-RISE REINFORCED CONCRETE
BUILDING IN BEIRUT

by

BAHAA TAYBA

A thesis
submitted in partial fulfillment of the requirements
for the degree of Master of Engineering
to the Department of Civil & Environmental Engineering
of the Faculty of Engineering and Architecture
at the American University of Beirut

Beirut, Lebanon
February 2020

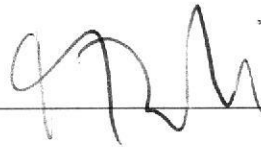
AMERICAN UNIVERSITY OF BEIRUT

QUANTIFYING THE EFFECT OF RETROFITTING ON THE
SEISMIC COLLAPSE PERFORMANCE OF A
REPRESENTATIVE MID-RISE REINFORCED CONCRETE
BUILDING IN BEIRUT

by

BAHAA TAYBA

Approved by:



Dr. Mayssa Dabaghi,
Civil and Environmental Engineering
Assistant Professor

Advisor



Dr. Mohamad Harajli,
Civil and Environmental Engineering
Provost, Professor

Member of Committee



Dr. George Saad,
Civil and Environmental Engineering
Associate Professor

Member of Committee



Dr. Elie Hantouche,
Civil and Environmental Engineering
Associate Professor

Member of Committee

Date of thesis/dissertation defense: February 17, 2020

AMERICAN UNIVERSITY OF BEIRUT

THESIS, DISSERTATION, PROJECT RELEASE FORM

Student Name: Tayba Bahaa Mohamad Tawfik
Last First Middle

Master's Thesis
Dissertation

Master's Project

Doctoral

I authorize the American University of Beirut to: (a) reproduce hard or electronic copies of my thesis, dissertation, or project; (b) include such copies in the archives and digital repositories of the University; and (c) make freely available such copies to third parties for research or educational purposes.

I authorize the American University of Beirut, to: (a) reproduce hard or electronic copies of it; (b) include such copies in the archives and digital repositories of the University; and (c) make freely available such copies to third parties for research or educational purposes
after : **One** --- year from the date of submission of my thesis, dissertation, or project.
Two years from the date of submission of my thesis, dissertation, or project.
Three --- years from the date of submission of my thesis, dissertation, or project.


Signature

18/03/2020
Date

ACKNOWLEDGMENTS

I would like to express my deepest thanks to my parents, without whom I would not be where I am nor who I am today. Sincere gratitude goes to my advisor Dr. Mayssa, who for the past two and half years, was my guide (and sometimes my partner) in navigating the confusing labyrinth of structural modelling. I would also like to thank the members of the committee professors Muhamad Harajli, George Saad, and Elie Hantouche, for constantly pushing me to strive to create the best possible version of this project and all faculty members at the civil engineering department in AUB. And my friends, for keeping me relatively sane throughout this short foray into academia.

Finally, I would like to thank the University Research Board (URB) for providing the necessary means and funding which made this research possible.

AN ABSTRACT OF THE THESIS OF

Bahaa Tayba- for Master of Engineering
Major: Civil Engineering

Title: Quantifying The Effect Of Retrofitting On The Seismic Collapse Performance Of A Representative Mid-Rise Reinforced Concrete Building In Beirut

Lebanon is situated in a region of significant seismic hazard. Seismic design codes, however, were not strictly enforced until 2012 with the publication of the second edition of the Lebanese earthquake standards. This, combined with a lack of construction regulation and oversight caused by the onset of the Lebanese civil war in 1975, has led to a structurally deficient building stock in need of rehabilitation. Limited studies that investigate methods of improving the seismic performance of buildings constructed prior to the 1990s are available.

This project aims to assess the effect of several retrofitting schemes on the seismic collapse performance of an 8-story non-ductile reinforced concrete frame building in Beirut. This typical structure is characterized by wide-shallow beams, high aspect ratio columns, insufficient transverse reinforcement, unreinforced wide beam-narrow column joints, and lap splices located in potential plastic hinge regions. Three retrofitted versions of the building are designed and considered in this study. In the first version, the columns are concrete jacketed using the minimum jacket thickness and reinforcement. In the second version, the concrete column jackets are designed to sustain the column seismic demands obtained using the equivalent lateral force method. The third version is identical to the second but longitudinal carbon-fiber reinforced polymer (CFRP) strips are added to the beam elements. The seismic assessment is accomplished using the Federal Emergency Management Agency (FEMA) P-695 methodology. Analytical models of the buildings are developed in the Open System for Earthquake Engineering Simulation (OpenSees) framework using the lumped plasticity approach, non-linear pushover and incremental dynamic analyses are performed, and collapse fragility functions calculated.

Results show that all the retrofitting procedures investigated in this study are effective. The probability of collapse at the maximum considered earthquake intensity is reduced from 87% for the unretrofitted structure to below the FEMA P-695 recommendation of 20% for all the retrofitted versions. Methods that strengthen the structural joints are found to be particularly effective. This study can be extended to other typical buildings and retrofitting schemes to form the basis for conducting a seismic loss analysis of the existing Lebanese building stock and a cost-benefit evaluation of seismic risk mitigation alternatives. The findings of this study can help raise awareness about the necessity of retrofitting older concrete buildings in Lebanon and provide retrofitting options and important information for stakeholders and policymakers dealing with such buildings.

CONTENTS

ACKNOWLEDGMENTS.....	v
ABSTRACT	vi
LIST OF ILLUSTRATIONS	ix
LIST OF TABLES	xi

Chapter

I. INTRODUCTION.....	1
A. Motivation and Background	1
B. Literature Review	2
C. Objectives and Scope.....	9
D. Organization of the Thesis.....	10
II. DESCRIPTION AND DESIGN OF THE UNRETROFITTED MIDRISE RC BUILDING	12
III. ANALYTICAL MODELING OF THE UNRETROFITTED BUILDING	17
A. Introduction.....	17
B. Concentrated/Lumped Plasticity Approach.....	18
1. Flexural Behavior.....	20
2. Shear and Axial Behavior	23
C. Joint Modelling.....	24
1. Background	24
2. Joint Spring Model.....	25
3. Model for Unreinforced Wide Beam-Narrow Column Joints	26
D. Damping and Mass Allocation	30
E. Analytical Model of the Unretrofitted Building	31
IV. SEISMIC PERFORMANCE ASSESSMENT METHODOLOGY AND APPLICATION TO THE UNRETROFITTED BUILDING	35
A. Seismic Hazard at the Site	36
B. Pushover Analysis.....	37

C.	Incremental Dynamic Analysis.....	40
D.	Definition of Global Collapse.....	41
E.	Fragility Analysis.....	43
V. DESCRIPTION AND DESIGN OF THE RETROFITTED BUILDINGS.....		49
A.	Objectives and Constraints of Retrofitting	49
B.	Selected Retrofitting Methods	50
1.	Concrete Jacketing	50
2.	Fiber-Reinforced Polymer (FRP) Strengthening	52
C.	Design of the Retrofitted Structures	53
1.	Retrofitted Building 1 (RB1)	54
2.	Retrofitted Building 2 (RB2)	55
3.	Retrofitted Building 3 (RB3)	58
VI. ANALYTICAL MODELING OF THE RETROFITTED BUILDINGS.....		63
A.	Beam and Column Modeling.....	64
B.	Proposed Joint Model	69
1.	Experimental Data on Wide Beam-Narrow Column Joints.....	69
2.	Joint Model Calibration to Experimental Data	73
3.	Predicted Versus Experimental Responses	76
VII. SEISMIC PERFORMANCE OF THE RETROFITTED VERSUS UNRETROFITTED BUILDINGS		80
A.	Pushover Analysis.....	80
B.	Incremental Dynamic Analysis.....	83
C.	Fragility Analysis.....	86
D.	Individual Spring Response.....	92
1.	Joints	92
2.	Columns	93
3.	Beams.....	95
VIII. SUMMARY, CONCLUSIONS AND RECOMMENDATIONS		97
A.	Summary and Conclusions	97

B. Limitations and Recommendations for Future Work	100
BIBLIOGRAPHY	103

LIST OF ILLUSTRATIONS

Figure	Page
1. Figure 1: Map of Lebanon displaying the major faults with the historical events marked (Elias et al. 2007[3])	2
2. Figure 2: Plan view of the configuration	13
3. Figure 3: Visual representation of the lumped plasticity approach to capture flexure (a) and flexure shear (b) behavior [4]	18
4. Figure 4: Backbone curve of the Ibarra-Krawinkler hysteretic model [44]	21
5. Figure 5: Joint scissor model developed by Alath and Kunnath [53].....	25
6. Figure 6: Hysteretic backbone for the model developed by Lowes and Altoontash [58].....	26
7. Figure 7: Analytical model utilized to represent the unretrofitted structure [18]	32
8. Figure 8: Pushover analysis curve of the unretrofitted building’s exterior frame	39
9. Figure 9 : MIDA results of the unretrofitted exterior frame	41
10. Figure 10: Illustration of Side-sway collapse criteria.....	42
11. Figure 11: Fragility curves of the exterior frame of the unretrofitted structure with record-to-record variability and total uncertainty	48
12. Figure 12: Plan view showcasing FRP Continuity	61
13. Figure 13: Cross section of the Ribbed slab	62
14. Figure 14: Analytical model of retrofitted buildings	64
15. Figure 15: Specimens tested by Elsouri and Harajli [61, 74]	72
16. Figure 16: Predicted and experimental joint moment-rotation responses for UIJ-F1	77
17. Figure 17: Predicted and experimental joint moment-rotation responses for UEJ-F1	78

18. Figure 18: Predicted and experimental joint moment-rotation responses for UIJ-F2	78
19. Figure 19: Predicted and experimental joint moment-rotation responses for UEJ-F2	79
20. Figure 20: Pushover curves of the unretrofitted and retrofitted frames.....	82
21. Figure 21: MIDA results for B0	84
22. Figure 22: MIDA results for RB1	84
23. Figure 23: MIDA results for RB2.....	85
24. Figure 24: MIDA results for RB3.....	85
25. Figure 25: Fragility curves of the unretrofitted and retrofitted frames accounting only for record to record uncertainty	87
26. Figure 26: Fragility curves of the unretrofitted and retrofitted frames accounting for the total uncertainty	88
27. Figure 27: Comparison between the maximum floor displacements of RB1 and RB2 when subjected to the same four ground motions scaled to $SaT = 0.1$ g.	90
28. Figure 28: Comparison between the maximum floor displacements of RB1 and RB2 when subjected to the same four ground motions scaled to $SaT = 0.9$ g.	91
29. Figure 29: Comparison between the maximum inter-story drift ratios (IDRs) of RB1 and RB2 when subjected to the same four ground motions scaled to $SaT = 0.9$ g.	91
30. Figure 30: Moment-rotation response of joint 3 at floor 8 in all models.....	93
31. Figure 31: Moment-rotation response and backbone curve of the rotational spring at the top of Column 3 on floor 8 in all models subjected to the same ground motion; the ground motion is scaled to $Sa(T)$ of 0.4g for RB0 and 1.1g for RB1, RB2 and RB3	94
32. Figure 32: Moment-rotation response and backbone curve of the rotational springs of beam 3 on floor 8 in all models subjected to the same ground motion; the ground motion is scaled to $Sa(T)$ of 0.4g for RB0 and 1.1g for RB1, RB2 and RB3	96

LIST OF TABLES

Table	Page
1. Table 1: Column Dimensions in the structure	152.
2. Table 2: Design Parameters of the Column of the Exterior Frame of B0	16
3. Table 3: Design Parameters of the Beams of the Exterior Frame of B0	16
4. Table 4: Calibrated rotation values for unretrofitted joints from Allabban[18]	29
5. Table 5: Calibrated hysteric pinching parameters for unretrofitted joints from Allabban [18]	30
6. Table 6: Properties of the Flexural Springs of the columns of B0	33
7. Table 7: Properties of the Shear and Axial Springs of the columns of B0	33
8. Table 8: Spring properties of beams of B0 for all floors	34
9. Table 9: Seismic Parameters of the exterior frame of the unretrofitted structure	37
10. Table 10: Pushover Results for the Unretrofitted structure	39
11. Table 11: Selected uncertainty parameters	45
12. Table 12: Fragility parameters of the as built structure	47
13. Table 13: Design details of columns of RB1	55
14. Table 14 Seismic Weight and Design Base Shear of the exterior frame of the studied buildings	57
15. Table 15: Design Details of columns of RB2 and RB3	57
16. Table 16: CFRP Material properties	59
17. Table 17: Design details of CFRP added to the beams on floor 1 of exterior frame of RB3	62
18. Table 18: Design details of CFRP added to the beams on floor 2 of exterior frame of RB3	62
19. Table 19: Design details of CFRP added to the beams on floors 3-8 of exterior frame of RB3	62
20. Table 20: Spring properties of columns of RB1	65

21. Table 21 : Spring properties of columns of RB2 and RB3.....	66
22. Table 22 Spring properties of beams of B0, RB1 and RB2 for all floors.....	67
23. Table 23: Spring properties of beams of floor 1 of RB3	67
24. Table 24: Spring properties of beams of floor 2 of RB3	68
25. Table 25: Spring properties of beams of floors 3-8 of RB3	68
26. Table 26: Specimen columns in Elsouiri and Harajli [61, 74].....	71
27. Table 27:Specimen Beams in Elsouiri and Harajli [61, 74]	72
28. Table 28: Proposed Joint Model Rotation Parameters	76
29. Table 29:Proposed Joint moment Values	76
30. Table 30: Proposed hysteretic pinching parameters	76
31. Table 31: Comparison of predicted and observed ultimate moment strength	79
32. Table 32: Summary of Push-Over analysis results of the unretrofitted and retrofitted frames.....	82
33. Table 33: Summary of fragility results using Record-to-Record Uncertainty.	86
34. Table 34: Summary of fragility results using Total uncertainty.....	87

CHAPTER I

INTRODUCTION

A. Motivation and Background

Lebanon has been subject to several catastrophic earthquake events of moment magnitudes M_w exceeding 7. These include the destructive 551AD $M_w = 7.5$ earthquake-tsunami combination, which laid waste to the majority of the coastal settlements of the region. This seismic activity is attributed to the presence of the Levantine fault system, which runs from the Red Sea to the Taurus Mountains, passes through Lebanon, and forms the boundary between the Arabian and Sinai-Levantine plates. Within Lebanon, this fault system is mainly comprised of the Yammouneh, Rachaya and Mount Lebanon Thrust active faults [1], which are displayed in Figure 1.

Given the extent of the seismic activity previously recorded in Lebanon, it should come as a cause for concern that the country's seismic design code was not enforced until 2012 [2]. As a result, a large part of the building stock in Beirut, and more generally in Lebanon, was designed to resist gravity loads only. This issue is further aggravated by the overall lack of oversight and construction quality control during the Lebanese Civil War (1975-1990). This project focuses on reinforced concrete structures designed and built during that period. These structures are non-ductile and expected to perform poorly in the event of a major earthquake. They are prime candidates for retrofitting and strengthening programs, which would be essential in preserving the livelihood and safety of their

occupants. However, the selection of the retrofiting program requires an understanding of the effect of the retrofits on the behavior and seismic performance of the structure.

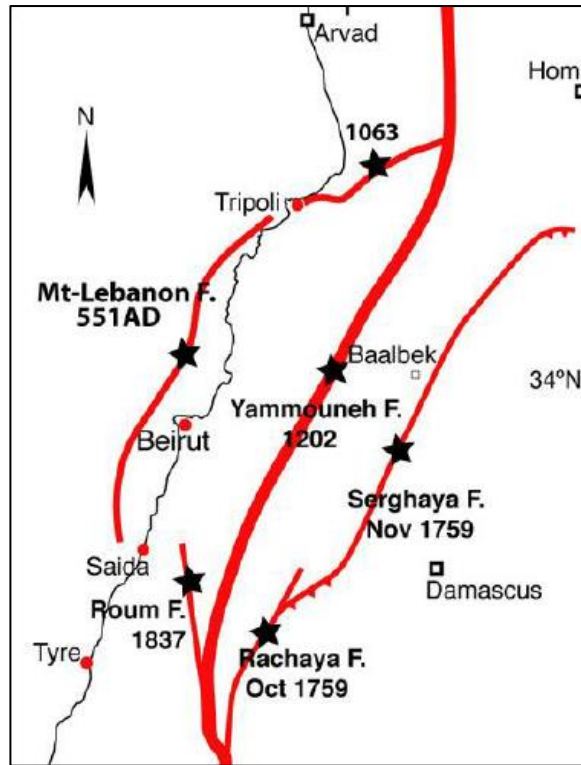


Figure 1: Map of Lebanon displaying the major faults with the historical events marked (Elias et al. 2007[3])

B. Literature Review

The seismic performance of non-ductile reinforced concrete (NDRC) frame structures has been the subject of growing interest during the past decade, as computational and modelling methods have improved to better capture the non-linear behavior of RC frames. NDRC structures are gravity-load designed structures that lack the proper detailing and reinforcement to ensure a ductile response during seismic events [4]. A standard method for assessing seismic performance is through the use of collapse fragility curves.

These curves present the probability of collapse of a structure as a function of a parameter representing the intensity or strength of a ground motion. Fragility curves are generally assumed to follow a lognormal cumulative distribution function [5]. For example, Galanis and Moehle [6], Suwal et. al [7], and Baradaran Shoraka [4] each investigated the performance of older NDRC frames by subjecting non-linear models of the frames to seismic ground motions and developing fragility curves using the incremental dynamic analysis method (IDA) developed by Vamvatsikos and Cornell [8]. Galanis and Moehle [6] used the fragility curves to examine the possibility of using predictors such as beam to column strength ratio as collapse indicators in NDRC frames, while Baradaran Shoraka [4] carried out a complete collapse and seismic loss assessment. Suwal et al. [7] on the other hand, investigated the effect of defining the analytical model parameters based on ASCE 41-13 [9] versus ACI 369 [10]; they found that the two codes result in slightly different structural performance predictions. Sattar and Liel [11] quantified the effects of heavy nonstructural infill walls on the seismic performance of non-ductile RC frames and found that the presence of heavy infill walls tends to increase the collapse risk. Liel et al.[12] compared the performance of similarly dimensioned non-ductile and ductile RC frames to find that the non-ductile frames were roughly 40 times more likely to suffer collapse compared to their code conforming counterparts. All these studies deal with structures that represent the design and construction practices implemented in the United States, namely RC frames with square columns, and may not be directly applicable to the building stock present in Lebanon, which is characterized by wide concealed beams and high aspect ratio columns [13].

In a recent study, Makhoul et al. [14] conducted a vulnerability study on the city of Byblos, Lebanon, and found that over 60% of concrete frame structures would suffer moderate to heavy damage in the event of a strong earthquake. However, their study made use of collapse fragility curves developed for NDRC frames in neighboring countries such as Greece [15] and Turkey [16].

Elkhoury and Harajli [13] reviewed the characteristics and seismic deficiencies of older construction in Lebanon, and assessed the seismic risk of several representative buildings using elastic response spectrum analysis. Old buildings usually consist of RC frames with wide beams and high aspect ratio columns, to conceal them within slabs and partition walls. This practice results in elements that are vulnerable to plastic hinging and failure around their weaker axis. Because these buildings were designed to resist gravity loads only, they lack the detailing necessary to ensure a ductile flexural response under strong ground shaking, namely: (1) the amount and spacing of transverse reinforcement in beam and column elements is insufficient to confine the concrete; (2) the transverse reinforcement is not extended into the beam-column joints, contrary to the recommendations of ACI 352 [17] for reinforced concrete joints in seismic areas; and (3) the column reinforcement is typically spliced close to the face of the column within potential plastic hinge regions. Moreover, heavy masonry infill walls are used for the facades and space partitions. These walls increase the seismic mass and can lead to weak story failure when they are discontinued at the ground level, which is a common practice.

Al Labban [18] investigated the global collapse performance of 4-, 8- and 12-story NDRC frame structures with no shear walls and located in Beirut, similar to those studied

by Elkhoury and Harajli [13]. Al Labban [18] developed non-linear analytical models of the structures using the lumped plasticity approach, performed nonlinear incremental dynamic analysis to calculate structural response, and developed seismic collapse fragility curves for each building. The stiffness contribution of the masonry walls was neglected in the analytical models. Results from Al Labban [18] indicate that the joints fail prematurely thus significantly contributing to collapse of the buildings.

Various retrofitting methods have been proposed to address some of the seismic deficiencies of NDRC buildings. They include: jacketing columns and beams using steel (e.g., [19]), concrete (e.g., [4, 20, 21]), or fiber reinforced polymers (FRP) (e.g., [21-23]); confining joints using FRP sheets (e.g., [23, 24]) or steel plates (e.g., [25]); adding lateral force-resisting elements such as shear walls and steel bracing (e.g., [21, 26]); and adding seismic isolation and energy dissipation systems (e.g., [27, 28]).

The literature on retrofitting can be divided into two main categories. The first category deals with the effect of retrofitting on the force-deformation relations and performance of the retrofitted elements. Hany et al. [29] compared the effect of carbon FRP (CFRP) jackets with and without CFRP anchor rods on the axial force-deformation response of rectangular concrete columns. They found that the use of CFRP jackets alone results in an increase in the axial stress capacity and that adding CFRP anchor rods greatly improves the ductility of axially loaded columns while also providing a greater increase in the axial stress capacity compared to non-anchored jackets. Harajli and Hantouche [25] studied the effect of active confinement by way of steel anchor rods pre-tensioned against steel bearing plates on the flexural strength and ductility capacity of wide RC columns with

lap splices placed near the base of the column, as was typical in Lebanon prior to the 1990s. They compared them to similar columns passively confined using CFRP jackets with CFRP anchor rods, similar to [29]. They found that the use of active confinement through pre-tensioned steel anchor rods results in larger improvements to the strength and ductility capacity of the tested specimens than the CFRP method. Additionally, Hassan and Bilal [30] attempted to strengthen a beam-column joint by embedding high strength U-shaped steel bars into the joint core. This however was found to not strengthen the joint, as the benefits provided by the extra bars were countered by the weakening of the joint due to the drilling action. Karayannis et. al [31] investigated the effect of jacketing joints using thin concrete jackets that cover both beams and columns and found that concrete jackets improve the strength and, depending on the amount of added reinforcement, the ductility capacity of the joint. This finding is in agreement with the earlier work done by Alcocer and Jirsa [32], which showed that column jacketing, even without any beam jacketing, leads to an increase in joint shear strength and concrete confinement. El-Amouri and Ghobarah [33] investigated combining glass FRP (GFRP) sheets with steel plates anchored by steel rods on the performance of exterior joints. They found that the use of GFRP sheets with steel plates greatly improves the specimen's strength and ductility capacity. Additional U-shaped steel plates further improved specimen performance by preventing the GFRP from debonding. The above studies are all limited to square columns with the exception of the study by Hany et al. [29], which considered wide rectangular columns.

The second category of literature on the topic of retrofitting examines the overall performance of retrofitted structures. For example, Baradaran Shoraka [4] directly

investigated the effect of several retrofitting methods on the seismic performance of older NDRC frames with square columns and beams, described in terms of collapse fragility functions. The methods considered are concrete jacketing of the columns, adding shear walls, and weakening the beams. The buildings were modeled using the lumped plasticity approach on Opensees. The study found that the concrete column jacketing they used, when combined with additional steel reinforcement, lead to the largest increase in seismic collapse performance even when only the columns on the lower floors were jacketed.

Niroomandi et al. [22] used a finite element model to study the effect of retrofitting the joints of an NDRC frame using FRP sheets on the overall roof drift capacity. They found that the FRP retrofitting of joints leads to significantly increased ductility capacity and to the upgrade of an ordinary moment-resisting frame to an intermediate moment-resisting frame. Harrington and Liel [20] used a fiber modeling approach to investigate the effect of column jacketing on the seismic performance of older NDRC frames. They found that retrofitting leads to increased ductility capacity and a reduced drift demand to capacity ratio. Liel and Deierlein [21] investigated the cost-effectiveness of several types of retrofits on the seismic performance of older type NDRC frames with square columns, described in terms of collapse fragility functions. The frames were modeled using a lumped plasticity approach. The retrofitting methods they considered are concrete jacketing of columns, CFRP jacketing of columns (without anchor rods), and the addition of shear walls. CFRP jacketing was accounted for in the analytical models by adjusting the rotational capacities of the columns based on experimental data, while concrete jackets were modelled by merely modifying the section area. They found that the CFRP jacketing resulted in a minimal improvement in fragility in low-rise (4-story) and an almost negligible

improvement in mid-rise (8-story) structures when compared with the two other methods. They found that the RC jacketing they used provided the most considerable improvement in seismic collapse performance. Ronagh and Eslami [23] studied the effect of FRP retrofitting of joints on how damage propagates in a frame subjected to lateral forces in a pushover analysis. They found that the use of FRP retrofitting increases the lateral load capacity of the concrete frame. Vega-Behar et al. [34] investigated the effect of retrofitting joints and inadequate lap splices on the seismic performance of NDRC frames modeled using a distributed plasticity approach. The FEMA Hazus MH-2.1 [35] methodology was used to define the performance limit states and calculate the fragility curves. This study found that retrofitting the joints without retrofitting the columns results in decreased performance. However, this study has some modeling limitations; the only effect of joint retrofitting that it accounts for is the reduction in bond slip.

The previously reviewed literature highlights the sparse volume of publications tackling the effect of retrofitting on the global seismic collapse performance of NDRC frame buildings. To our knowledge, besides the lap splice improvement studied in Vega-Behar et al. [34], there are no studies that deal with the effect of retrofitting joints on collapse fragility, or with the effect of retrofitting on the seismic performance of NDRC frames with wide beam-narrow column joints, which are typical in Lebanon. This presents an excellent opportunity to research the effectiveness of various retrofitting methods in addressing some of the structural deficiencies that are ubiquitous in the older building stock in Beirut.

C. Objectives and Scope

The main objective of this study is to assess the effect of various retrofitting methods on the seismic collapse performance of mid-rise NDRC frame structures with no shear walls and built in Beirut before the 1990s. These structures are characterized by wide and shallow beams, high aspect ratio columns, insufficient transverse reinforcement, unreinforced wide beam-narrow column joints, and lap splices located in potential plastic hinge regions. This study will focus on a representative 8-story building that was studied by El-Khoury and Harajli [13]. The seismic response and performance of this building was already assessed in a study by Allabban [18]. This study, which is briefly reviewed in this thesis, found that the joints perform poorly and are the primary contributors to collapse, and that the building has a probability of collapse of 87.4% when subjected to a maximum considered earthquake (MCE) ground motion.

To achieve the main objective, retrofitting schemes that target the structural deficiencies of the studied representative building are first identified. The structural deficiencies include: (1) columns are weak along their minor axis; (2) columns are non-ductile due to insufficient transverse reinforcement; (3) joints are weak and non-ductile due to lack of or poor detailing of reinforcement; (4) lap splices are located in potential plastic hinge regions. The retrofitting methods investigated in this study are concrete jacketing of the columns [20], which increases the shear and moment strengths and the ductility capacity of the strengthened members, allows moving lap splices away from potential plastic hinge regions and also strengthens the joints by enlarging the joint area [26], and the use of CFRP sheets to increase beam moment capacity. Three different retrofitted structures

are then designed. The designs all include concrete column jacketing, with varying jacket dimensions, and with or without CFRP sheets added to the beams.

Next, for each retrofitted structure, a nonlinear analytical model is developed in the Open System for Earthquake Engineering Simulation (OpenSees) [36] using the lumped plasticity approach. The effect of each retrofitting technique used is incorporated into the analytical model without sacrificing the capability of the model to predict global collapse. Then, the global collapse performance of each retrofitted building is assessed following the FEMA-P695 methodology [37] by using incremental dynamic analysis (IDA) [8] to develop collapse fragility curves, which are then compared with that of the unretrofitted building. Finally, the retrofitted designs are compared based on their effect on collapse performance, in particular on the probability of collapse of the structure when subjected to an MCE ground motion, as well as the ease of their practical implementation, and recommendations are made accordingly.

D. Organization of the Thesis

This thesis is organized into eight chapters. Chapter 0 of the thesis discusses the background and motivation behind the topic. It also includes an in-depth literature review as well as a summary of the objective at hand. Chapter 0 describes the midrise NDRC building that is assessed and retrofitted in this study. Chapter 0 presents the approaches used to develop a non-linear analytical model of the unretrofitted building. These modeling approaches are later extended to also model the retrofitted buildings. Chapter 0 presents the analysis methods used for the seismic performance assessment of all the building models considered in this study, namely, pushover analysis, incremental dynamic analysis, and the

derivation of seismic collapse fragility curves while also summarizing the results, previously presented by Allabban [18], of the seismic performance assessment of the unretrofitted building. These results confirm the poor expected seismic performance of the unretrofitted building if subjected to strong ground shaking. Chapter 0 specifies the objectives that the retrofitted buildings should aim to achieve, describes the selected retrofitting methods, and presents the design of the three retrofitted structures that are assessed in this study. Chapter 0 extends the discussion of Chapter 0 and describes the approaches used to account for the implemented retrofits in the analytical models of the retrofitted buildings. Chapter 0 presents the results of the seismic collapse assessment of the retrofitted buildings for the pushover and incremental dynamic analyses and also includes an in depth discussion of the performance of individual elements of the models. Finally, Chapter 0 summarizes the accomplished work, presents the conclusions of the study, discusses its limitations, and makes recommendations for improvement and future work.

CHAPTER II

DESCRIPTION AND DESIGN OF THE UNRETROFITTED MIDRISE RC BUILDING

The objective of this study is to assess the effect of various retrofitting methods on the seismic collapse performance of older RC frame buildings in Beirut. Therefore, it is important to select a building configuration that is representative of the building stock in Beirut in the 1980s. To that end, the configuration used in this study is based upon the typical building configuration used by El-Khoury and Harajli [13], as well as on interviews with senior practicing engineers with design experience during the 1990s. Additional design was carried out by Allabban [18] following the ACI318-95 [38] building code. In this chapter, the design and detailing of the unretrofitted structure is described. The design and detailing of the retrofitted structures are described in Chapter 0.

As mentioned previously, this study focuses on an 8-story representative structure located at a class D site in Beirut and whose plan configuration is shown in Figure 2. This building is referred to as the *unretrofitted building* and labelled as B0 in this study. Similar 8-story buildings are prevalent in the Beirut and Lebanese building stock. The building has a rectangular and symmetric plan. The height of all floors is 3.2 m. In the longitudinal direction, the structural system is comprised of four reinforced concrete frames with columns and beams that all display high aspect ratios. The frames are connected by one-way ribbed slabs spanning in the transverse direction. The substructure includes basement retaining walls, which are assumed to behave rigidly. Consequently, the basement walls are

not modelled or designed in this study, and the superstructure is assumed to be fixed at the ground level. The building was designed by El-Khoury and Harajli [13] and Allabban [18] to resist gravity loads only and in accordance with ACI 318-95 [38]. The material properties selected are representative of the construction industry at the time, namely, a concrete compressive strength f'_c of 17.6MPa and steel yield strength f_y of 420MPa for both longitudinal and transverse steel.

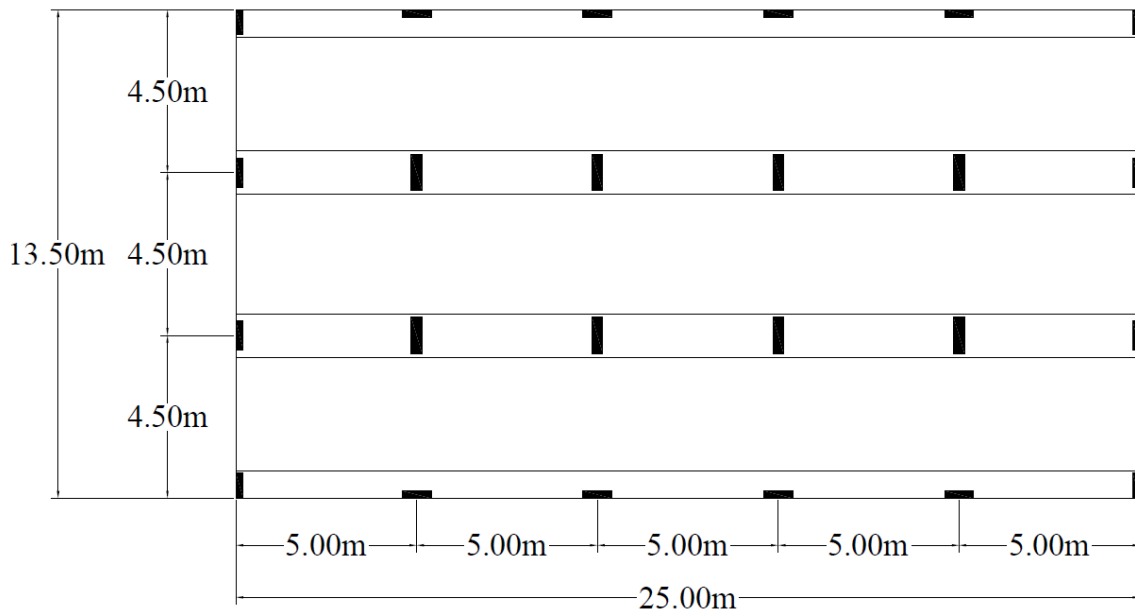


Figure 2: Plan view of the configuration

Table 1 shows the column sizes throughout the building, as taken from El-Khoury and Harajli [13]. The beams are all concealed within the slab and have a height of 24 cm. The exterior beams are 75 cm wide, and the interior beams are 120 cm wide. The ribbed slab spanning in the transverse direction has a total depth of 24 cm, a top slab thickness of 9 cm, and ribs that are 15 cm wide with a center to center spacing of 55 cm. This

configuration contains no shear walls or other lateral load resisting systems. The interviews conducted with professionals revealed that moment-resisting shear walls were not common in the construction of that time.

The steel reinforcement of the columns was designed by Allabban [18] according to the ACI318-95 [38] code to resist gravity loads only. The following service loads were accounted for in the design:

- 3.5 KN/m^2 for infill walls and tiling,
- 4.1 KN/m^2 for the slab own weight,
- 2.0 KN/m^2 for the service residential live load.

The gravity load combination used was $1.4DL + 1.7LL$, which brings the ultimate distributed load to:

$$W_u = 1.4DL + 1.7LL = 14.04 \text{ KN/m}^2 \quad (1)$$

This loading was then used to calculate the total load on each frame, with the own weight of the structure included in the dead weight. The density of concrete was assumed to be equal to 25 KN/m^3 . The columns were designed to resist these gravity loads as compression members only, with no lateral forces. Therefore, minimum shear reinforcement allowed by ACI318-95 [38] was adopted according to the following equation:

$$A_v = 0.34b_w s / f_y, \quad (2)$$

where, A_v is the area of shear reinforcement, b_w is the member width, and s is the shear reinforcement spacing. Beams were designed by El-Khoury and Harajli [13] as flexural members with the reinforcement calculated based upon the moments at critical sections.

For the exterior frame of the building, which is the focus in this study, the dimensions and reinforcements of the columns and beams are shown in Table 2 and Table 3, respectively. Table 2 also provides the expected gravity load demands on the columns of B0 calculated from the load combination $1.0DL + 0.25LL$.

The member detailing is adequate for gravity loading, but not for lateral loading. Beam longitudinal reinforcement is continuous, with splices in low moment areas and hooks only at the beam ends. Column reinforcement is spliced at the base (against the recommendation of ACI318-14 [39]). Additionally, the beam and column transverse reinforcement do not extend into the joint region [13]. This leads to non-ductile joints that are vulnerable to plastic hinging. The high aspect ratio of the members is also of concern as it leads to earlier plastic hinging along the weaker axes in particular. More details about the design of this NDRC building can be found in El-Khoury and Harajli [13] and Allabban [18].

Table 1: Column Dimensions in the structure

Frame	Column	Floors	Dimensions (mm)
Interior	Interior	1-4	300x1000
		5-8	250x700
	Exterior	1-4	200x800
		5-8	200x700
Exterior	Interior	1-4	200x800
		5-8	200x700
	Exterior	1-4	200x700
		5-8	200x600

Table 2: Design Parameters of the Column of the Exterior Frame of B0

Exterior Columns of Exterior Frame							
Floor	Depth (mm)	Width (mm)	P (kN)	Main Reinf.	ρ (%)	Shear Reinf. (mm)	ρ_{sh} (%)
1	200	700	538	8T20	1.77	4T8@200	0.14
2	200	700	470	8T20	1.77	4T8@200	0.14
3	200	700	402	8T20	1.77	4T8@200	0.14
4	200	700	334	8T20	1.77	4T8@200	0.14
5	200	600	266	8T16	1.33	4T8@200	0.17
6	200	600	199	8T16	1.33	4T8@200	0.17
7	200	600	133	8T16	1.33	4T8@200	0.17
8	200	600	66	8T16	1.33	4T8@200	0.17
Interior Columns of Exterior Frame							
Floor	Depth (mm)	Width (mm)	P (kN)	Main Reinf.	ρ (%)	Shear Reinf. (mm)	ρ_{sh} (%)
1	800	200	1005	8T22	1.94	2T8@200	0.25
2	800	200	879	8T22	1.94	2T8@200	0.25
3	800	200	752	8T20	1.55	2T8@200	0.25
4	800	200	626	8T20	1.55	2T8@200	0.25
5	700	200	499	8T16	1.14	2T8@200	0.25
6	700	200	374	8T16	1.14	2T8@200	0.25
7	700	200	250	8T16	1.14	2T8@200	0.25
8	700	200	125	8T16	1.14	2T8@200	0.25

Table 3: Design Parameters of the Beams of the Exterior Frame of B0

Beam Span	Dimensions (mm)	Side	Longitudinal Reinforcement		ρ (%)		Shear Reinf. (mm)	ρ_{sh} (%)
			Top	Bottom	Top	Bot		
1	240x750	Left	5T14	5T14	0.5	0.5	4T6@200	0.075
		Right	6T16	5T14	0.8	0.5		
2	240x750	Left	6T16	5T14	0.8	0.5	4T6@200	0.075
		Right	5T16	5T14	0.7	0.5		
3	240x750	Left	5T16	5T14	0.7	0.5	4T6@200	0.075
		Right	5T16	5T14	0.7	0.5		
4	240x750	Left	5T16	5T14	0.7	0.5	4T6@200	0.075
		Right	6T16	5T14	0.8	0.5		
5	240x750	Left	6T16	5T14	0.8	0.5	4T6@200	0.075
		Right	5T14	5T14	0.5	0.5		

CHAPTER III

ANALYTICAL MODELING OF THE UNRETROFITTED BUILDING

A. Introduction

For seismic collapse assessment, non-linear models of the unretrofitted and retrofitted structures should be developed. The models should be capable of accurately simulating the behavior of the structures well into the non-linear stage of analysis while also remaining computationally efficient. For each of the unretrofitted and retrofitted structures, a 2D model of the structure in the longitudinal direction is constructed using OpenSees [36]. This approach is made possible due to the fact that the representative structure being studied is entirely symmetrical and thus the effects of torsion can be ignored [9, 40]. P-delta effects are directly incorporated into the numerical model, and structural masses are lumped at each floor.

In this study, only a single frame is modeled to simplify the model and reduce the computational time and convergence problems. The exterior frame is selected because it has more columns oriented along their major (strong) axis; therefore it is stiffer and attracts larger earthquake forces than the interior frame and is more representative of the behavior of the overall structure [41]. This is confirmed by the work of Allabban [18] who modeled and assessed using incremental dynamic analysis (IDA) the seismic performance of the external and internal frames, both individually and when connected by rigid links. Allabban [18] found that, at equal spectral acceleration levels, the exterior frame possesses a higher probability of collapse than the interior frame. Allabban [18] also found that, when both

frames are analyzed concurrently (connected by rigid links), damage and collapse start and are more predominant in the exterior frame. Additionally, Allabban [18] found that the collapse fragility curve of the exterior frame is similar to that of the combined frame, especially at spectral amplitudes $S_a(T_1)$ close to the maximum considered earthquake (MCE) amplitude.

B. Concentrated/Lumped Plasticity Approach.

A lumped plasticity approach is used to model the stiffness and hysteretic relationships of the structural elements. This approach consists of lumping the non-linear structural deformations of a frame element into springs at both ends of the element. Each frame element is then modeled as the assembly of a linear elastic 2D line element and zero-length springs, as shown in Figure 3. The spring force deformation relationships are carefully calibrated such that the assembly adequately simulates the element behavior.

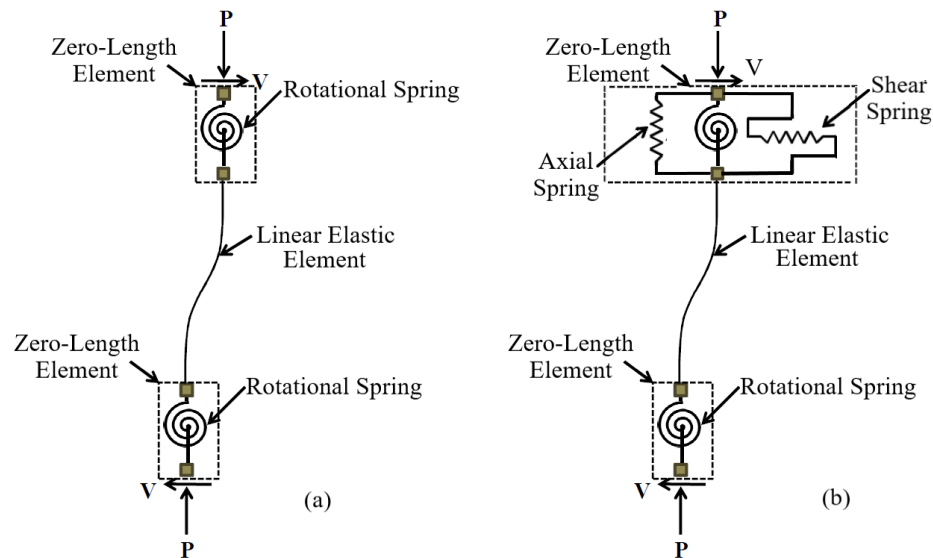


Figure 3: Visual representation of the lumped plasticity approach to capture flexure (a) and flexure shear (b) behavior [4]

The main advantage of this modeling technique is its ability to capture and distinguish between in-cycle and cyclic strength deterioration. Additionally, it provides a more computationally efficient approach to structural modeling when compared to the fiber modeling approach [42, 43]. The most significant weakness of this method is its difficulty with capturing stiffness changes at the onset of cracking; this, however, is not an issue in this project since the focus is on the global structural collapse performance [44].

In seismic collapse assessment studies of ductile frames, capturing the flexural response of the frame elements using rotational springs would be adequate, as shown in Figure 3 (a) [4]. However, when it comes to non-ductile reinforced concrete (NDRC) frames, shear or even axial failure of columns are common, thus shear and axial springs should also be included, as shown in Figure 3 (b) [4]. To establish which failure mode is more likely to occur, and therefore, which modeling approach to use for a particular frame, the V_p/V_n ratio for every column is calculated, where V_p is the shear demand on the column at flexural yielding and V_n is the design shear strength of the column [9]. V_p is calculated according to the following equation:

$$V_p = \frac{(M_{y,top} + M_{y,bot})}{L}, \quad (3)$$

where M_y is the expected yield moment strength of the column, calculated according to the equations proposed by Panagiotakos and Fardis [45], and L is the column length. V_n is the nominal shear strength of the column calculated based on ASCE 41 [46] as follows:

$$V_n = k \left[\frac{A_v f_{yt} d}{s} + \lambda_c \left(\frac{0.5 \sqrt{f'_c}}{a/d} \right) \sqrt{\left(1 + \frac{P}{0.5 \sqrt{f'_c} A_g} \right) 0.8 A_g} \right] (MPa), \quad (4)$$

where A_v is the area of shear reinforcement, f_{yt} is the transverse steel strength, d is the effective depth of the column, s is the spacing of transverse reinforcement, L is the column length, $\lambda_c = 1$ for normal-weight concrete, f'_c is the concrete compressive strength, a is the shear span taken as $L/2$, P is the axial force, A_g is the column gross section area, and k is a factor that degrades with ductility demand μ_T ; ranging from $k = 1.0$ when $\mu_T \leq 2.0$, to $k = 0.7$ when $\mu_T \geq 6.0$. The value of k is linearly interpolated for μ_T values in between. A value of $k = 1$ is used to calculate V_n in the V_p/V_n ratio. The axial load P is calculated using the expected gravity load on each column according to its tributary area and the load combination $1.0DL + 0.25LL$, and is provided in Table 2 for the columns of the unretrofitted building.

Following Sattar and Liel [47], columns with a $V_p/V_n < 0.7$ are taken to be dominated by flexural behavior and those with a $V_p/V_n > 0.7$ may be subject to shear failure and are thus modeled as flexure-shear members by adding shear and axial springs. As shown later in this chapter, the majority of the columns of the unretrofitted structure possess a $V_p/V_n > 0.7$, therefore they are modeled as depicted in Figure 3 (b) to capture the onset of shear failure.

1. Flexural Behavior

The force deformation relationships of the beam-column rotational springs are modeled using the modified Ibarra and Krawinkler lumped plasticity model [48]. This model, whose positive backbone is shown in Figure 4, consists of a trilinear backbone curve with energy dissipation parameters controlling the hysteretic response. The model is

capable of capturing in-cycle strength deterioration as well as the effect of bond-slip. The backbone is defined by the following parameters: the secant value of the effective stiffness to 40% of the yield moment ($K_e = EI_{stf40}$); the yield moment (M_y); the capping moment (M_c); the plastic chord rotation capacity ($\theta_{cap,pl}$); and the post capping rotation capacity (θ_{pc}). Moreover, eight terms (c_{1-4}) and (λ_{1-4}) are used to define the cyclic deterioration and normalized cyclic energy dissipation, respectively. Following the work of Haselton et al. [44] the eight terms (c_{1-4}) and (λ_{1-4}) are reduced to only two terms (c) and (λ).

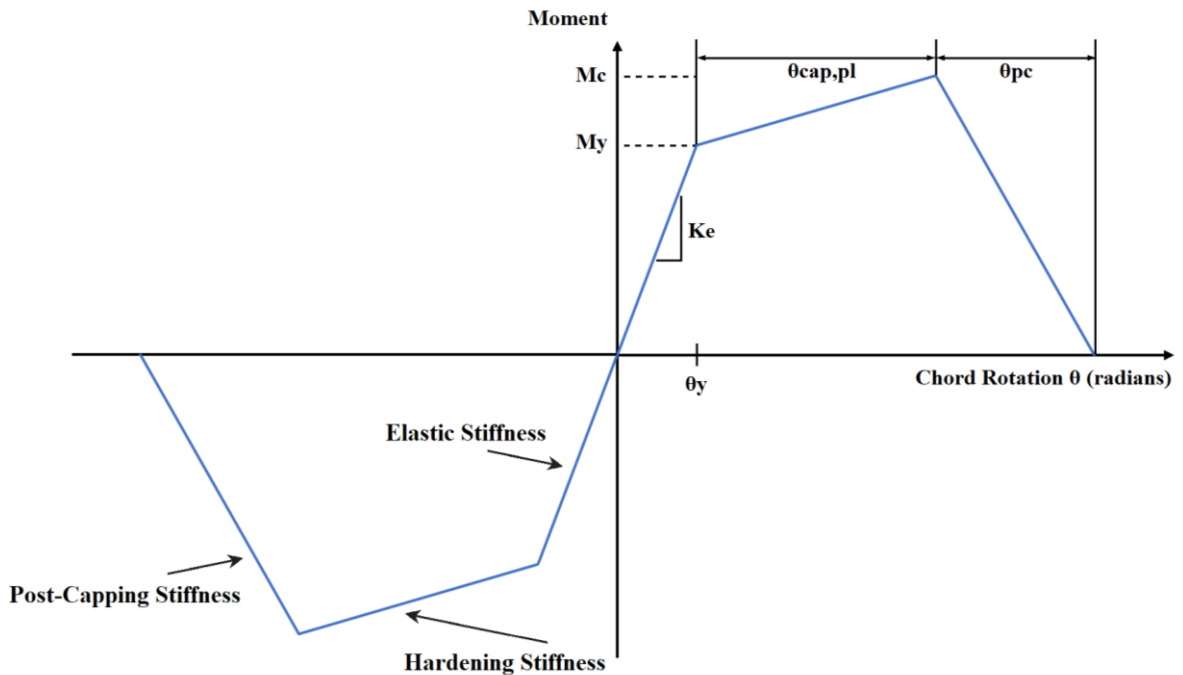


Figure 4: Backbone curve of the Ibarra-Krawinkler hysteretic model [44]

Haselton et al. [42] developed a set of regression equations to predict each of the parameters mentioned above. These predictive relations were established by calibrating the model parameters to 255 concrete specimen tests that failed in flexure and flexure shear, then relating them to design parameters such as geometry, reinforcement details, material

properties etc. The exception is the yield moment which is calculated according to the equations proposed by Panagiotakos and Fardis [45]. For the elements dominated by flexure, i.e., where $V_p/V_n < 0.7$, a recalibrated version of these equations is used in this study. These were calibrated to the 220 specimens that failed in flexure only and were published in Galanis [49]. The recalibrated equations are shown below:

$$\frac{EI_{stf40}}{EI_g} = 0.77(0.1 + v)^{0.8} \left(\frac{L_s}{H}\right)^{0.43}, \quad (5)$$

$$\theta_{cap,pl} = 0.13(1 + 0.55a_{sl})(0.16)^v(0.02 + 40\rho_{sh})^{0.55}(0.99412)^{f'_c}, \quad (6)$$

$$\theta_{pc} = (1.13)(0.018)^v(0.02 + 40\rho_{sh})^{1.14} \leq 0.10, \quad (7)$$

$$M_c/M_y = 1.13, \quad (8)$$

$$\lambda = (170.7)(0.27)^v(0.10)^{s/d}, \quad (9)$$

$$c = 1.0, \quad (10)$$

where E is the modulus of elasticity of concrete, I_g is the gross moment of inertia of the section, I_{stf40} is the effective cross-sectional moment of inertia at 40% of the yield moment, $v = P/A_g f'_c$ is the axial load ratio, L_s is the shear span being the distance between element end and point of inflection, H is the height of the cross-section parallel to the lateral/transverse load, s is the spacing of transverse reinforcement at the hinge region, d is the effective depth of the section, ρ_{sh} is the ratio of transverse reinforcement at the hinge region, a_{sl} is assigned as 0 if slip is not possible or 1 if slip is possible, c_{units} is defined as a conversion constant being 1.0 if units are MPa and 6.9 if units are ksi , s_n is the rebar buckling coefficient given as $s/d_b \sqrt{c_{units} f_y / 100}$, and ρ is the reinforcement ratio of compression steel in columns and of tension rebars in beams.

2. *Shear and Axial Behavior*

For columns with $V_p/V_n > 0.7$, shear and axial springs are added to the top of the frame elements as shown in Figure 3 (b). Their purpose is to capture the effect of strength degradation due to excessive shear and axial forces. This is done by using a bilinear force-deformation relationship that consists of a linear initial stiffness followed by a degrading stiffness once a shear or axial limit curve is reached. This behavior is incorporated into Opensees [36] as the Limit State Material developed by Elwood [50].

For the purpose of defining the onset of shear failure, the work of Elwood and Moehle [51] is used. An empirical equation was calibrated from 50 column tests which failed in shear (although they yielded prior to shear failure):

$$\frac{\Delta_s}{L} = \frac{3}{100} + 4\rho'' - \frac{1}{40} \frac{v_s}{\sqrt{f'_c}} - \frac{1}{40} \frac{P}{A_g f'_c} \geq \frac{1}{100}, \quad (11)$$

where Δ_s/L is the drift ratio at which shear failure occurs, ρ'' is the shear reinforcement ratio, and v_s is the nominal shear stress V/bd .

The onset of axial failure, on the other hand, is defined according to the following equation also developed empirically by Elwood [52]:

$$\left(\frac{\Delta}{L}\right)_{axial} = \frac{4}{100} \times \frac{1 + (\tan \theta)^2}{\tan \theta + P(s/A_{st} f_{yt} d_c \tan \theta)}, \quad (12)$$

where $(\Delta/L)_{axial}$ is the drift ratio at axial failure, A_{st} is the area of transverse reinforcement, f_{yt} is the transverse reinforcement yield strength, d_c is the depth of the column core from the centerline to the centerline of the ties and θ is the crack angle measured from the horizontal and assumed to be 65°

It is worth noting that the shear and axial springs are only implemented in the model of the unretrofitted structure. They are not included in the models of the retrofitted structures because one of the retrofitting objectives is to reduce the V_p/V_n ratio below 0.7 to ensure a flexure dominated response.

C. Joint Modelling

1. Background

Several different approaches for modeling joints exist throughout the published literature. They are explored and summarized in Celik and Ellingwood [51]. In this work and the earlier study by Allabban [18], the joints of the unretrofitted structure lack transverse reinforcement and are modeled using the scissor model with rigid end zones, as developed by Alath and Kunnath [53]. This model consists of a single rotational spring at the center of the joint, with rigid members representing the actual joint dimensions, as shown in Figure 5. Celik and Ellingwood [54] validated this model against experimental data from seismic loading tests on reinforced concrete joints with inadequate reinforcement [55, 56].

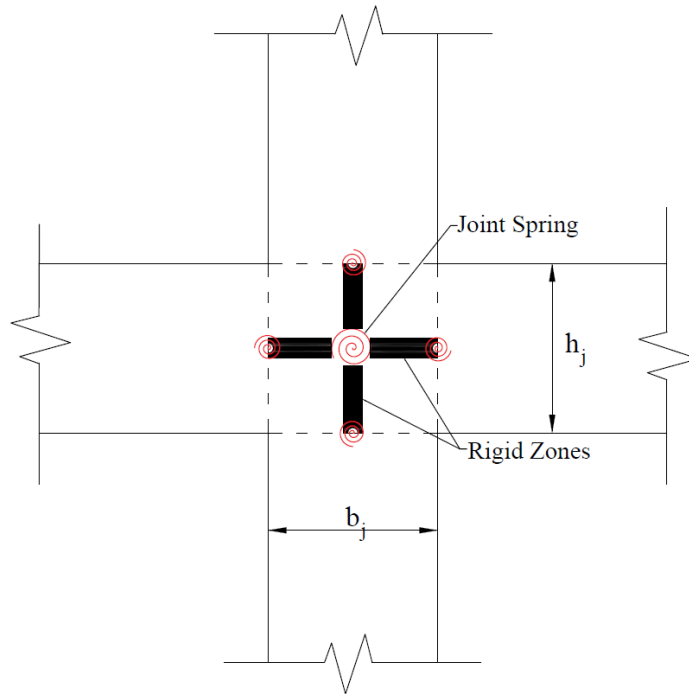


Figure 5: Joint scissor model developed by Alath and Kunnath [53]

2. *Joint Spring Model*

The hysteretic model of the joint spring moment-rotation relation consists of a backbone curve defined by four points, and incorporates in-cycle deterioration and pinching behavior, which is characteristic of joints lacking transverse reinforcement [55, 57]. The four points defining the backbone curve are: (1) joint shear cracking (M_{cr}, θ_{cr}); (2) reinforcement yielding (M_y, θ_y); (3) joint shear capacity or adjoining member capacity (M_u, θ_u); and (4) residual strength (M_r, θ_r). Points 2 and 3 are taken to be the minimum of the joint, beam or column capacity. The moment capacity of beams is scaled downwards by a factor α to account for the effect of bond slip on beam capacity.

Additionally, three more parameters are used to control the hysteretic and pinching properties of the model. These parameters are $rDisp$, which defines the ratio of the

deformation at which reloading occurs to the maximum or minimum historic deformation demand, $fForce$, which defines the ratio of the force at which reloading begins to the force corresponding to the maximum or minimum historic deformation demand, and $uForce$, which defines the ratio of the strength developed upon unloading from a negative load to the maximum strength developed under monotonic loading. The parameters are all displayed in Figure 6.

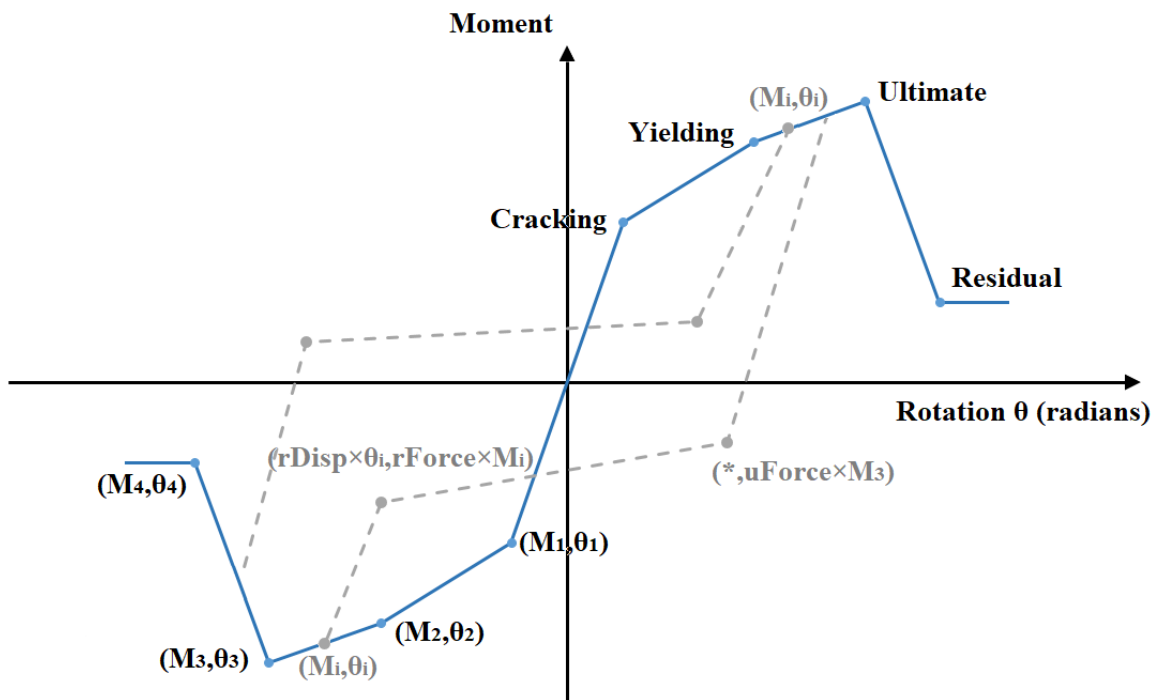


Figure 6: Hysteretic backbone for the model developed by Lowes and Altoontash [58]

3. *Model for Unreinforced Wide Beam-Narrow Column Joints*

The various parameters of the joint model hysteretic curve are calibrated based on experimental tests. Most of the previous literature on the topic calibrated the model to the joints of square columns (e.g., Celik and Ellingwood [54], De Risi et al. [59] and Park and

Mosalam [60]). However, the beams and columns of the buildings analyzed in Allabban [18] and in this study are rectangular with high aspect ratios. Therefore, a new calibration was performed by Allabban [18] to the experimental tests of Elsouri and Harajli [61, 62], one of the few tests on beam-column joints with proportions and aspect ratios similar to those of the buildings studied by Allabban [18]. These tests were conducted on specimens with inadequate detailing and lacking transverse reinforcement, which resulted in non-ductile behavior. The scissor approach and the joint spring model calibrated by Allabban [18] are used in this study to model the joints of the unretrofitted building. Details of the model calibrated by Allabban [18] are presented in the next paragraphs.

The calculation of the yield and ultimate moments (M_y and M_u) was based on the recommendations of Celik and Ellingwood [54], where the maximum possible moment transferable through the joint is based on the minimum of the following strengths:

- The moment capacity of the adjoining beams;
- The moment capacity of the adjoining columns;
- The moment based on the maximum joint shear strength $(\overline{\tau}_{jh})_{max}$.

In particular, the following equations were used:

$$(M_j)_{y,u} = \min \left[\frac{(M_c^T)_{y,u} + (M_c^B)_{y,u}}{\eta_c}, \frac{(\alpha M_B^+) + (M_B^-)_{y,u}}{\eta_B}, M((\overline{\tau}_{jh})_{max}) \right] \quad (13)$$

for interior joints,

$$(M_j)_{y,u} = \min \left[\frac{(M_c^T)_{y,u} + (M_c^B)_{y,u}}{\eta_c}, \frac{(\alpha M_B^+)_{y,u}}{\eta_B}, M((\overline{\tau_{jh}})_{max}) \right] \quad (14)$$

for the positive backbone of exterior joints, and

$$(M_j)_{y,u} = \min \left[\frac{(M_c^T)_{y,u} + (M_c^B)_{y,u}}{\eta_c}, \frac{(M_B^-)_{y,u}}{\eta_B}, M((\overline{\tau_{jh}})_{max}) \right] \quad (15)$$

for the negative backbone of exterior joints, where $\eta_c = 1 - h_j/L_c$ and $\eta_B = 1 - b_j/L_b$,

where b_j is the joint panel width, h_j is the joint panel height, L_b is the total length of the left and right beams, L_c is the total length of top and bottom columns. The subscripts C and B refer to columns and beams, respectively, the superscripts T and B refer to top and bottom members, respectively, and the subscripts y and u refer to the yielding and ultimate strengths, respectively. α is a factor that accounts for the effect of rebar slip in beams due to inadequate development length within the joint. In the work of Celik and Ellingwood [54], α varied between 0.4 and 0.7, but the value of α adopted in Allabban [18] and in this work is the one recommended by Hoffman et al. [63], namely that α is the ratio of the development length provided to the development length required by ACI318-95 [38].

The maximum joint shear stress $(\overline{\tau_{jh}})_{max}$ used in Equations (13)-(15) was obtained using the ACI318 [39] equations, whereby the strength of interior joints is taken to be $1.25\sqrt{f'_c}$ (MPa) for interior joints and $1.0\sqrt{f'_c}$ (MPa) for exterior joints. The corresponding moment $M(\overline{\tau_{jh}})$ is calculated using the equations derived by Celik and Ellingwood [54], which relate the joint moment and rotation to the joint shear stress and shear strain, respectively. These joint moment M_j is calculated from the joint shear τ_{jh} as follows:

$$M_j = \tau_{jh} A_{jh} \frac{1}{\lambda} \quad (16)$$

where $\lambda = (1 - b_j/L_b)/jd - 1/L_c$ for all exterior and interior joints below the roof and $\lambda = (1 - b_j/L_b)/jd - 2/L_c$ for top floor joints only, and A_{jh} is the joint area in the horizontal plane, b_j is the joint panel width, L_b is the total length of the left and right beams, L_c is the total length of top and bottom columns, and jd is the beam moment arm. As for the joint rotation θ_j , it is equal to the joint shear strain γ_j .

The cracking (M_{cr}) and residual (M_r) moments were taken by Allabban [18] to be $0.35M_u$ and $0.4M_u$, respectively, based on the experimental data of Elsouiri and Harajli [61, 62].

All the joint rotation values ($\theta_{cr}, \theta_y, \theta_u, \theta_r$) were also calibrated to the experiments of Elsouiri and Harajli [61, 62] in the work of Allabban [18]. The result of these calibrations are displayed in Table 4, where h_b and h_c are the the beam and column depths, respectively.

As for the hysteretic and pinching parameters $uForce$, $rForce$, and $rDisp$, their calibration was carried out by fitting the overall hysteretic responses calculated using the proposed predictive model to the experimental responses. The values of the hysteretic and pinching parameters selected by Allabban [18] are shown in Table 5.

Table 4: Calibrated rotation values for unretrofitted joints from Allabban[18]

Joint Type	Cracking (θ_{cr})	Yield (θ_y)	Ultimate (θ_u)	Residual (θ_r)
Exterior	0.005	0.0125	$0.0024(h_b/h_c) + 0.0167$	$\theta_u + 0.02$
Interior		$0.0075(h_b/h_c) + 0.0097$	$0.0306(h_b/h_c) + 0.008$	

Table 5: Calibrated hysteric pinching parameters for unretrofitted joints from Allabban [18]

Hysteric Parameter	$uForce$	$rForce$	$rDisp$
Exterior	-0.1	0.15	-0.1
Interior	-0.1	0.15	0.15

D. Damping and Mass Allocation

As was done by Galanis [49], the mass sources considered in the model are the dead load and 0.25 times the live load. The total seismic mass at each floor is distributed between the external and internal frames in proportion to the initial stiffnesses of the two frames, but only the external frame is modeled and analyzed in this study. Then the seismic masses are lumped at the beam end nodes and assigned to the lateral degrees of freedom. Negligible mass sources are assigned to the other degrees of freedom to avoid a sparse mass matrix and numerical instability [49].

Also following Galanis [49], mass and stiffness proportional Rayleigh damping is used. The damping ratio adopted is $\zeta = 2\%$ for the first and third modes as calculated by eigenvalue analysis. The formulation used is as follows:

$$[C] = \alpha[M] + \beta[K], \quad (17)$$

where $[C]$ is the damping matrix, $[M]$ is the mass matrix, $[K]$ is the initial stiffness matrix, α is the mass proportional factor, and β is the stiffness proportional factor. In order to prevent spurious damping moments caused by the change in stiffness of non-linear elements when using the initial stiffness matrix, the recommendations of Ibarra et al. [48] are followed. Stiffness proportional damping is assigned to the linear elastic elements only, and not to the non-linear rotational springs. Note that the stiffness $K_{beam-column}$ of the

beam-column assembly shown in Figure 3 (a) is related to the stiffnesses of its linear-elastic element $K_{elastic}$ and rotational spring components K_{spring} by

$$K_{beam-column} = \frac{1}{K_{elastic} + K_{spring}} = \frac{K_{elastic} * K_{spring}}{K_{elastic} + K_{spring}}. \quad (18)$$

Following [49], the non-linear springs are assigned a stiffness that is n times larger than that of the linear elastic element. The stiffness values of the elastic element and of the springs are then adjusted according to

$$K_{elastic} = \frac{n + 1}{n} K_{beam-column}; \quad K_{spring} = (n + 1) K_{beam-column}. \quad (19)$$

This approximate solution satisfies both dynamic and static equilibrium [49]. In this study, $n = 10$ is chosen. Note that since no damping is assigned to the non-linear rotational springs, the stiffness proportional damping factor, β , assigned to the elastic elements must be modified to

$$\beta_{mod} = \beta \times \left(\frac{n+1}{n}\right). \quad (20)$$

E. Analytical Model of the Unretrofitted Building

Using the modeling approaches presented in the previous sections, a non-linear model of the unretrofitted structure is developed in the Open System for Earthquake Engineering Simulation (OpenSees) [36]. Similar modeling approaches are used to develop the non-linear models of the retrofitted structures, also in OpenSees, as later presented in Chapter 0. Note that only the performance of the bare frames is assessed and incorporated into the analysis in this study. Non-structural elements such as infill walls and their effect

on collapse performance are not accounted for. Adding infill walls to the analytical model could be a valid avenue to explore in future projects.

Figure 7 shows the model used to assess the unretrofitted structure, as adopted by Allabban [18] and as described in the previous sections. It also illustrates the modeling details of the joint region, including the layout of the springs, nodes and rigid links. Table 6 and Table 7 display the properties of the rotational springs and of the shear and axial springs of the columns of B0, respectively. Table 8 lists the properties of the flexural springs of the beams of B0. All the model parameters are calculated using expected material properties for the steel.

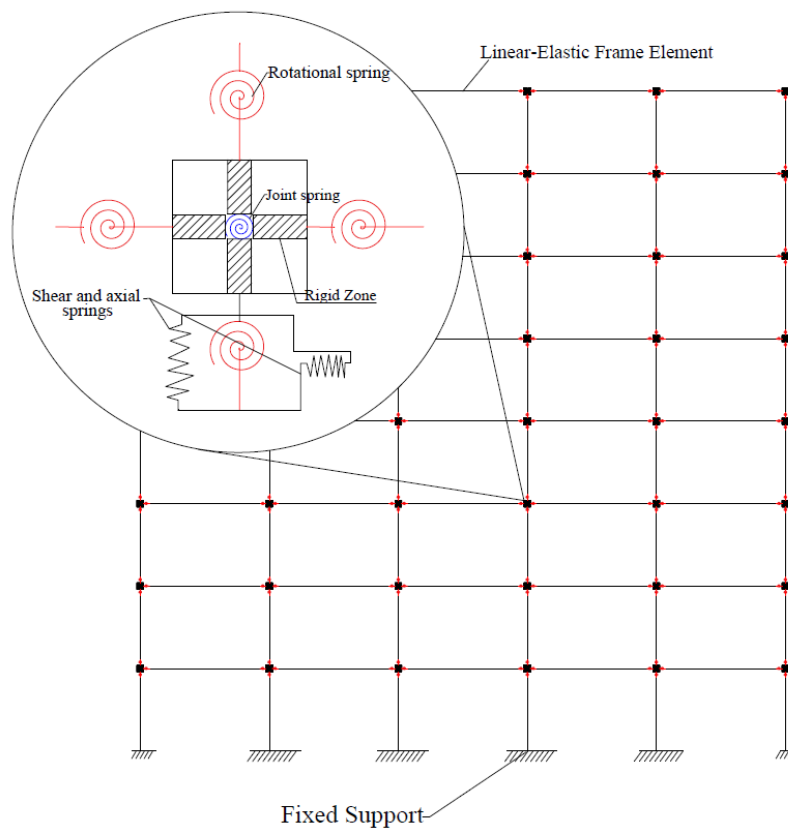


Figure 7: Analytical model utilized to represent the unretrofitted structure [18]

Table 6: Properties of the Flexural Springs of the columns of B0

Exterior Columns of Exterior Frame								
Floor	$P/A_g f'_c$	M_y (KN.m)	V_p/V_n	EI_{stf}/EI_g	M_c/M_y	$\theta_{cap,pl}$	θ_{pc}	λ
1	0.22	83	0.54	0.75	1.13	0.0298	0.0255	7
2	0.19	82	0.55	0.70	1.13	0.0314	0.0285	8
3	0.16	82	0.55	0.65	1.13	0.033	0.0318	8
4	0.13	82	0.56	0.59	1.13	0.0347	0.0355	8
5	0.12	58	0.41	0.57	1.13	0.0377	0.0422	9
6	0.09	54	0.39	0.51	1.13	0.0399	0.0479	9
7	0.06	49	0.36	0.44	1.13	0.0423	0.0543	10
8	0.03	44	0.33	0.37	1.13	0.0488	0.0616	10
Interior Columns of Exterior Frame								
Floor	$P/A_g f'_c$	M_y (KN.m)	V_p/V_n	EI_{stf}/EI_g	M_c/M_y	$\theta_{cap,pl}$	θ_{pc}	λ
1	0.35	603	1.03	0.55	1.13	0.030	0.024	61
2	0.31	606	1.07	0.51	1.13	0.032	0.029	65
3	0.26	550	1.00	0.47	1.13	0.035	0.035	69
4	0.22	525	0.98	0.42	1.13	0.038	0.042	74
5	0.20	322	0.71	0.42	1.13	0.039	0.045	70
6	0.15	291	0.77	0.36	1.13	0.043	0.055	75
7	0.10	260	0.43	0.35	1.13	0.047	0.068	81
8	0.05	228	0.39	0.35	1.13	0.052	0.083	87

Table 7: Properties of the Shear and Axial Springs of the columns of B0

Exterior Columns of Exterior Frame						
Floor	$P/A_g f'_c$	M_y (KN.m)	V_p/V_n	EI_{stf}/EI_g	Δ_s/L	Δ_a/L
1	-	-	-	-	-	-
2	-	-	-	-	-	-
3	-	-	-	-	-	-
4	-	-	-	-	-	-
5	-	-	-	-	-	-
6	-	-	-	-	-	-
7	-	-	-	-	-	-
8	-	-	-	-	-	-
Interior Columns of Exterior Frame						
Floor	$P/A_g f'_c$	M_y (KN.m)	V_p/V_n	EI_{stf}/EI_g	Δ_s/L	Δ_a/L
1	0.35	603	1.03	0.55	0.0108	0.047
2	0.31	606	1.07	0.51	0.0125	0.050
3	0.26	550	1.00	0.47	0.0142	0.054
4	0.22	525	0.98	0.42	0.0159	0.059

5	0.20	322	0.71	0.42	0.0180	0.061
6	0.15	291	0.77	0.36	0.0200	0.068
7	-	-	-	-	-	-
8	-	-	-	-	-	-

Table 8: Spring properties of beams of B0 for all floors

Rotational Spring at the Left Side								
Beam Span	M_{y+} (KN.m)	M_{y-} (KN.m)	EI_{stf}/EI_g	M_c/M_y	$\theta_{cap,pl+}$	$\theta_{cap,pl-}$	θ_{pc}	λ
1	67	67	0.35	1.13	0.035	0.035	0.037	19
2	67	103	0.35	1.13	0.039	0.032	0.037	19
3	67	86	0.35	1.13	0.037	0.033	0.037	19
4	67	86	0.35	1.13	0.037	0.033	0.037	19
5	67	103	0.35	1.13	0.039	0.032	0.037	19
Rotational Spring at the Right Side								
Beam Span	M_{y+} (KN.m)	M_{y-} (KN.m)	EI_{stf}/EI_g	M_c/M_y	$\theta_{cap,pl+}$	$\theta_{cap,pl-}$	θ_{pc}	λ
1	103	67	0.35	1.13	0.032	0.039	0.037	19
2	86	67	0.35	1.13	0.033	0.037	0.037	19
3	86	67	0.35	1.13	0.033	0.037	0.037	19
4	103	67	0.35	1.13	0.032	0.039	0.037	19
5	67	67	0.35	1.13	0.035	0.035	0.037	19

CHAPTER IV

SEISMIC PERFORMANCE ASSESSMENT METHODOLOGY AND APPLICATION TO THE UNRETROFITTED BUILDING

To achieve the main objective of this study, which is to assess and compare the effectiveness of various retrofitting approaches on the seismic collapse performance of an 8-story NDRC frame structure in Beirut, the reduction in the probability of global collapse of the retrofitted structures compared to the unretrofitted one is quantified. To result in an acceptable performance, and following FEMA P695 [37], the retrofits should reduce the probability of collapse of the structure when subjected to an MCE ground motion to less than 20%.

Following the FEMA-P695 methodology [37], the seismic performance of each of the unretrofitted and retrofitted structures is assessed using non-linear structural analysis of the corresponding analytical models developed in OpenSees and presented in Chapters 0 and 0, respectively. In particular, non-linear static pushover analysis is used to verify the system overstrength and ductility, and incremental dynamic analysis (IDA), as developed by Vamvatsikos and Cornell [8], is used to assess structural collapse and obtain the collapse fragility curve, which is a plot of the probability of collapse as a function of a ground motion intensity measure. The fragility curve is then used to determine the probability of collapse at the MCE intensity. In the next sections, the methodology used by Allabban [18] and in this study to assess the seismic performance of the unretrofitted building is

presented, and its results are summarized. More details can be found in Allabban [18]. The same methodology is also applied to the retrofitted buildings in Chapter 0.

A. Seismic Hazard at the Site

This project uses the results of the probabilistic seismic hazard analysis carried out by Huijjer et al. [1], which provides, for Lebanon, maps of the maximum considered earthquake (MCE) spectral acceleration parameters S_S and S_1 , which corresponds to ground motion intensities with a 2% probability of exceedance in 50 years [64]. Using ASCE 7-10 [64], the MCE spectral intensities at a class D site in Beirut are obtained, namely $S_{Ms} = 1.45$ g at short periods and $S_{M1} = 0.675$ g at a period of 1 second. Due to the lack of strong seismic ground motion recordings available in Lebanon, the FEMA P-695 far-field strong motion set is utilized to provide the ground motion acceleration data. It consists of 22 pairs of horizontal ground motions that adequately capture the variability in ground motion acceleration and frequency content [37]. Following the FEMA-P695 methodology, the intensity measure selected is the 5% damped first mode spectral acceleration $S_a(T_1; \zeta = 5\%)$ because it is scalable and generally found to be efficient [65].

Following FEMA P-695 [37] and ASCE 7-10 [64], the fundamental period, T , for each building is calculated as follows:

$$T = C_u T_a = C_u C_t h_n^x, \quad (21)$$

where h_n is the height of the building, C_u is the coefficient for the upper period limit, and C_t and x are approximate period parameters. For the 8-story structure in question, using $h_n = 25.6$ m, $C_u = 1.4$, $C_t = 0.0466$ and $x = 0.9$, the calculated fundamental period is

provided in Table 9 along with the MCE spectral acceleration S_{MT} at the fundamental period of the structure and its seismic weight. Note that the seismic weight displayed is that of the exterior frame of the unretrofitted building.

Table 9: Seismic Parameters of the exterior frame of the unretrofitted structure

Fundamental Period T (sec)	S_{MT} (g)	Seismic Weight (KN)
1.21	0.559	7975

Note that the retrofitting methods considered in this study do not include seismic isolation or dampers and are limited to concrete jacketing of the columns and adding CFRP sheets to the beams. As a result, since the fundamental period is assumed to only depend on the building height and type, the fundamental period and, therefore, the MCE spectral acceleration S_{MT} at the fundamental period of the structure remain unchanged as a result of the retrofitting procedures. As for the seismic weight, it is affected by the concrete jacketing and is thus calculated in Chapter 0 for each of the retrofitted structures.

B. Pushover Analysis

Pushover analysis is performed according to the guidelines in FEMA P695 [37], which follow the procedures of ASCE 41-13 [9]. Lateral forces are applied to the structure and are gradually increased, and the roof displacement is recorded. The lateral forces are distributed as follows:

$$F_x \propto m_x \phi_{1,x}, \quad (22)$$

where F_x is the lateral force applied at level x , m_x is the seismic mass at level x and $\phi_{1,x}$ is the ordinate of the fundamental mode shape at level x . Figure 8 shows the pushover analysis curve of the exterior frame of the unretrofitted 8-story building.

From the pushover curve, the maximum base shear V_{max} that can be sustained by the frame is obtained and so is the ultimate displacement δ_u defined as the roof displacement when the base shear level degrades to 80% of V_{max} . These parameters are utilized to determine the overstrength factor Ω as well as the period-based ductility μ_T , which are obtained from the following equations:

$$\Omega = V_{max}/V, \quad (23)$$

$$\mu_T = \delta_u/\delta_y, \quad (24)$$

where V is the design base shear and δ_y is the roof displacement at yield.

The design base shear of the frame is calculated following ASCE 7-10 [64],

$$V = C_s W, \quad (25)$$

where C_s is the seismic response coefficient determined following ASCE 7-10 Section 12.8.1.1 and W is the effective seismic weight of the exterior frame. For $T = 1.21$ s,

$$C_s = \frac{S_{D1}}{T(R/I_e)}, \quad (26)$$

where the design spectral response acceleration parameter at a period of 1.0 sec is $S_{D1} = 0.45g$ for a site class D site in Beirut, the response modification factor, R , is taken as 3 as

the structure is considered to be an ordinary moment-resisting frame, and the importance factor, I_e , is 1 as per residential buildings [37, 66].

Table 10 lists the design and maximum base shears of the unretrofitted frame, its roof drift ratios at yield and ultimate, as well as the calculated values of the ductility μ_T and overstrength Ω factors.

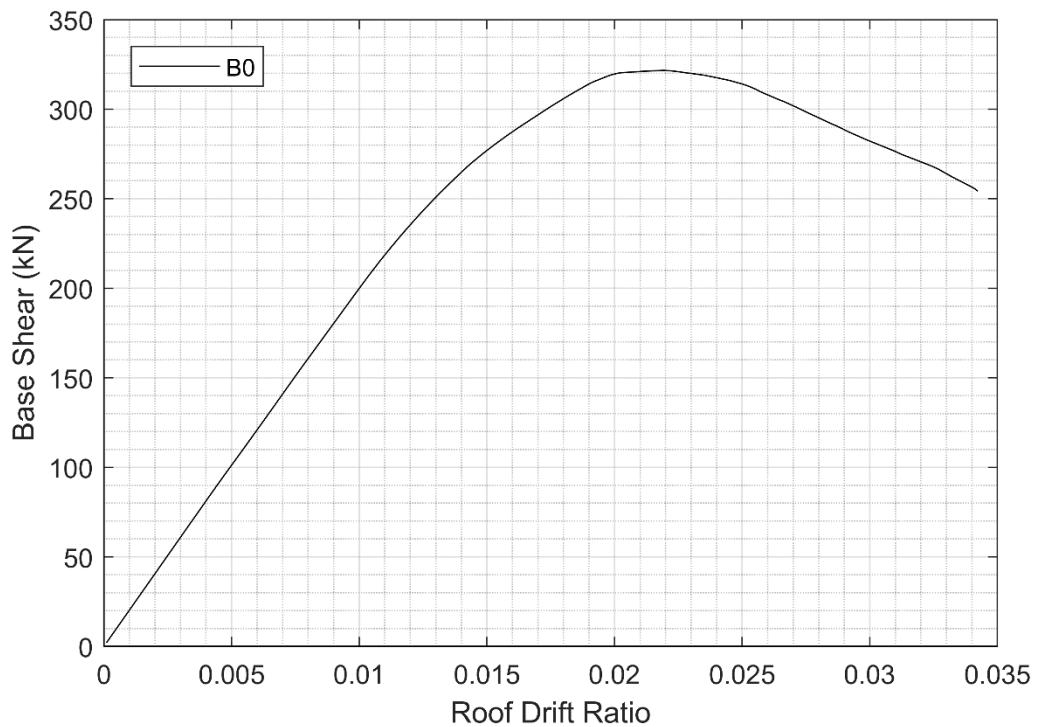


Figure 8: Pushover analysis curve of the unretrofitted building's exterior frame

Table 10: Pushover Results for the Unretrofitted structure

Building Model	V (KN)	V_{max} (KN)	Ω	δ_y/h_n	δ_u/h_n	μ_T
B0	990	322	0.32	0.013	0.034	2.62

It is immediately apparent that the pushover response of the building is alarming. The overstrength factor falls below one, meaning that this structure cannot resist the design

base shear required as per ASCE 7-10 specifications for Lebanon. This will affect the retrofiting methods chosen and will be discussed in the following chapter.

C. Incremental Dynamic Analysis

Incremental dynamic analysis (IDA) is performed in accordance with the procedure developed by Vamvatsikos and Cornell [8], whereby the structural model is subjected to several ground motions that are gradually scaled until a particular limit state is reached. This study focuses on the collapse limit state. For each ground motion and scale factor, several response quantities (e.g., inter-story drift ratios, inelastic deformations, etc.) defined as engineering demand parameters (EDP), can be calculated. The choice of EDP to calculate is based on the definition of collapse considered in the study. For every ground motion, one IDA curve, which is a plot of IM versus EDP, is obtained. Such analysis is denoted as multi-incremental dynamic analysis (MIDA) and results in as many different IDA curves as ground motions used.

The ground motions used in this study are the FEMA P695 set of 22 pairs of far-field ground motions. This set of recorded ground motions is robust and was defined to limit subjectivity in any non-linear dynamic analysis. It provides enough data to accurately determine and quantify record-to-record variability. The records are normalized to allow scaling, meaning that each ground motion is normalized by its peak ground velocity (PGV), a step that intends to remove additional variability between records due to inherent differences in event magnitude, distance to source, source type, and site conditions, without eliminating overall record-to-record variability [37]. They are then scaled following the procedure described in FEMA P695 appendix A.

Figure 9 shows the results of the MIDA of the external frame of the unretrofitted 8-story structure for the selected ground motions. The MIDA analysis was carried out in varying increments up until a maximum $Sa(T)$ of 0.9 g.

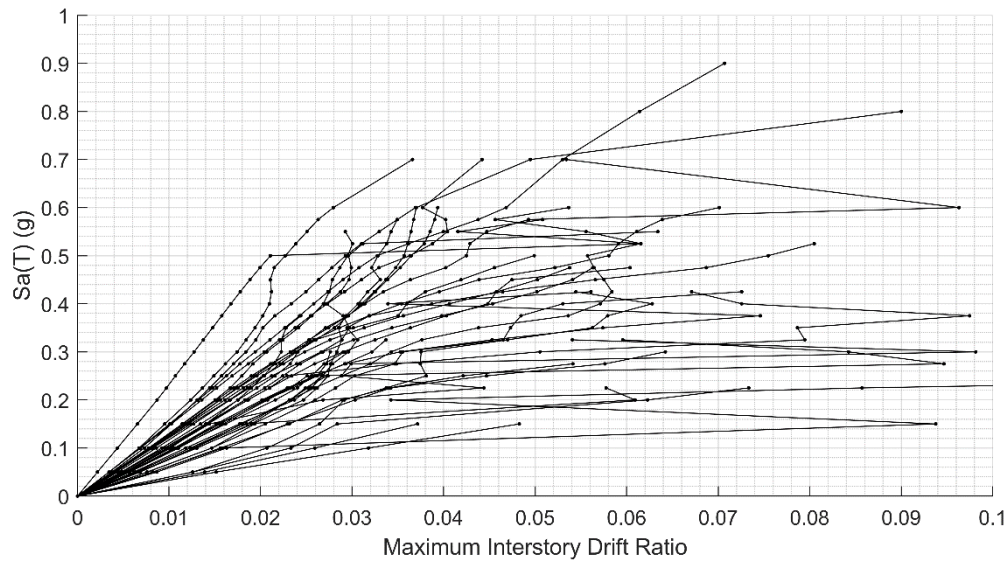


Figure 9 : MIDA results of the unretrofitted exterior frame

D. Definition of Global Collapse

In this study, a deterministic definition of collapse based on selected EDPs is adopted. Note that the focus is on the global collapse of structures, as opposed to the collapse of individual elements within the model. ASCE 41-13 [9] defines the EDP values for several damage limit states such as life safety and collapse prevention. This work, however, focuses on the total collapse of the structure and the overarching objective of this study is to implement retrofits that reduce the probability of collapse of the structure to less than 20% when subjected to an MCE ground motion.

Several modes of collapse are considered. The first is side-sway or lateral collapse, which is expected to be the dominant form of collapse in all retrofitted structures. Inter-story drift ratio (IDR) has been shown to be an efficient indicator of this form of collapse and has been extensively used as an EDP in the literature [6, 9, 37]. Therefore, IDR is also used as the EDP to identify side-sway collapse in this study. For non-ductile concrete frames, side-sway collapse is assumed to occur at an IDR of 5% [67]. For ductile or retrofitted frames, failure is defined by dynamic instability, which is when the slope of the IDA curve drops below 20% [68], or if the recorded IDR reaches 10% before dynamic instability occurs. The side-sway collapse of non-ductile frames can also be identified by dynamic instability should the slope of the IDA curve drop below 20% before IDR reaches a value of 5%. Figure 10 showcases these collapse criteria.

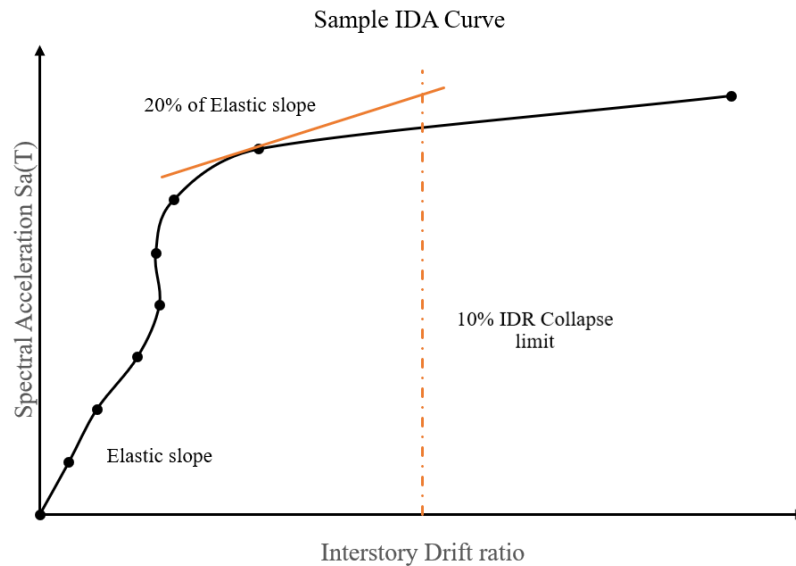


Figure 10: Illustration of Side-sway collapse criteria

Other forms of collapse are possible in non-ductile RC frames [69] and are considered in this study only for the unretrofitted frame because it has seismic deficiencies,

including columns possessing $V_p/V_n > 0.7$. One of the collapse modes considered for the unretrofitted building is gravity collapse. The EDP used to indicate this failure is the horizontal displacement of the columns. Following Baradaran Shoraka et al. [69], gravity collapse is defined as the point where the axial capacity of the columns at any floor is reduced below the gravity load demand at that floor. The axial capacity of columns is obtained from Eq. (12).

The other collapse mode considered for the unretrofitted building is shear collapse, which is defined following Sattar and Liel [47] as the point where the shear strength of the columns at any floor, calculated from equation (11), reduces to 40% of the initial floor capacity, determined by summing the V_n values of all the columns in the floor according to equation (4). The 40% value is chosen based on the recommendation of Sattar and Liel [47]. This value is arbitrary, and research has shown that the collapse results do not vary significantly based on this value.

E. Fragility Analysis

One of the main objectives of this study is to produce sets of collapse fragility curves for both the unretrofitted and retrofitted structures. Collapse fragility curves are fitted lognormal cumulative distributions that relate the probability of collapse to a specific ground motion intensity level, the 5% damped first mode spectral acceleration $S_a(T; \zeta = 5\%)$ in this case [5]. A lognormal fragility curve is fully defined by two parameters: the median collapse intensity \hat{S}_{CT} , which is defined as the intensity at which there is a 50%

probability of collapse; and the logarithmic standard deviation of the collapse intensity β , which is also known as the dispersion and accounts for the uncertainty in collapse. Four sources of uncertainty are considered in this work following the recommendation of FEMA P695 and other established literature [5, 37]. These sources are as follows:

- Record to Record Uncertainty β_{RTR} , which is obtained directly from fitting the lognormal function to the collapse data. This is the variability caused by the variations among the selected ground motions due to factors such as frequency content, ground motion duration, and pulses.
- Design Requirements Uncertainty β_{DR} : related to the quality and standards of the design requirements used during the design stage and to the extent to which these requirements prepare the structural system for seismic forces and failure modes.
- Test Data Uncertainty β_{TD} : Uncertainty related to the quality of the test data which is used to define the modelling parameters of the system.
- Modelling Uncertainty β_{UDL} : Uncertainty based on the quality of the index archetype model used. Factors include how well it represents the full spectrum of structural response as well as the model's ability to capture all modes of failure.

With the exception of the record-to-record uncertainty, uncertainty values will be adopted based on the FEMA P-695 evaluation rubric. The design requirements are rated as Fair (C) and β_{DR} is set equal to 0.35 for the unretrofitted structure. This is due to using gravity-based design in a seismic region, which could lead to brittle failure. β_{DR} is set equal to 0.2 for the retrofitted structures due to using more stringent design requirements which implement more safeguards against collapse.

Test Data Uncertainty β_{TD} is assigned a value of 0.2 as the data is rated as Good (B) for both the unretrofitted and retrofitted structures. The primary database being used for member behavior is the PEER structural performance database [70], which consists of 255 samples that were tested to failure in both flexure and shear flexure modes. Test data quality is rated as B in spite of the large range of parameters varied in the database because many of the samples did not undergo significant strength deformation before failure. Additionally, the effect of slabs was not accounted for in the tests conducted and only column members were tested.

Finally, the modelling uncertainties are based on the ability of the model to robustly and accurately capture all forms of collapse. For the unretrofitted structure, the model is rated as Fair (C) with a β_{UDL} of 0.35. This is due to the ongoing progress on the shear an axial model used within the model. Additionally, the shear model used can only capture shear failure if it occurs after flexural yielding. For the retrofitted structures, although the retrofitting procedures implemented eliminate the possibility of shear failure and thus require the model to only account for the flexural response, the modeling uncertainty is not decreased because a high level of uncertainty is associated with the joint model, later developed in Chapter 0 using a small sample of experimental tests. Table 11 summarizes the uncertainty values adopted for the retrofitted and unretrofitted structures in this study.

Table 11: Selected uncertainty parameters

Uncertainty Source	Unretrofitted Structure	Retrofitted Structures
Design Requirements β_{DR}	0.35	0.2
Test Data β_{TD}	0.2	0.2
Modeling β_{UDL}	0.35	0.35

The total uncertainty β_{TOT} is calculated using the following equation:

$$\beta_{TOT} = \sqrt{\beta_{RTR}^2 + \beta_{DR}^2 + \beta_{TD}^2 + \beta_{MDL}^2}. \quad (27)$$

In this study, fragility functions are fitted using the maximum likelihood method [71]. This fitting method relies on determining the parameters that are most likely to result in the observed data. The fragility curve parameters β_{RTR} and \hat{S}_{CT} are obtained by maximizing the following log likelihood function:

$$\{\hat{\mu}, \hat{\beta}\} = \max \sum_{i=1}^m \left\{ \ln \binom{n_i}{z_i} + z_i \ln \phi \left(\frac{\ln x_i - \mu}{\beta} \right) + (n_i - z_i) \ln \left(1 - \phi \left(\frac{\ln x_i - \mu}{\beta} \right) \right) \right\}, \quad (28)$$

where $\hat{\beta}$ is equal to β_{RTR} and is the standard deviation of the natural logarithm, $\hat{\mu}$ is the mean of the natural logarithm, m is the total number of $S_a(T_1)$ intensity levels considered, $S_a(T_1) = x_i$ is the i th intensity level, $i = 1 \dots m$, $\phi(\cdot)$ is the normal cumulative distribution function, n_i is the number of ground motions used at the i th intensity level, and z_i is the number of ground motions that cause collapse at the i th intensity level. \hat{S}_{CT} is equal to the exponential of $\hat{\mu}$.

Table 12 shows the values of the fragility curve parameters \hat{S}_{CT} and β_{RTR} fitted to the collapse data of the unretrofitted frame, and the resulting total uncertainty β_{TOT} . Figure 11 shows the corresponding fragility curves, when only record-to-record uncertainty is accounted for, as well as when the total uncertainty is accounted for. Figure 11 also shows that the probability of collapse at $S_{MT} = 0.559g$ is equal to 0.87 (87%) when only record-to-record uncertainty is accounted for, and is reduced to 0.731 (73.1%) when the total uncertainty is accounted for. These values are high, especially when compared to the

FEMA P-695 requirements that the collapse probability at the S_{MT} should not exceed 20% for any single configuration within the archetype [37]. The current collapse probability is about four times higher than the FEMA recommendation. This serves as the basis upon which the retrofitting of the NDRC structure will be undertaken.

Allabban [18] found that the collapse of the unretrofitted building occurs due to shear failure in the columns at the top floors for all the scaled ground motions causing collapse. This is a consequence of the frame being designed for gravity loading only. In addition, the results indicate that damage is concentrated in the beam-column joints, which fail prior to the beams and columns [18].

Table 12: Fragility parameters of the as built structure

Building Model	\hat{S}_{CT} (g)	β_{RTR}	β_{TOT}
B0	0.378	0.341	0.633

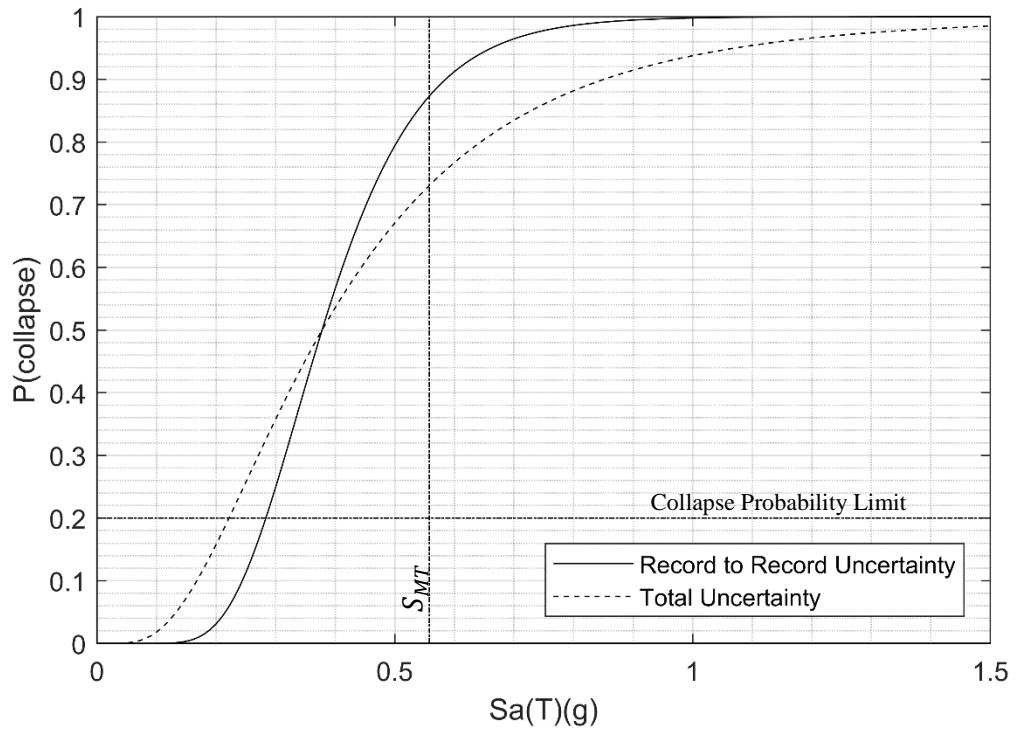


Figure 11: Fragility curves of the exterior frame of the unretrofitted structure with record-to-record variability and total uncertainty

CHAPTER V

DESCRIPTION AND DESIGN OF THE RETROFITTED BUILDINGS

A. Objectives and Constraints of Retrofitting

One of the most alarming results from the pushover analysis of the NDRC structures assessed in Allabban [18] is that the overstrength factor Ω is actually below 1; it is equal to 0.33 for the 8-story building, which is retrofitted in this study. As a result, one of the objectives of retrofitting is to increase both the strength of the structure and its deformation or ductility capacity. Therefore, retrofits that only increase the ductility capacity of the structure are not considered in this study.

As mentioned in Chapter 0, the MIDA analysis of the unretrofitted structures showed that the joints are the first components to fail. Therefore, the structural joints are a major target for retrofitting. This is expected because, as discussed earlier, the joints have seismically deficient detailing and reinforcement. Seismic joint retrofitting is not commonly done in practice due to its practical difficulties [21]. However, for the building considered in this study, reinforcing the structural joints is necessary to attain the required seismic performance.

Moreover, note that at the exterior joints of floors 5 to 8, the ratio of the beam to column moments at yielding ($\sum M_{y,columns}/\sum M_{y,beams}$) is much lower than that of floors 1 to 4. Moreover, this ratio is less than 1.2 at the exterior joints of floor 8, thus violating the “strong column, weak beam” design requirement in ACI318, which states that

$\sum M_{y,columns}/\sum M_{y,beams}$ should be no less than 1.2 [39]. These characteristics are consistent with the observations from the damage propagation analysis performed on the unretrofitted structure and detailed in Allabban [18], whereby the exterior columns of the higher floors are the first to fail due to their lower $\sum M_{y,columns}/\sum M_{y,beams}$ ratios. Therefore, another requirement for the retrofitting process is to ensure that $\sum M_{y,columns}/\sum M_{y,beams} > 1.2$ at all joints. This requirement is particularly important for the retrofitted design in which the beams are strengthened as that could reduce the $\sum M_{y,columns}/\sum M_{y,beams}$ ratio.

Finally, the practicality of implementing the retrofits is considered as well. Some retrofitting measures are not considered in this study because they are expensive or difficult to apply in practice. The retrofitting techniques selected can be easily applied to a wide range of existing NDRC structures in Beirut. The addition of lateral force resisting systems, such as shear walls or steel braces, is not considered in this study. Seismic isolation and energy dissipation methods are also beyond the scope of this study; they are commonly employed in retrofitting high importance structures such as bridges and historical buildings and would be impractical and difficult to implement at a large scale to common residential structures [22, 26, 28].

B. Selected Retrofitting Methods

1. Concrete Jacketing

The first method chosen is member enlargement by concrete jacketing. This method is chosen due to its ability to increase the structural capacity of the retrofitted

structure. It has been used previously and extensively in seismic retrofitting [4, 21, 72] due to its relative ease of implementation and low cost.

a) Columns

Columns are prime candidates for concrete jacketing because column jacketing can remedy a variety structural deficiencies. Jacketing increases both the moment carrying capacity and shear strength of columns, and the addition of longitudinal and transverse reinforcement within the jacket allows detailing of the columns for ductile response up to seismic standards [72]. Additionally, column jacketing increases the $\sum M_{y,columns}/\sum M_{y,beams}$ ratio thus promoting the more ductile beam collapse mechanism.

b) Beams

In this study, beams are not strengthened by concrete jacketing because they generally seem to not contribute to the collapse of the structure [18]. Therefore, jacketing of the beams is not expected to yield a significant improvement in collapse performance, contrary to jacketing of the columns. On the contrary, Barandaran Shoraka [69] investigated weakening the beams in an NDRC frame in order to increase the $\sum M_{y,columns}/\sum M_{y,beams}$ ratio, which yielded a slight increase in collapse performance. Additionally, the concealed nature of the beams in the archetype configuration [13] places a large architectural and practical restriction on beam jacketing.

c) Joints

To remedy the lack of transverse reinforcement and the poor seismic performance of the joints in the unretrofitted structure, the concrete jackets and transverse reinforcement added to the columns are extended through the slab and onto the next floor of the structure.

This procedure increases the joint area and provides the joint with increased shear strength, stiffness and ductility [32] due to the presence of additional concrete and reinforcement.

2. *Fiber-Reinforced Polymer (FRP) Strengthening*

The use of FRPs to strengthen existing structures is widespread. However, Liel and Deierlein [21] found that the transverse FRP wrapping of columns, the most commonly used FRP strengthening method, provided negligible benefit to the seismic collapse performance of a NDRC frame. That is because transverse wrapping increases ductility but has a smaller effect on moment capacity, and as mentioned earlier in this chapter, increasing the column moment capacity is one of the main retrofit objectives. To increase the moment capacity of columns using FRP, longitudinal FRP reinforcement should be utilized and combined with FRP anchor rods. This requires drilling into the beam-column joint area for embedment, which is difficult and rarely done in practice.

Several examples exist in the literature of FRP strengthening being performed on joints [22, 23, 33, 73]. However, FRP joint strengthening is not considered in this study because most experimental studies were carried out on specimens comprising of exposed joints with no slab interference or on joints with beams and columns having similar thicknesses. In the building being retrofitted in this study, the beams are shallow, wide, and concealed within the slab, making FRP joint strengthening difficult to implement correctly.

As mentioned previously, the strength of a joint is limited by the moment capacity of the adjoining beams, the moment capacity of the adjoining columns, and the shear strength of the joint itself; see Equations (13)-(15). Therefore, if joint strength is limited by the moment strength of the adjoining beams, which becomes more likely when the columns

and joints are concrete jacketed, joint strength can be increased by strengthening the beams. While concrete jacketing of the beams is not practical for the studied building, the addition of longitudinal FRP strips along the bottom and top lengths of the beam can be implemented more easily. This is done according to the recommendations of ACI 440 [74]. Note that adding FRP strips to beams increases their moment capacity, and does not affect their ductility [74]. Also note that the addition of FRP strips to beams is only implemented in combination with concrete jacketing of the columns and joints, such that acceptable $\sum M_{y,columns}/\sum M_{y,beams}$ ratios are maintained at the joints.

C. Design of the Retrofitted Structures

Three retrofitted versions of the 8-story NDRC frame building are considered in this study. Retrofitted building 1 (RB1) utilizes the minimum applicable concrete column jacket, namely a thickness of 10 cm. Retrofitted building 2 (RB2) uses concrete column jackets designed and detailed to satisfy the shear and moment seismic demand requirements for columns. Retrofitted building 3 (RB3) is identical to RB2, but sheets of CFRP are added to the beams to increase their moment strength.

In the next sections, the designs of the retrofitted buildings are presented in more detail. Both the exterior and interior frames are retrofitted because retrofitting only the exterior frame, which carries more lateral loads, is not expected to improve the overall performance of the building. In fact, the interior frame has a limited ductility capacity and, if not retrofitted, would not be able to sustain the deformations of the ductile retrofitted exterior frame. However, since the modeling and analysis in this study are limited to the

exterior frame, the presentation of the retrofitted designs in the next sections is limited to the exterior frame.

1. Retrofitted Building 1 (RB1)

For RB1, all the columns are concrete jacketed using the minimum jacket thickness, namely 10 cm of concrete combined with the minimum allowable steel ratio in columns of 1%, per ACI-318 [39].

Table 13 provides for the exterior frame of RB1 the dimensions, expected gravity load demands, and the longitudinal and transverse reinforcement of the jacketed columns. The compressive strength of the concrete used for the jackets is $f'_c = 33$ MPa. The steel used for the longitudinal and transverse reinforcement has a nominal yield strength $f_y = 420$ MPa .

Note that the longitudinal reinforcement of the original column is considered effective in contributing to the strength of the jacketed column, but not the transverse reinforcement [72]. Also note that the column jackets of all the retrofitted buildings are extended through the slab, resulting in enlarged and strengthened joints. Finally, the lap splices in the jackets of all the retrofitted buildings are moved away from potential plastic hinge regions and placed near the midspan of columns.

Table 13: Design details of columns of RB1

Exterior Columns of Exterior Frame								
Floor	Depth (mm)	Width (mm)	P (kN)	Main Reinf.	Jacket Reinf.	ρ (%)	Shear Reinf. (mm)	ρ_{sh} (%)
1	400	1000	672	8T20	14T16	1.4	2T12@100	0.25
2	400	1000	587	8T20	14T16	1.4	2T12@100	0.25
3	400	1000	501	8T20	14T16	1.4	2T12@100	0.25
4	400	1000	415	8T20	14T16	1.4	2T12@100	0.25
5	400	900	330	8T16	12T16	1.3	2T12@100	0.28
6	400	900	247	8T16	12T16	1.3	2T12@100	0.28
7	400	900	165	8T16	12T16	1.3	2T12@100	0.28
8	400	900	82	8T16	12T16	1.3	2T12@100	0.28
Interior Columns of Exterior Frame								
Floor	Depth (mm)	Width (mm)	P (kN)	Main Reinf.	Jacket Reinf.	ρ (%)	Shear Reinf. (mm)	ρ_{sh} (%)
1	1000	400	1152	8T22	14T16	1.4	2T12@100	0.23
2	1000	400	1007	8T22	14T16	1.4	2T12@100	0.23
3	1000	400	861	8T20	14T16	1.2	2T12@100	0.23
4	1000	400	715	8T20	12T16	1.2	2T12@100	0.23
5	800	400	570	8T16	12T16	1.1	2T12@100	0.25
6	800	400	427	8T16	12T16	1.1	2T12@100	0.25
7	800	400	284	8T16	12T16	1.1	2T12@100	0.25
8	800	400	142	8T16	12T16	1.1	2T12@100	0.25

2. *Retrofitted Building 2 (RB2)*

For the second retrofitted building considered, RB2, the column jackets are designed to meet the shear and moment demands calculated using the equivalent lateral force procedure (ELFP) of ASCE 41-13 [9], which is similar to that of ASCE 7-10 [58] and was outlined in Chapter 00. Note that the beams of RB2 are not retrofitted although their moment capacity is lower than the moments obtained from the ELFP. The design and detailing of the column sections is performed to satisfy the requirements of ACI318-14 [39]

for the columns and joints of intermediate moment frames. According to Bousias et al. [72], the concrete jacketed members can be regarded as monolithic reinforced concrete members with the dimensions of the jacketed columns and the longitudinal reinforcement of both the concrete jacket and the original member. For this assumption to stand, the jacket reinforcement must be extended past the member end section in order to allow for proper development. As for the transverse reinforcement of the original member, it is ignored in the calculations. Note that, since the original columns have a concrete strength $f'_c = 17.6$ MPa while the concrete used for the jackets has $f'_c = 33$ MPa, an effective concrete compressive strength is used to calculate the strength of the jacketed columns and joints [32]:

$$A_j \sqrt{f'_{c,j}} = A_1 \sqrt{f'_{c,1}} + A_2 \sqrt{f'_{c,2}}, \quad (29)$$

where A_j is the joint area, $f'_{c,j}$ is the effective concrete strength for the jacketed member, A_1 and A_2 are the cross sectional areas of the original member and the jacket respectively and $f'_{c,1}$ and $f'_{c,2}$ are the concrete strengths of the original member and the jacket respectively. The required jacket dimensions and the amounts of longitudinal and transverse reinforcement are calculated accordingly.

Note that, similar to the unretrofitted building, the design base shear for the retrofitted buildings is also calculated per equations (25) and (26). The fundamental period T of the retrofitted buildings, which is calculated from equation (21), remains unchanged at $T = 1.21$ s. However, the response modification factor R is modified from 3 to 5 to reflect the improvements made in the retrofitted structures, which can be considered as

intermediate moment frames in the longitudinal direction. The values of T , R and the seismic weight W of the retrofitted structures is provided in Table 14, along with the resulting design base shear V . The design base shear of the retrofitted structures is lower than that of B0 despite their higher seismic weight. This is a result of the increase of the response modification factor. The corresponding values for the unretrofitted building (B0) are also listed in Table 14 for completeness.

The description of the designed jacketed columns of the exterior frame of RB2 is provided in Table 15, namely the dimensions, expected gravity load demands, and the longitudinal and transverse reinforcement of the jacketed columns.

Table 14 Seismic Weight and Design Base Shear of the exterior frame of the studied buildings

Building	Fundamental Period T (s)	Response Modification Factor R	Seismic Weight W (KN)	Design Base Shear V (KN)
B0	1.21	3	7975	990
RB1	1.21	5	8959	667
RB2	1.21	5	9012	671
RB3	1.21	5	9012	671

Table 15: Design Details of columns of RB2 and RB3

Floor	Exterior Columns of Exterior Frame							
	Depth (mm)	Width (mm)	P (kN)	Main Reinf.	Jacket Reinf.	ρ (%)	Shear Reinf. (mm)	ρ_{sh} (%)
1	400	900	672	8T20	14T16	1.3	2T12@100	0.25
2	400	900	587	8T20	14T16	1.3	2T12@100	0.25
3	400	900	501	8T20	14T16	1.3	2T12@100	0.25
4	400	900	415	8T20	14T16	1.3	2T12@100	0.25
5	400	800	330	8T16	12T16	1.1	2T12@100	0.28

6	400	800	247	8T16	12T16	1.1	2T12@100	0.28
7	400	800	165	8T16	12T16	1.1	2T12@100	0.28
8	400	800	82	8T16	12T16	1.1	2T12@100	0.28
Interior Columns of Exterior Frame								
Floor	Depth (mm)	Width (mm)	P (kN)	Main Reinf.	Jacket Reinf.	ρ (%)	Shear Reinf. (mm)	ρ_{sh} (%)
1	1100	500	1176	8T22	28T22	2.5	4T12@100	0.40
2	1100	500	1019	8T22	26T14	1.9	4T12@100	0.40
3	1000	400	861	8T20	20T14	1.7	2T12@100	0.23
4	1000	400	715	8T20	20T14	1.7	2T12@100	0.23
5	900	400	570	8T16	12T16	1.1	2T12@100	0.25
6	900	400	427	8T16	12T16	1.1	2T12@100	0.25
7	900	400	284	8T16	12T16	1.1	2T12@100	0.25
8	900	400	142	8T16	12T16	1.1	2T12@100	0.25

3. *Retrofitted Building 3 (RB3)*

Beams are not commonly the target of seismic strengthening, particularly flexural strengthening. However, in the case of RB1 and RB2, the strength of all joints is limited by the moment capacity of the adjoining beams. As a result, increasing the beam moment capacity leads to a larger joint moment capacity. Therefore, for RB3, longitudinal CFRP reinforcement is added to the top and bottom faces of the beams of RB2 to increase their moment strength and thus increase the joint capacity. The CFRP sheets are designed using ACI-440 [74] to meet the moment demands in the beams obtained from the ELFP per ASCE 41-13 [9]. However, an upper bound is imposed on beam strengthening in RB3 to maintain satisfactory $\sum M_{y,columns}/\sum M_{y,beams}$ ratios. Transverse CFRP wraps are also included to ensure that the longitudinal CFRP strips do not debond under seismic loading.

The design equations used to determine the size and amounts of longitudinal and transverse CFRP layers are presented in the next paragraphs. Table 16 lists the properties of the CFRP material used.

Table 16: CFRP Material properties

Property	SI units
t_f (layer thickness)	0.2 mm
E_f (Elastic modulus)	230000 MPa
ϵ_{fu} (Rupture Strain)	0.015

Flexural design is performed to design the longitudinal CFRP reinforcement such that the moment capacity M_n of a CFRP strengthened beam section satisfies $\phi M_n \geq M_u$, where ϕ is the strength reduction factor according to ACI318, M_u is the moment demand and M_n is calculated as

$$M_n = (A_s f_y - A'_s f'_s) \left(d - \frac{a}{2} \right) + \psi E_f A_f \epsilon_f \left(h - \frac{a}{2} \right) + A'_s f'_s (d - d'), \quad (30)$$

where A_s and A'_s are the areas of tension and compression steel respectively, f_y and f'_s are the stresses acting on the tension and compression steel respectively, d is the section effective depth, a is the depth of the compression block according to ACI 318, ψ is a strength reduction factor based on a reliability analysis detailed in ACI 440 [74] and is taken as 0.85, E_f is the elastic modulus of the CFRP material, A_f is the CFRP area utilized, ϵ_f is the strain at failure of the section, h is the section height and d' is the effective depth of the compression reinforcement. ϵ_f is calculated based on the failure mode of the section

and can either be due to concrete crushing or FRP debonding. The strain at debonding ϵ_{fd} is calculated as follows:

$$\epsilon_{fd} = 0.41 \times \sqrt{\frac{f'_c}{t_f \times n_f \times E_f}} < 0.9 \epsilon_{fu}, \quad (31)$$

where t_f is the thickness of a single CFRP layer, n_f is the number of longitudinal layers applied and E_f is elastic modulus of the CFRP material. Should concrete crushing occur before debonding, ϵ_f is calculated as follows:

$$\epsilon_f = \epsilon_{cu} \left(\frac{h - c}{c} \right), \quad (32)$$

where ϵ_{cu} is the crushing strain of concrete taken as 0.003, h is the section height and c is the depth of the neutral axis obtained from cracked equivalent section analysis.

In order to ensure the proper moment transfer from the CFRP strengthened beams into the joint area, the CFRP strips are made continuous over the length of beam, as illustrated in Figure 12 for the exterior frame. As can also be observed in Figure 12, the relative orientation of the beams and columns of the interior frame does not allow placement of continuous CFRP strips on the top and bottom faces of the beams of the interior frame. Therefore only the beams of the exterior frame are strengthened using CFRP.

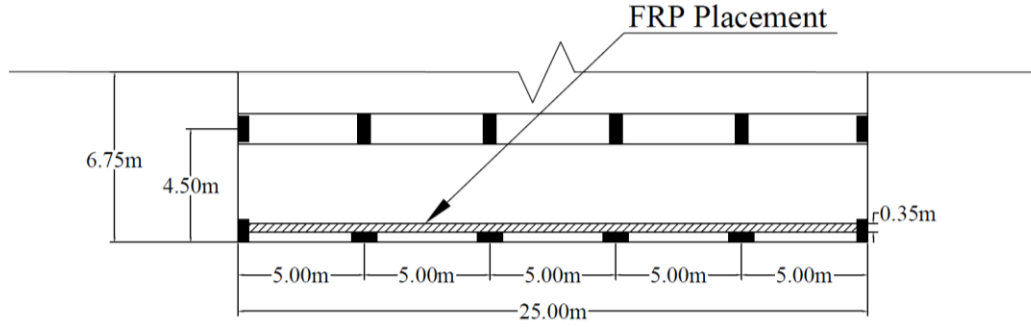


Figure 12: Plan view showcasing FRP Continuity

As for the transverse CFRP wraps, they are not designed to provide shear strength but only to ensure that the longitudinal CFRP strips do not debond under seismic loading. Following ACI 440 [74], spaced transverse strips are included over a minimum length l_o from the face of each joint, where l_o is calculated as follows:

$$l_o = g + 0.044f_y d_{bl} + \sqrt{\frac{n_f E_f t_f}{\sqrt{f'_c}}}, \quad (33)$$

where g is the distance from the columns face to the first strip, and f_y and d_{bl} are the yield strength and diameter of the steel reinforcing bars respectively. The total area A_{Anchor} of these transverse strips is determined by the following equation:

$$A_{Anchor} = \frac{A_f f_{fe}}{(E_f K_v \epsilon_{fu})_{anchor}}, \quad (34)$$

where A_f and f_{fe} are the area and stresses at failure of the longitudinal CFRP strips and K_v is a modification factor calculated according to the ACI 440 report [74].

Table 17 to Table 19 describes the size and the number of longitudinal and transverse CFRP layers used to strengthen each beam. In order to facilitate the placement of

the transverse CFRP strips, the slab is sliced at the location of the hourdis blocks. This is shown in Figure 13.

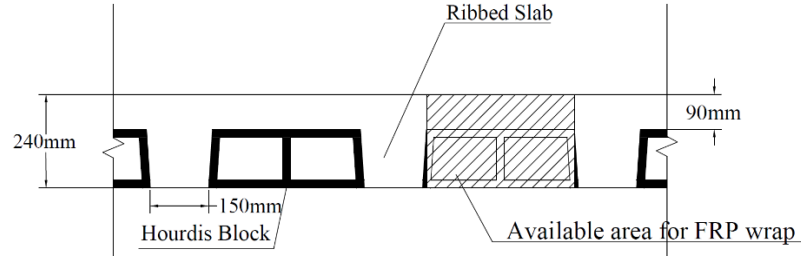


Figure 13: Cross section of the Ribbed slab

Table 17: Design details of CFRP added to the beams on floor 1 of exterior frame of RB3

Beam	$n_{f,bot}$	$A_{fLong,bot}$ (mm^2)	$n_{f,top}$	$A_{fLong,bot}$ (mm^2)	A_{anchor} (total) (mm^2)	n_{anchor}
1	2	100	2	100	420	2
2	2	100	1	50	420	2
3	2	100	1	50	420	2
4	2	100	1	50	420	2
5	2	100	2	100	420	2

Table 18: Design details of CFRP added to the beams on floor 2 of exterior frame of RB3

Beam	$n_{f,bot}$	$A_{fLong,bot}$ (mm^2)	$n_{f,top}$	$A_{fLong,bot}$ (mm^2)	A_{anchor} (total) (mm^2)	n_{anchor}
1	2	150	3	150	630	2
2	2	150	2	100	630	2
3	2	150	2	100	630	2
4	2	150	2	100	630	2
5	2	150	3	150	630	2

Table 19: Design details of CFRP added to the beams on floors 3-8 of exterior frame of RB3

Beam	$n_{f,bot}$	$A_{fLong,bot}$ (mm^2)	$n_{f,top}$	$A_{fLong,bot}$ (mm^2)	A_{anchor} (total) (mm^2)	n_{anchor}
1	3	210	3	210	875	3
2	3	210	3	210	875	3
3	3	210	3	210	875	3
4	3	210	3	210	875	3
5	3	210	3	210	875	3

CHAPTER VI

ANALYTICAL MODELING OF THE RETROFITTED BUILDINGS

As mentioned in Chapter V, both the exterior and interior frames of RB1, RB2 and RB3 are retrofitted, and both contribute to resisting the seismic loads. The use of a perimeter framing system where only the exterior frame is jacketed to resist lateral loads is non-beneficial due to the ductility limitation of the unretrofitted frame members. However, and as was done for the unretrofitted building B0, only the exterior frame of RB1, RB2 and RB3 is modeled in this study, also using the lumped plasticity approach. The seismic masses are distributed between the external and internal frames in proportion to the initial stiffnesses of the two frames. Figure 14 shows the analytical model used for the retrofitted buildings, the details of which are presented next.

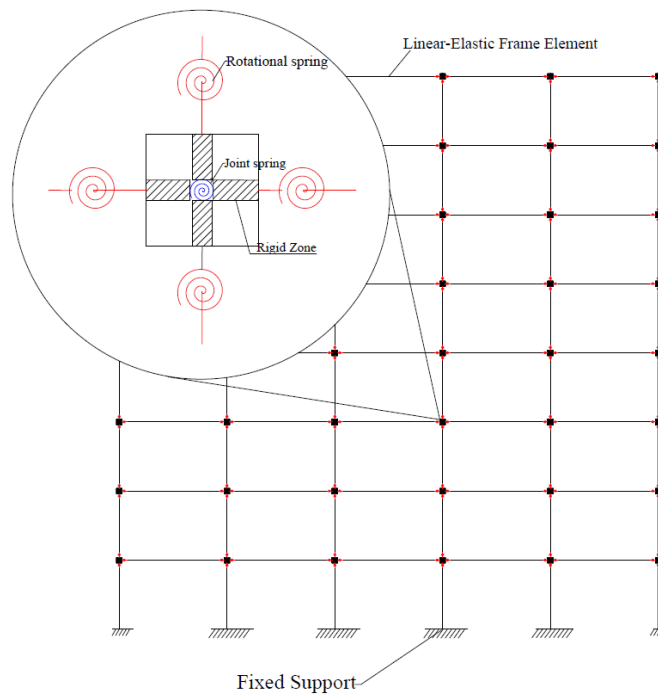


Figure 14: Analytical model of retrofitted buildings

A. Beam and Column Modeling

As was done for the unretrofitted building, the beams and columns of the retrofitted structures are modelled using linear-elastic elements with rotational springs at both ends. The springs are defined using the model described in Ibarra et al.[48], which was already presented in Chapter 0, in Equations (5) to (10). The spring model parameters are recalculated to reflect the changes in the moment-rotation relations due to concrete jacketing of columns and CFRP strengthening of beams. For the three retrofitted buildings, the equation developed by Panagiotakos and Fardis [45] and that is used to calculate the yield moment for elements of the unretrofitted building is also used for the jacketed columns. This is possible due to treating the concrete jacketed column members as monolithic RC members, following the work of Bousias et al. [72]. Since the original

columns have a concrete strength $f'_c = 17.6$ MPa while the concrete used for the jackets has $f'_c = 33$ MPa, the effective concrete compressive strength obtained from Equation (29) is used to calculate the model parameters of the jacketed columns [32].

Table 20 shows the spring properties of the columns of RB1, while Table 21 shows the spring properties of the columns of RB2 and RB3, which are identical. Note that shear and axial springs are not included in the models of the retrofitted buildings because all the jacketed columns have a V_p/V_n ratio less than 0.7, as can be observed in Table 20 and Table 21.

Table 20: Spring properties of columns of RB1

Exterior Columns of Exterior Frame								
Floor	$P/A_g f'_c$	M_y (KN.m)	V_p/V_n	EI_{stf}/EI_g	M_c/M_y	$\theta_{cap,pl}$	θ_{pc}	λ
1	0.071	411	0.425	0.40	1.13	0.047	0.076	89
2	0.062	398	0.416	0.37	1.13	0.051	0.079	91
3	0.053	386	0.407	0.35	1.13	0.051	0.082	92
4	0.044	373	0.398	0.35	1.13	0.052	0.085	93
5	0.040	305	0.339	0.35	1.13	0.056	0.096	94
6	0.030	293	0.330	0.35	1.13	0.057	0.100	95
7	0.020	281	0.320	0.35	1.13	0.058	0.100	97
8	0.010	268	0.309	0.35	1.13	0.059	0.100	98
Interior Columns of Exterior Frame								
Floor	$P/A_g f'_c$	M_y (KN.m)	V_p/V_n	EI_{stf}/EI_g	M_c/M_y	$\theta_{cap,pl}$	θ_{pc}	λ
1	0.110	1422	0.508	0.35	1.13	0.044	0.059	126
2	0.096	1370	0.496	0.35	1.13	0.045	0.062	129
3	0.082	1227	0.451	0.35	1.13	0.047	0.066	132
4	0.068	1174	0.438	0.35	1.13	0.048	0.070	134
5	0.062	852	0.372	0.35	1.13	0.051	0.079	132
6	0.046	805	0.358	0.35	1.13	0.052	0.084	135
7	0.031	756	0.343	0.35	1.13	0.054	0.089	138
8	0.015	707	0.327	0.35	1.13	0.055	0.095	141

Table 21 : Spring properties of columns of RB2 and RB3

Exterior Columns of Exterior Frame								
Floor	$P/A_g f'_c$	M_y (KN.m)	V_p/V_n	$E I_{stf} / E I_g$	M_c/M_y	$\theta_{cap,pl}$	θ_{pc}	λ
1	0.071	411	0.425	0.40	1.13	0.047	0.076	89
2	0.062	398	0.416	0.37	1.13	0.048	0.079	91
3	0.053	386	0.407	0.35	1.13	0.049	0.082	92
4	0.044	373	0.398	0.35	1.13	0.050	0.085	93
5	0.040	305	0.339	0.35	1.13	0.053	0.096	94
6	0.030	293	0.330	0.35	1.13	0.054	0.100	95
7	0.020	281	0.320	0.35	1.13	0.055	0.100	97
8	0.010	268	0.309	0.35	1.13	0.056	0.100	98
Interior Columns of Exterior Frame								
Floor	$P/A_g f'_c$	M_y (KN.m)	V_p/V_n	$E I_{stf} / E I_g$	M_c/M_y	$\theta_{cap,pl}$	θ_{pc}	λ
1	0.076	3175	0.596	0.35	1.13	0.059	0.100	136
2	0.066	2500	0.474	0.35	1.13	0.060	0.100	138
3	0.082	1563	0.573	0.35	1.13	0.044	0.066	132
4	0.068	1507	0.562	0.35	1.13	0.045	0.070	134
5	0.062	852	0.372	0.35	1.13	0.048	0.079	132
6	0.046	805	0.358	0.35	1.13	0.050	0.084	135
7	0.031	756	0.343	0.35	1.13	0.051	0.089	138
8	0.015	707	0.327	0.35	1.13	0.053	0.095	141

As for the beams of the retrofitted buildings, the spring model parameters of RB1 and RB2 are identical to those of the unretrofitted building B0 because their beams are identical. These model parameters were already presented in Table 8 but are repeated in Table 22 for completeness. The parameters of the beams of RB3 are different due to the addition of CFRP longitudinal reinforcement. The model parameters for floor 1, floor 2 and floors 3 to 8 are presented in Table 23, Table 24 and Table 25, respectively. Note that the effect of longitudinal CFRP strips on the rotation capacity of the beams is negligible and is

ignored [74]. Also, the effect of the transverse CFRP wraps is not included as they are provided only to ensure that the longitudinal CFRP strips do not debond under seismic loading. Only the yield moment M_y is assumed to be affected and is calculated from cracked section analysis of the retrofitted beam section. The other spring model parameters are left unchanged.

Table 22 Spring properties of beams of B0, RB1 and RB2 for all floors

Rotational Spring at the Left Side								
Beam Span	M_{y+} (KN.m)	M_{y-} (KN.m)	EI_{stf}/EI_g	M_c/M_y	$\theta_{cap,pl+}$	$\theta_{cap,pl-}$	θ_{pc}	λ
1	67	67	0.35	1.13	0.035	0.035	0.037	19
2	67	103	0.35	1.13	0.039	0.032	0.037	19
3	67	86	0.35	1.13	0.037	0.033	0.037	19
4	67	86	0.35	1.13	0.037	0.033	0.037	19
5	67	103	0.35	1.13	0.039	0.032	0.037	19
Rotational Spring at the Right Side								
Beam Span	M_{y+} (KN.m)	M_{y-} (KN.m)	EI_{stf}/EI_g	M_c/M_y	$\theta_{cap,pl+}$	$\theta_{cap,pl-}$	θ_{pc}	λ
1	103	67	0.35	1.13	0.032	0.039	0.037	19
2	86	67	0.35	1.13	0.033	0.037	0.037	19
3	86	67	0.35	1.13	0.033	0.037	0.037	19
4	103	67	0.35	1.13	0.032	0.039	0.037	19
5	67	67	0.35	1.13	0.035	0.035	0.037	19

Table 23: Spring properties of beams of floor 1 of RB3

Rotational Spring at the Left Side								
Beam Span	M_{y+} (KN.m)	M_{y-} (KN.m)	EI_{stf}/EI_g	M_c/M_y	$\theta_{cap,pl+}$	$\theta_{cap,pl-}$	θ_{pc}	λ
1	82	82	0.35	1.13	0.035	0.035	0.037	19
2	82.	110	0.35	1.13	0.039	0.032	0.037	19
3	82	94	0.35	1.13	0.037	0.033	0.037	19
4	82	94	0.35	1.13	0.037	0.033	0.037	19

5	82	110	0.35	1.13	0.039	0.032	0.037	19
Rotational Spring at the Right Side								
Beam Span	M_{y+} (KN.m)	M_{y-} (KN.m)	EI_{stf}/EI_g	M_c/M_y	$\theta_{cap,pl+}$	$\theta_{cap,pl-}$	θ_{pc}	λ
1	110	82	0.35	1.13	0.032	0.039	0.037	19
2	94	82	0.35	1.13	0.033	0.037	0.037	19
3	94	82	0.35	1.13	0.033	0.037	0.037	19
4	110	82	0.35	1.13	0.032	0.039	0.037	19
5	82	82	0.35	1.13	0.035	0.035	0.037	19

Table 24: Spring properties of beams of floor 2 of RB3

Rotational Spring at the Left Side								
Beam Span	M_{y+} (KN.m)	M_{y-} (KN.m)	EI_{stf}/EI_g	M_c/M_y	$\theta_{cap,pl+}$	$\theta_{cap,pl-}$	θ_{pc}	λ
1	82	90	0.35	1.13	0.035	0.035	0.037	19
2	82	118	0.35	1.13	0.039	0.032	0.037	19
3	82	101	0.35	1.13	0.037	0.033	0.037	19
4	82	101	0.35	1.13	0.037	0.033	0.037	19
5	82	118	0.35	1.13	0.039	0.032	0.037	19
Rotational Spring at the Right Side								
Beam Span	M_{y+} (KN.m)	M_{y-} (KN.m)	EI_{stf}/EI_g	M_c/M_y	$\theta_{cap,pl+}$	$\theta_{cap,pl-}$	θ_{pc}	λ
1	118	82	0.35	1.13	0.032	0.039	0.037	19
2	101	82	0.35	1.13	0.033	0.037	0.037	19
3	101	82	0.35	1.13	0.033	0.037	0.037	19
4	118	82	0.35	1.13	0.032	0.039	0.037	19
5	90	82	0.35	1.13	0.035	0.035	0.037	19

Table 25: Spring properties of beams of floors 3-8 of RB3

Rotational Spring at the Left Side								
Beam Span	M_{y+} (KN.m)	M_{y-} (KN.m)	EI_{stf}/EI_g	M_c/M_y	$\theta_{cap,pl+}$	$\theta_{cap,pl-}$	θ_{pc}	λ
1	98	98	0.35	1.13	0.035	0.035	0.037	19
2	98	134	0.35	1.13	0.039	0.032	0.037	19
3	98	118	0.35	1.13	0.037	0.033	0.037	19
4	98	118	0.35	1.13	0.037	0.033	0.037	19
5	98	134	0.35	1.13	0.039	0.032	0.037	19

Rotational Spring at the Right Side								
Beam Span	M_{y+} (KN.m)	M_{y-} (KN.m)	EI_{stf}/EI_g	M_c/M_y	$\theta_{cap,pl+}$	$\theta_{cap,pl-}$	θ_{pc}	λ
1	134	98	0.35	1.13	0.032	0.039	0.037	19
2	118	98	0.35	1.13	0.033	0.037	0.037	19
3	118	98	0.35	1.13	0.033	0.037	0.037	19
4	134	98	0.35	1.13	0.032	0.039	0.037	19
5	98	98	0.35	1.13	0.035	0.035	0.037	19

Regarding the joints, they are also modelled using the scissors approach [58] and the 4 point hysteretic joint spring model developed by Alath and Kunnath [53], which were presented in Chapter 0. However, the parameters of the joint spring model need to be updated to reflect the increase in joint area and the addition of transverse reinforcement within the joints. Recall that a four-point hysteretic model was fitted to unreinforced wide beam-narrow column joints by Allabban [18], and the results were summarized in Chapter 0 and used in the model of the unretrofitted building. In the next section, the model is again calibrated to wide beam-narrow column joints, which are commonly constructed in Lebanon and the Middle East, but this time the joints contain transverse reinforcement. The results of the experiments performed by Elsouri and Harajli [75] are used for this calibration.

B. Proposed Joint Model

1. Experimental Data on Wide Beam-Narrow Column Joints

Elsouri and Harajli [60, 61, 74] studied the response of wide beam-narrow column joints under seismic loading by testing two sets of specimens: a set of unreinforced non-

ductile specimens, and another set of more ductile specimens in which the reinforcement detailing was slightly improved, namely by adding transverse steel reinforcement within the joint core. The first set of specimens [60, 61] was used by Allabban [18] to calibrate the joint model used for the unretrofitted structure. For the retrofitted structures, the second set [74] is used in this study. This set is comprised of four full-scale wide beam-narrow column joints reinforced partly in accordance with the ACI318-08 seismic specifications, with transverse reinforcement extending into the joint area and beam reinforcement provided with adequate development and hooks. The dimensions of the members they tested are similar to construction practices prevalent in the region. The material properties they used are $f'_c = 35 \text{ MPa}$, $f_y = 420 \text{ MPa}$, and $f_{yt} = 420 \text{ MPa}$. Figure 15 shows the specimens in question.

The specimens consist of two exterior joints (UEJ-F1 and UEJ-F2) and two interior joints (UIJ-F1 and UIJ-F2). Typical of older construction in Lebanon, the beams are wide and shallow and the columns are narrow, and all have high aspect ratios ranging from 2.8 to 3.25. In specimens UEJ-F1 and UIJ-F1, the longer side of the column is oriented parallel to the direction of the beam, similar to the interior joints of the building frames analyzed in this study. On the other hand, in specimens UEJ-F2 and UIJ-F2, the longer side is perpendicular to the direction of the beam, similar to the exterior joints of the building frames analyzed in this study. The main characteristics of these specimens are summarized in Table 26 and Table 27.

There are, however, some differences between the joints of the tested specimens and those present in RB1-RB3. The main difference is that the tested specimens were built

from scratch, and not obtained by concrete jacketing the columns and extending the jackets and their longitudinal and transverse reinforcement into the joint. But following Bousias [71], properly jacketed concrete members are assumed to behave similarly to monolithically cast members. Another difference is that the beam longitudinal reinforcement of the specimens is properly developed and spliced away from the joints, while the bottom longitudinal reinforcement in the beams of RB1-RB3 have insufficient development length and are spliced at the joint. The factor α , introduced in Chapter 0 and calculated as the ratio of the development length provided to that required by ACI318 [38], is used to account for the effect of the inadequate development length of the beam longitudinal reinforcement on joint strength. Despite the small number of specimens used for the calibration and the differences between the specimens and the joints of the retrofitted buildings of this study, the joint model calibrated to the above specimens is assumed to represent the behavior of the jacketed joints of RB1-RB3.

Table 26: Specimen columns in Elsouri and Harajli [61, 74]

Specimen Columns							
Name	Depth (mm)	Width (mm)	P (KN)	Main Reinf.	ρ (%)	Shear Reinf. (mm)	ρ_{sh} (%)
UEJ-F1	650	200	520	10T16	1.55	2 Φ 8@100	0.50
UEJ-F2	200	650	390	12T16	1.86	4 Φ 8@100	0.31
UIJ-F1	700	200	560	12T16	1.72	2 Φ 8@100	0.50
UIJ-F2	200	650	390	18T16	2.78	4 Φ 8@100	0.31

Table 27: Specimen Beams in Elsouri and Harajli [61, 74]

Name	Dimensions (mm)	Longitudinal Reinforcement		$\rho(\%)$		Shear Reinf. (mm)	$\rho_{sh}(\%)$
		Top	Bottom	Top	Bot		
UEJ-F1	250x800	8T14	8T16	0.73	0.95	4 Φ 8@75	0.34
UEJ-F2	250x800	8T14	8T16	0.73	0.95	4 Φ 8@75	0.34
UIJ-F1	250x800	8T14	8T16	0.73	0.95	4 Φ 8@75	0.34
UIJ-F2	250x800	8T14	8T16	0.73	0.95	4 Φ 8@75	0.34

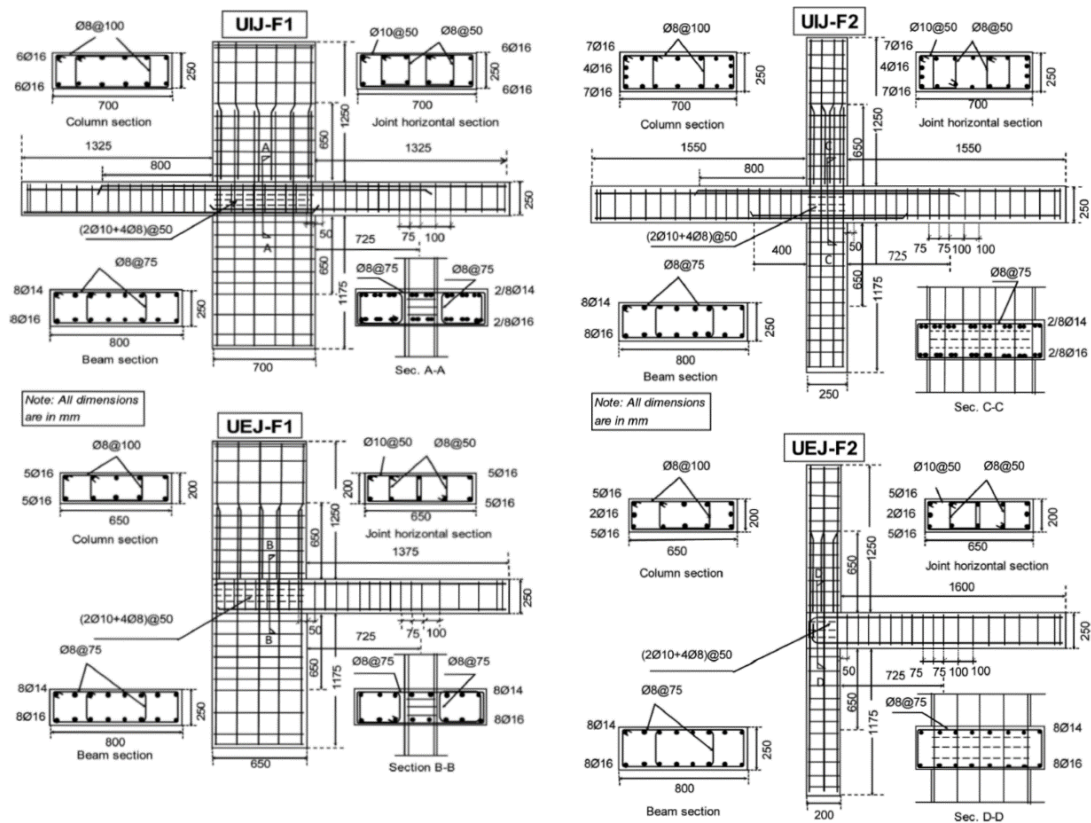


Figure 15: Specimens tested by Elsouri and Harajli [61, 74]

The four specimens were tested in a seismic actuator under quasi-static cyclic loading up to a drift of 4%. Specimens UEJ-F2 and UIJ-F2 were further tested using half cycles to a drift of 8.5%. The lateral load versus drift responses of the four specimens are

used to calculate the corresponding joint moment versus joint rotation responses, which are plotted in Figure 16.

2. *Joint Model Calibration to Experimental Data*

Following Celik and Ellingwood [53], and as previously described in Chapter 0, the force deformation relationship of the joint spring is defined using a four-point hysteretic pinching curve. The four points defining the backbone curve (cracking, yielding, ultimate strength, and residual strength; see Figure 6) and the three hysteretic and pinching parameters are calibrated to the experimental data presented above. Note that cyclic strength and stiffness degradation is ignored in the model.

- Cracking:

The cracking point is defined by the onset of joint shear cracks in the joint region. Elsouiri and Harajli [74] found that, in most specimens, cracks occur at drifts between 0.5% and 1 %. For the purpose of this predictive model the cracking rotation θ_{cr} is taken to be 0.005 radians. To predict the cracking moment, the average of the ratio of the cracking to ultimate moments obtained from the experiments is used, namely

$$M_{cr} = 0.28M_u, \quad (35)$$

where M_{cr} is the cracking moment and M_u is the maximum joint moment.

- Yielding:

Yielding is defined as the point where the beam steel reinforcement begins to yield. This point can be determined from the change in the specimen stiffness in early cycles. UEJ-F1 and UIJ-F1 both develop yielding at rotations of 0.017-0.02 radians, while

joints UEJ-F2 and UIJ-F2 yield at 0.025 and 0.035 radians, respectively. This indicates that the orientation of the column relative to the beam (described by the beam section height to column section height ratio) has a more significant effect on the yield rotation θ_y as opposed to joint location (exterior versus interior). A simple linear relationship is fitted

$$\theta_y = 0.0124(h_b/h_c) + 0.0151. \quad (36)$$

The moment at yield is calculated using Equations (13) to (15), as was done by Allabban [18] and Celik and Ellingwood [53]. In these equations the joint shear strength is defined following ACI318-14 [39] as 1.25 and $1.0 \sqrt{f'_c}$ (MPa) for interior and exterior joints, respectively. These values were found by Elsouiri and Harajli [74] to reliably predict the joint shear strength for the specimens that they tested.

- Ultimate:

The ultimate point is determined from the experimental results as the point where the specimen reaches peak strength. Specimens UEJ-F1 and UIJ-F1 reach ultimate strength at rotations of 0.035 and 0.04 radians, respectively, while joints UEJ-F2 and UIJ-F2 reach ultimate strength at rotations of 0.06 and 0.07 radians, respectively, again indicating that the orientation of the column relative to the beam has a more significant effect on the ultimate rotation θ_u as opposed to joint location (exterior versus interior). A linear relationship is also fitted:

$$\theta_u = 0.0323(h_b/h_c) + 0.0271. \quad (37)$$

It is worth noting that the h_b/h_c ratio in the retrofitted frames lies between 0.2 and 0.6, while the samples tested by Elsouiri and Harajli [61, 74] have an h_b/h_c ratio ranging from 0.4 to 1.2.

The moment at ultimate is calculated using equations (13) to (15) as was done by Allabban [18] and Celik and Ellingwood [53].

- Residual:

Only one specimen, UEJ-F2, reaches the point of residual strength. The other three specimens only show slight strength degradation, without reaching residual strength.

Therefore, the equation proposed by Park and Mosalam [59] is used to predict the residual rotation θ_r ,

$$\theta_r = \theta_u + 0.02, \quad (38)$$

and the equation proposed by Allabban [18] is used to predict the residual moment strength:

$$M_r = 0.4M_u. \quad (39)$$

The proposed relations to predict the rotation and moment values of the backbone curve of the joint spring are summarized in Table 28 and Table 29, respectively.

As for the hysteretic and pinching parameters $uForce$, $rForce$, and $rDisp$, their calibration is carried out by fitting the overall hysteretic responses calculated using the proposed predictive model to the experimental responses. The selected values of the hysteretic and pinching parameters are shown in Table 30. Note that the values of $rForce$

and $rDisp$ for the reinforced joints are larger than for the unreinforced joints, which are listed in Table 5. This difference is expected because the addition of transverse reinforcement reduces the pinching behavior, consistent with larger values of $rForce$ and $rDisp$. $uForce$ is unchanged as it is related to the reloading and unloading values of the experiment.

Table 28: Proposed Joint Model Rotation Parameters

Backbone Point	Cracking (θ_{cr})	Yield (θ_y)	Ultimate (θ_u)	Residual (θ_r)
Rotation	0.005	$0.0124(h_b/h_c) + 0.0151$	$0.0323(h_b/h_c) + 0.0271$	$\theta_u + 0.02$

Table 29: Proposed Joint moment Values

Backbone Point	Cracking	Yield	Ultimate (M_u)	Residual
Moment	$0.28M_u$	$(M_{y,C}, \alpha M_{y,B}, M((\tau_{jh})_{max})^*$	$(M_{u,C}, \alpha M_{u,B}, M((\tau_{jh})_{max})^*$	$0.4(M_u)$

*: Minimum

Table 30: Proposed hysteretic pinching parameters

Hysteric Parameter	$uForce$	$rForce$	$rDisp$
Exterior	-0.15	0.4	0.4
Interior	-0.15	0.3	0.3

3. Predicted Versus Experimental Responses

To verify the proposed backbone curve parameters, an OpenSees model of the test setup used in Elsouri and Harajli [61, 74] is developed and used to simulate the

experimental results. The modeling methodology used is identical to that used to model the studied buildings. Linear elastic elements with non-linear zero-length plastic hinges are used to represent the beam and column elements while joints are modelled using the scissor approach with rigid end zones. The joint springs are assigned the parameters predicted using the equations in Table 28 and Table 29 and the pinching and hysteretic parameters in Table 30. The loading protocols used by Elsouiri and Harajli [74] are used as displacement control parameters.

The simulated joint moment versus joint rotation responses are compared to the experimental results in Figures 16-19. Note that for specimens UIJ-F1 (Figure 16) and UEJ-F1 (Figure 17), the simulated response is extended past the experimental one in order to capture strength degradation.

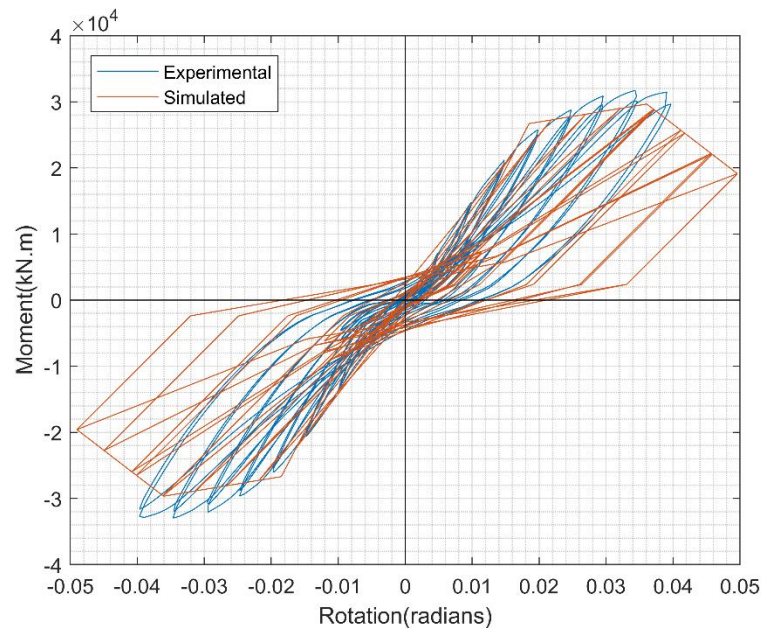


Figure 16: Predicted and experimental joint moment-rotation responses for UIJ-F1

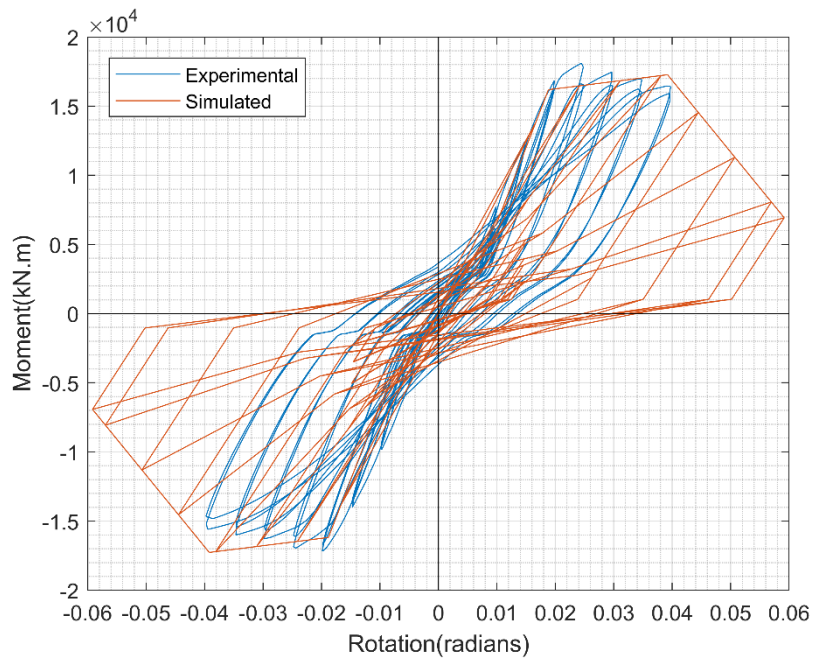


Figure 17: Predicted and experimental joint moment-rotation responses for UEJ-F1

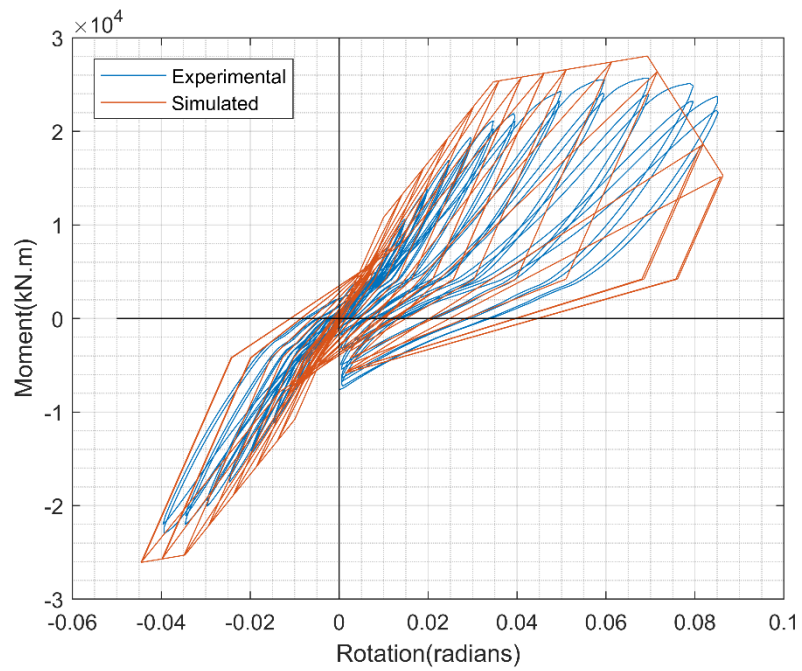


Figure 18: Predicted and experimental joint moment-rotation responses for UIJ-F2

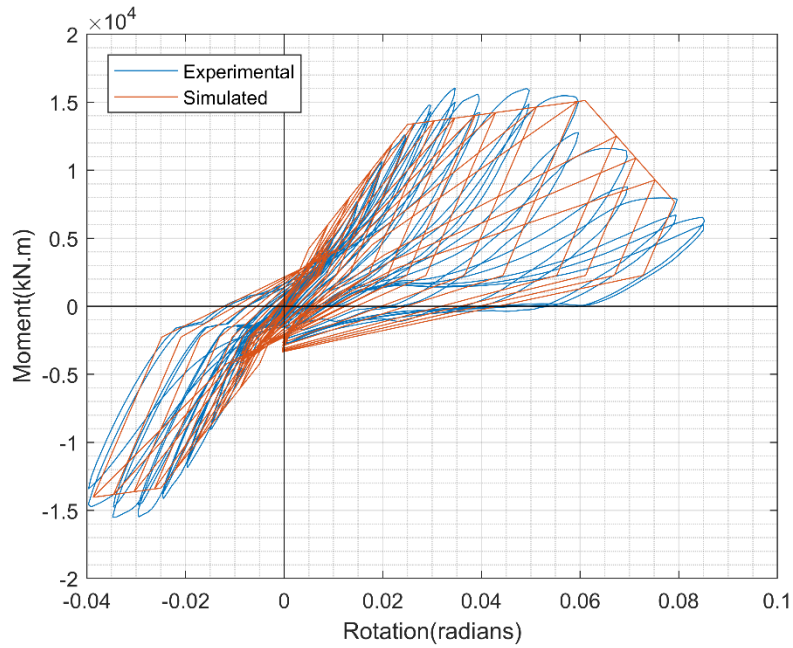


Figure 19: Predicted and experimental joint moment-rotation responses for UEJ-F2

Figures 16-19 show that the proposed joint model results in predicted joint responses that are in overall good agreement with the experimental responses. There are minor differences in the predicted and observed moment and rotation values. For example, Table 31 shows the fitted moment parameters compared to the maximum moment recorded in the experiment for every sample. The differences can be attributed to the simple linear relationships that were fitted to the experimental data. More experimental tests are needed to improve the predictive ability of the model.

Table 31: Comparison of predicted and observed ultimate moment strength

Connection	Simulated M_u (KN.m)	Experimental M_u (KN.m)
UEJ-F1	153	160.
UEJ-F2	134	142.
UIJ-F1	263	281
UIJ-F2	248.	227

CHAPTER VII

SEISMIC PERFORMANCE OF THE RETROFITTED VERSUS UNRETROFITTED BUILDINGS

As was done in Chapter IV for the unretrofitted building, the FEMA-P695 methodology [37] is used to assess the seismic performance of the retrofitted structures and to compare their performance with the unretrofitted one. The corresponding analytical models developed in OpenSees and presented in Chapter 0 are used to perform non-linear static pushover analysis and incremental dynamic analysis (IDA), from which the collapse fragility curves of the different retrofitted buildings are calculated. The fragility curves are then used to determine the probability of collapse of the retrofitted buildings at the MCE intensity, and thus compare the effectiveness of the various retrofitting approaches on the seismic collapse performance of the 8-story NDRC frame structure being studied.

A. Pushover Analysis

Figure 20 shows the pushover analysis curves of the exterior frame of the unretrofitted (B0) and the three retrofitted (RB1-RB3) 8-story buildings, and Table 32 lists the design and maximum base shears, the roof drift ratios at yield and ultimate, as well as the calculated values of the ductility μ_T and overstrength Ω factors for the exterior frame of the same buildings.

As apparent from Figure 20, the retrofitted structures perform much better than the unretrofitted one, with the maximum base shear V_{max} increasing by 68%, 96% and 166%

for RB1 (the building with the minimum jacket thickness), RB2 (the building whose concrete jackets were designed to sustain the shear and moment demands in the columns) and RB3 (same as RB2, with the addition of CFRP longitudinal and transverse reinforcement to the beams to satisfy their moment demands), respectively. However, the overstrength factor Ω remains below 1, at 0.81 and 0.94 for RB1 and RB2, respectively. Recall that the retrofitted structures are assumed to have a response modification factor of $R = 5$ for an intermediate moment frame as opposed to $R = 3$ for an ordinary moment frame, which is used for the unretrofitted structure. This result is not unexpected as retrofitted structures tend to perform less well than newly built ones [9]. Additionally, the beams are not retrofitted in RB1 and RB2 and they do not satisfy the moment demands. The performance of RB3 shows the largest improvement with an overstrength factor of 1.28.

It can also be observed from Figure 20 that retrofitting also positively affects the ductility of the structure with the roof drift ratio at ultimate δ_u/h_n increasing from 0.034 for B0, to 0.053, 0.057 and 0.045 for RB1, RB2, and RB3 respectively. This is an expected result as the concrete jackets contain additional transverse reinforcement, which increases concrete confinement and member ductility. Additionally, the jacket reinforcement is extended through the joints, which increases the confinement of the joint area and improves joint performance. As for RB3, it exhibits a higher ductility than B0 but lower than that of RB1 and RB2. However, it should also be noted that the pushover analysis for RB3 failed to converge before reaching 80% of V_{max} , and failure to converge does not always mean collapse, so there is a possibility that RB3 can reach a higher δ_u . Additionally, an increase

in linear stiffness is noted when going from B0 through to RB3, an increase that is clearly shown in Figure 20 and expected due to the increase in column and joint section size when going from B0 to RB1 and RB1 to RB2 and the increase in joint stiffness when going from RB2 to RB3.

Table 32: Summary of Push-Over analysis results of the unretrofitted and retrofitted frames

Building Model	$V_{Design}(kN)$	$V_{max}(kN)$	Ω	δ_y/h_n	δ_u/h_n	μ_T
B0	990	322	0.32	0.013	0.034	2.62
RB1	667	540	0.81	0.015	0.053	3.53
RB2	671	632	0.94	0.015	0.057	3.95
RB3	671	857	1.28	0.016	0.045	2.77

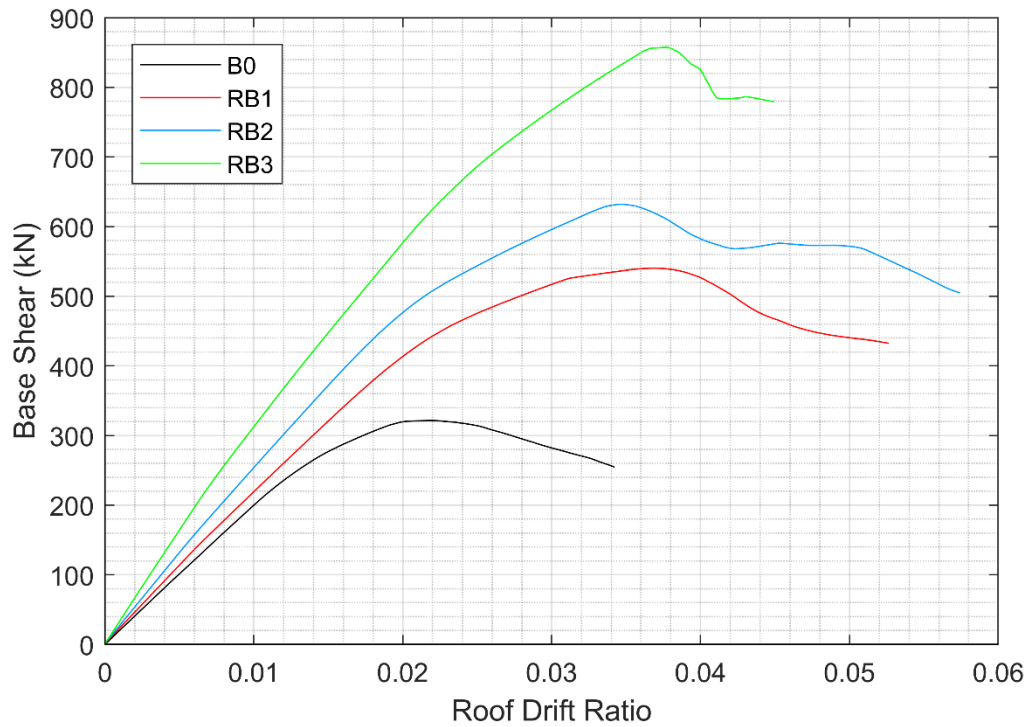


Figure 20: Pushover curves of the unretrofitted and retrofitted frames

B. Incremental Dynamic Analysis

Figure 21 to Figure 24 show the results of the MIDA using the FEMA P695 [37] far-field ground motions for the four building models. The MIDA is carried out in varying increments up until collapse. As mentioned in Chapter 0, failure of the retrofitted frames is defined by dynamic instability, which is when the slope of the IDA curve drops below 20% [67] or if the recorded IDR reaches 10% before dynamic instability occurs, while for the unretrofitted frame, shear collapse and gravity collapse are also considered and side-sway collapse is assumed to occur at an IDR of 5%.

It can be observed from Figure 21 that the maximum $Sa(T)$ achieved for B0 is 0.9 g, with the majority of earthquake records causing failure by $Sa(T) = 0.6$ g. On the other hand, higher values of $Sa(T)$ are consistently reached for RB1-RB3, and many records are scaled up to $Sa(T) = 1.5$ g without collapse, as can be observed in Figure 22 to Figure 24. This demonstrates that the retrofitted buildings are generally able to sustain more intense ground motions before collapse and perform better than the unretrofitted building. Additionally, for B0, collapse is entirely caused by shear failure, while for RB1-RB3, collapse is caused by the IDR exceeding 10% or dynamic instability occurring. Often, both occur simultaneously.

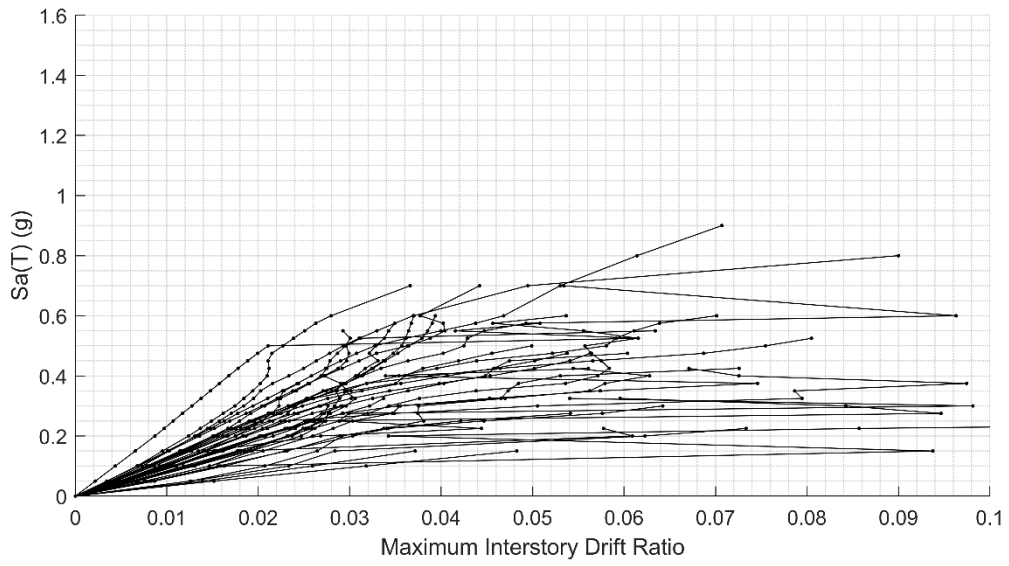


Figure 21: MIDA results for B0

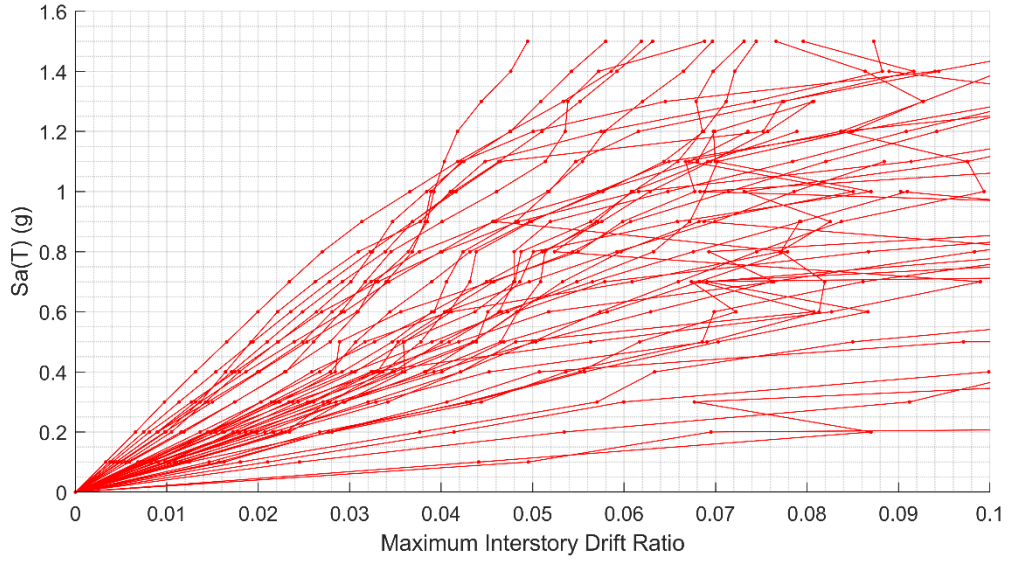


Figure 22: MIDA results for RB1

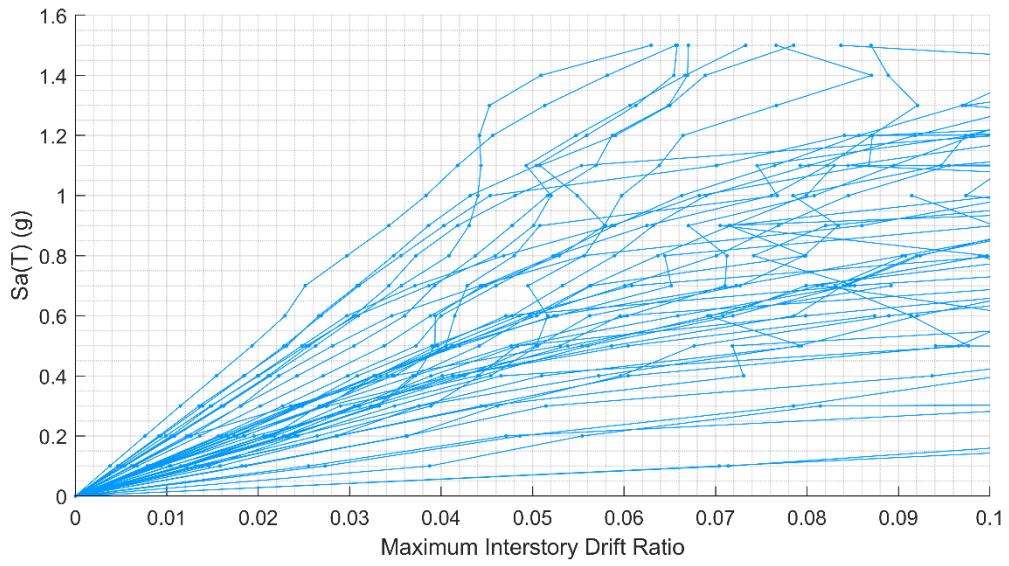


Figure 23: MIDA results for RB2

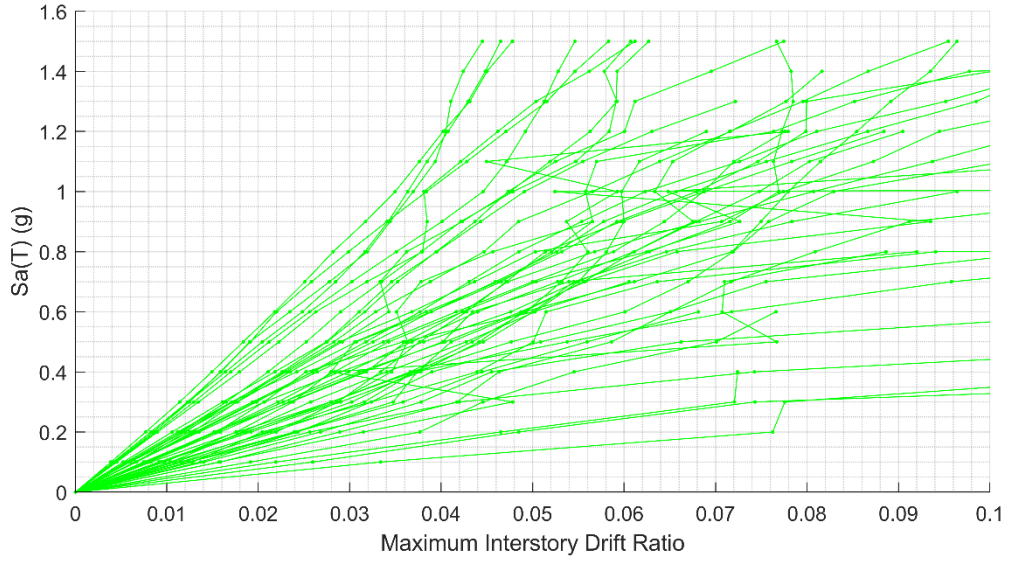


Figure 24: MIDA results for RB3

C. Fragility Analysis

The collapse data obtained from the MIDAs of the studied buildings is used to fit their lognormal collapse fragility curves. Table 33 shows the values of the fitted fragility curve parameters \hat{S}_{CT} and β_{RTR} for B0 (repeated from Chapter 0), RB1, RB2 and RB3, and the resulting probability of collapse at the MCE spectral intensity, S_{MT} , when only record-to-record variability, β_{RTR} , is accounted for. Table 34 provides the values of the total uncertainty, β_{TOT} , and the probability of collapse at the MCE spectral intensity when this total uncertainty is accounted for. Recall from Chapter 0 that β_{TOT} includes the additional values of the model, design and test data uncertainties.

Moreover, Figure 25 shows the corresponding collapse fragility curves of the four buildings when only record-to-record uncertainty is accounted for, while Figure 26 shows the fragility curves when the total uncertainty β_{TOT} is included. Figure 25 and Figure 26 also show the MCE spectral intensity $S_{MT} = 0.559g$, at which the probabilities of collapse are calculated and listed in Table 33 and Table 34.

Table 33: Summary of fragility results using Record-to-Record Uncertainty.

Model	S_{CT} (g)	β_{RTR}	S_{MT} (g)	P(Collapse MCE)
B0	0.378	0.34	0.559	0.874
RB1	1.128	0.74	0.559	0.170
RB2	0.956	0.56	0.559	0.171
RB3	1.233	0.71	0.559	0.134

Table 34: Summary of fragility results using Total uncertainty

Model	S_{CT} (g)	β_{TOT}	S_{MT} (g)	P(Collapse MCE)
B0	0.378	0.63	0.559	0.731
RB1	1.128	0.81	0.559	0.210
RB2	0.956	0.66	0.559	0.228
RB3	1.233	0.71	0.559	0.174

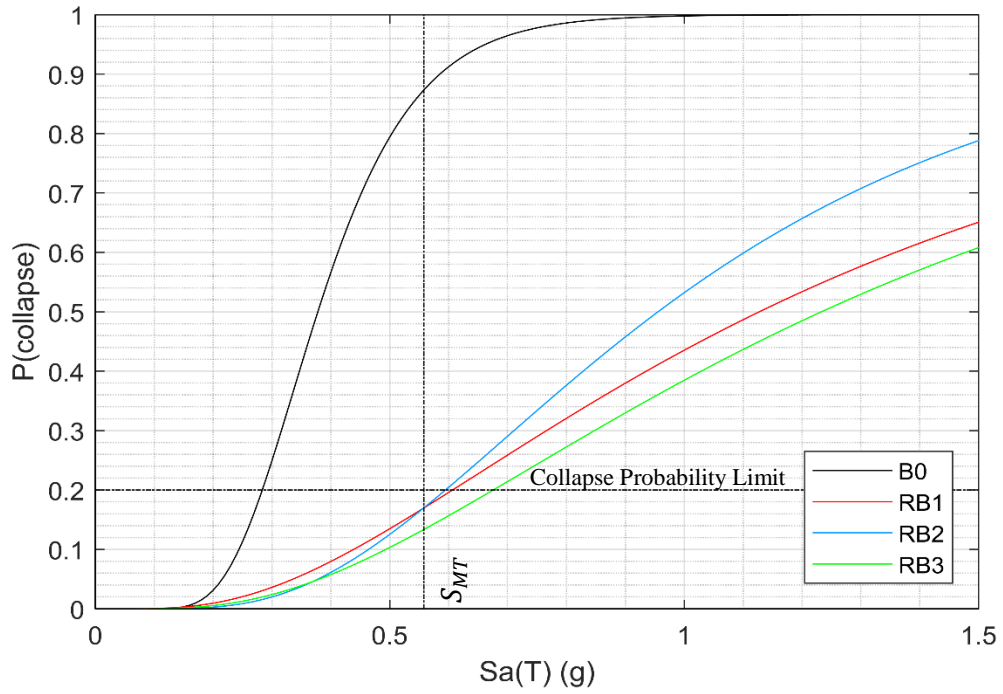


Figure 25: Fragility curves of the unretrofitted and retrofitted frames accounting only for record to record uncertainty

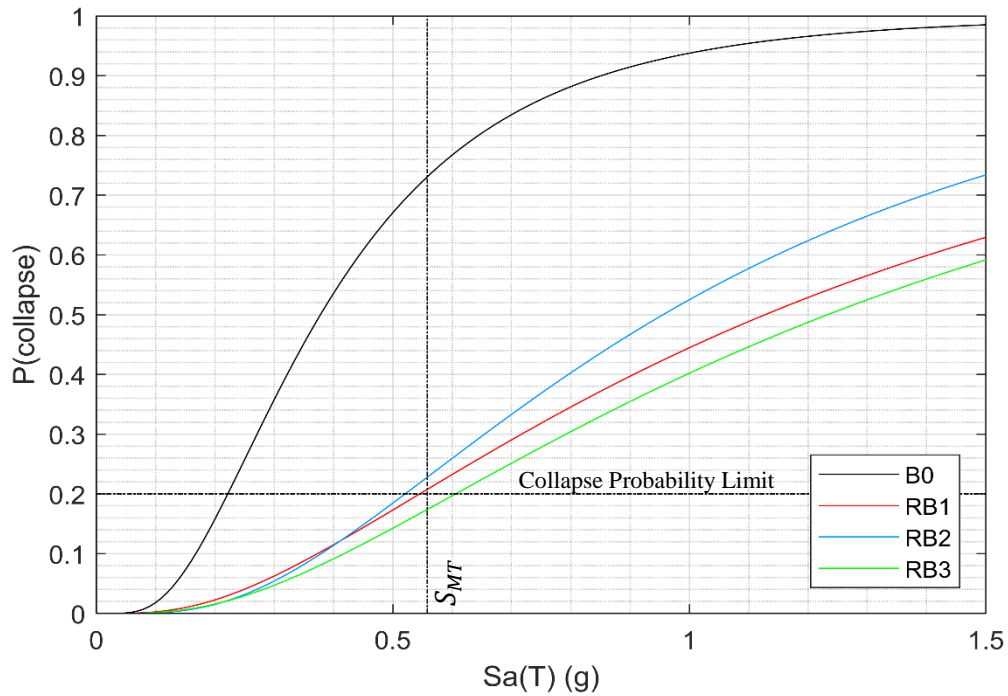


Figure 26: Fragility curves of the unretrofitted and retrofitted frames accounting for the total uncertainty

When the collapse fragility parameters and curves of the retrofitted and unretrofitted frames are compared in Table 33 and Figure 25, several observations can be made. First, a significant improvement in collapse performance due to retrofitting is immediately noted: the median collapse capacity \hat{S}_{CT} increases from 0.378 g for B0 to 1.128 g, 0.956 g and 1.233 g for RB1, RB2, and RB3, respectively, and the probability of collapse at the MCE ground motion drops from 87% for B0 to 17% for both RB1 and RB2, and to 13% for RB3. Recall that to result in an acceptable performance, and following FEMA P695 [37], the retrofits should reduce the probability of collapse of the structure when subjected to an MCE ground motion to less than 20%. Therefore, the three retrofitted buildings result in an acceptable performance, and, as expected, RB3 has the best

performance. When total uncertainty is taken into consideration (see Figure 26 and Table 34), the probabilities of collapse of the retrofitted structures increase slightly, to 21%, 23% and 17% for RB1, RB2, and RB3, respectively, but they are still deemed acceptable compared with the unretrofitted structure.

Another notable observation is that RB2 performs slightly better than RB1 at low spectral intensities, but RB1 performs better at higher spectral intensities, although the concrete jackets of RB2 are larger and more heavily reinforced than RB1 at the first two floors. In fact, compared with RB2, RB1 has a slightly larger median collapse capacity \hat{S}_{CT} and slightly lower probability of collapse at spectral intensities higher than 0.55 g, including at the MCE intensity. To better understand this observation, the maximum displacement recorded at every floor of RB1 and RB2 is compared for a set of ground motions scaled to the same intensity level. These displacements are shown in Figure 27 and Figure 28 for four earthquake records scaled to $Sa(T) = 0.1$ g and 0.9 g, respectively. Moreover, Figure 29 shows the maximum IDRs at every floor of RB1 and RB2 for the same records and scaling as Figure 28.

Figure 27 shows that at low ground motion intensities, the peak displacements of RB2 are smaller than those of RB1 at the lower floors (where the columns of RB2 are larger and more heavily reinforced), but they are similar at the higher floors. Figure 28 and Figure 29 show that when the ground motion intensity is increased to 0.9 g (larger than the MCE intensity), RB2 consistently displays lower displacements and IDRs at the bottom floors and higher displacements and IDRs at the top floors when compared to RB1. This difference in displacements can be attributed to RB2 having larger columns than RB1 in

floors 1 and 2. These larger columns undergo smaller displacements, and also create a stiffness change between floors 2 and 3, which, when coupled with the additional change in stiffness between floors 4 and 5, causes a slight whiplash effect that affects the distribution of deformations along the height of the structure and leads to larger displacements and IDRs at the upper floors of RB2. As a result of the larger IDR values, RB2 has a slightly larger probability of collapse than RB1 when subjected to intense ground motions. For example, as illustrated in Figure 29, the maximum IDR in RB2 exceeds 10% when subjected to record 33 scaled to $S_a(T) = 0.9$ g, thus indicating collapse, while RB1 doesn't collapse because its maximum IDR is less than 10%.

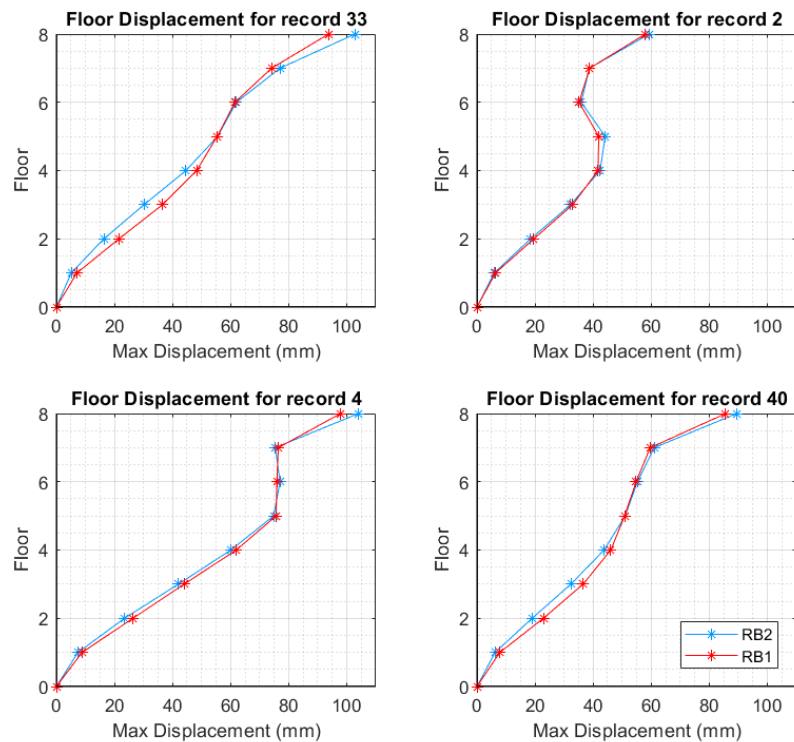


Figure 27: Comparison between the maximum floor displacements of RB1 and RB2 when subjected to the same four ground motions scaled to $S_a(T) = 0.1$ g.

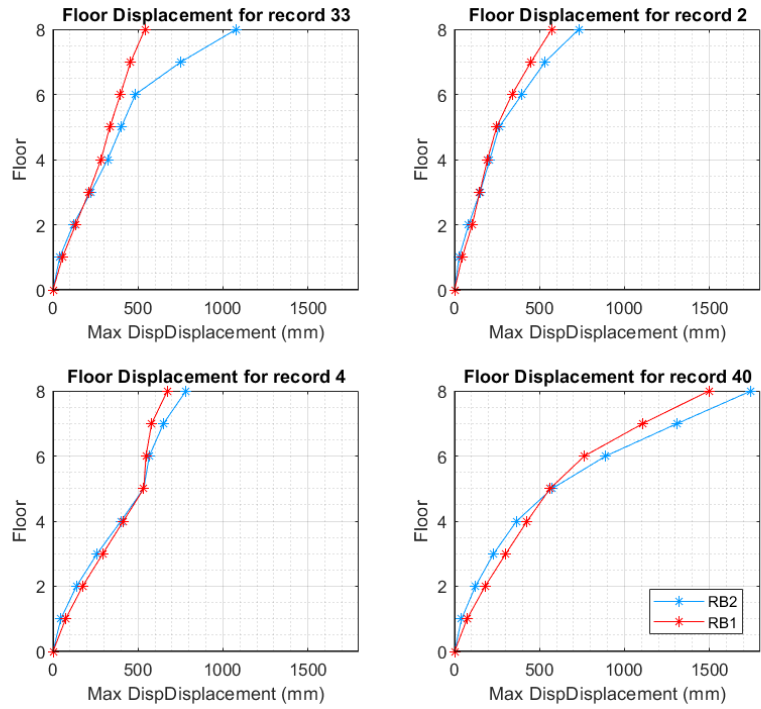


Figure 28: Comparison between the maximum floor displacements of RB1 and RB2 when subjected to the same four ground motions scaled to $S_a(T) = 0.9$ g.

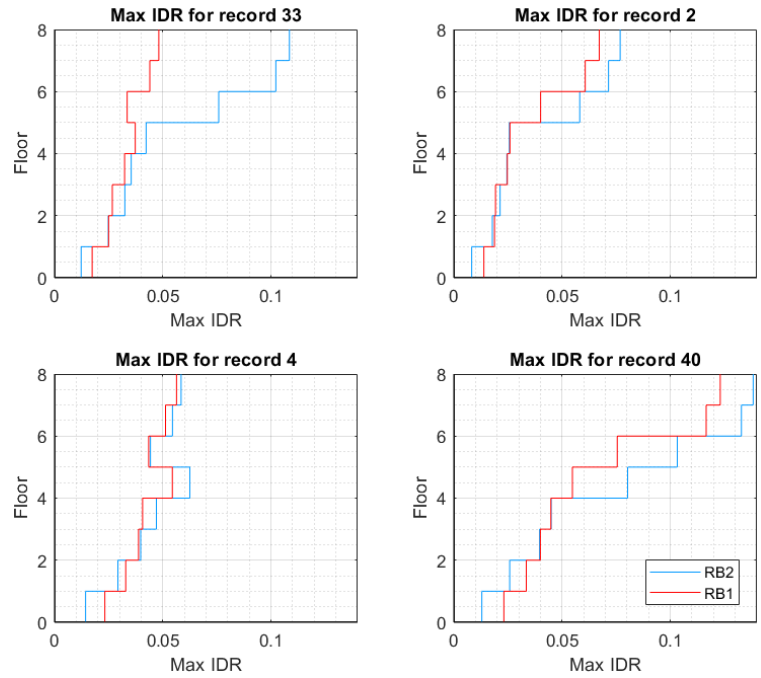


Figure 29: Comparison between the maximum inter-story drift ratios (IDRs) of RB1 and RB2 when subjected to the same four ground motions scaled to $S_a(T) = 0.9$ g.

D. Individual Spring Response

To better understand the differences in performance between the four studied buildings, the force deformation responses of a sample of individual springs in their structural models are examined more closely, compared and discussed. The same ground motion, but scaled to different intensity levels, is used in the following discussion.

1. Joints

For all models, the majority of the deformations are concentrated at the joint springs. Figure 30 shows the moment-rotation response of the rotational spring of Joint 3 at floor 8 in each of the four models, for the same ground motion scaled to three different $Sa(T)$ values. The spring backbone curves are also shown. Larger spectral acceleration values are used for the models of the retrofitted buildings to showcase the strength deterioration sustained at high spectral acceleration values. Figure 30 illustrates the strength and stiffness degradation of the joints with increasing ground motion intensity. Figure 30 also shows that the concrete jacketing of the columns and joints increases both the moment and rotation capacities of the joints. It also shows that the joints of RB1 and RB2 have similar responses, which is expected because they have identical beams and columns at the higher floors. On the other hand, the joint of RB3 has a larger moment capacity. This indicates that the strength of this joint in RB1 and RB2 is limited by the beam moment capacity, which is larger in RB3 because longitudinal CFRP sheets are added to the beams. Similar observations can be made for the other joints of the studied buildings.

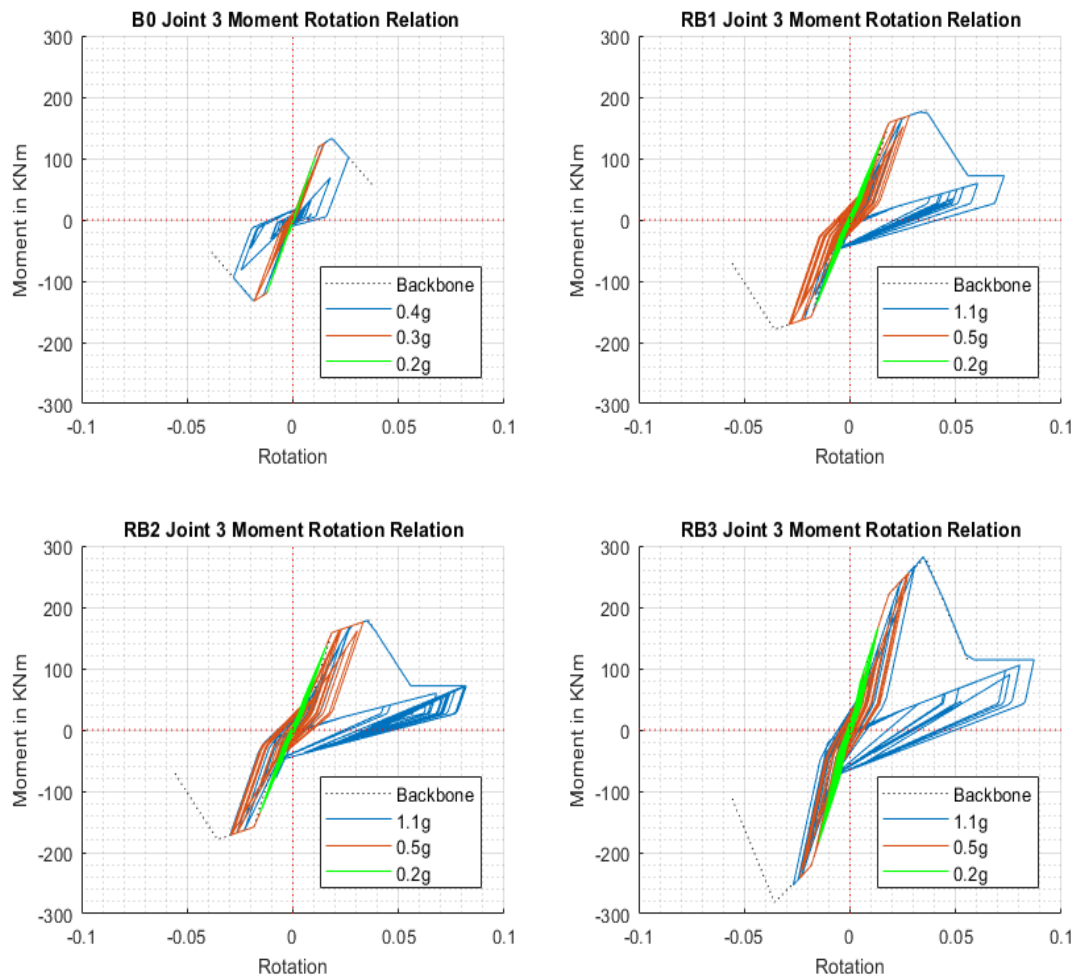


Figure 30: Moment-rotation response of joint 3 at floor 8 in all models

2. Columns

Figure 31 shows the moment-rotation response of the rotational spring at the top of column 3 on floor 8, for the same ground motion scaled to $Sa(T)$ of 0.4 g for B0, and 1.1 g for RB1, RB2 and RB3. At these scale factors, the buildings are close to, but do not reach, collapse. It is apparent here that these column springs remain in the linear-elastic range in both the unretrofitted and retrofitted models, contrary to the joint springs, which display a

non-linear response and reach the strength degradation phase. This observation is also valid for the other floors with the exception of floors 5 and 6 where the column springs experience some yielding prior to the failure of the joint spring, likely due to the change in column cross section dimensions between floors 4 and 5. The linear-elastic behavior of the column springs suggests that further increasing the moment capacity of columns alone is not expected to result in a large improvement in seismic fragility. This is confirmed when comparing the collapse fragility curves of RB1 and RB2, whereby the interior columns in the model of RB2 are stronger than those of RB1 at floors 1-4.

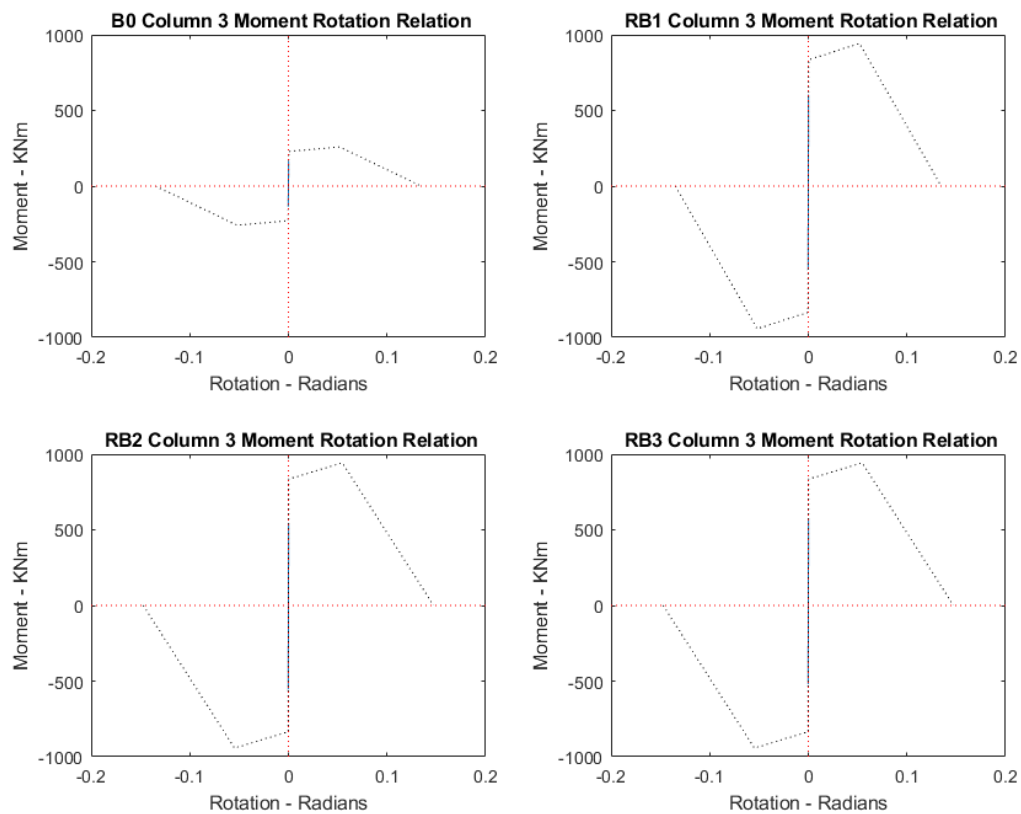


Figure 31: Moment-rotation response and backbone curve of the rotational spring at the top of Column 3 on floor 8 in all models subjected to the same ground motion; the ground motion is scaled to $Sa(T)$ of 0.4g for RB0 and 1.1g for RB1, RB2 and RB3

3. *Beams*

Figure 32 shows the moment-rotation responses of the rotational springs of beam 3 at floor 8 for the four models. Again, the same ground motion is used and scaled to $Sa(T)$ of 0.4 g for B0, and 1.1 g for RB1, RB2 and RB3. As mentioned previously, at these scale factors the buildings are close to, but do not reach, collapse. The beams are identical in B0, RB1 and RB2, and Figure 32 shows that the beam deformations increase as the retrofitting increases from B0 to RB1, and from RB1 to RB2, with some strength degradation even occurring in RB2. In fact, the beam of B0 responds mostly in the linear-elastic range, while the adjoining joint responds in the non-linear range and exhibits strength and stiffness degradation when subjected to the same scaled ground motion (see Figure 30 for the response of the joint of B0 to the ground motions scaled to 0.4 g). This indicates that the beam moment capacity does not limit joint strength in B0 (recall from equations (14) to (16) that the moment strength of a joint is the minimum of the moment corresponding to the joint shear strength, the beam moment capacity, and the column moment capacity). After jacketing the columns and the joints in RB1 and RB2, their joint strength increases (see Figure 30) but becomes limited by the moment capacity of the adjoining beams, as demonstrated by the yielding and large deformations of the beams of RB1 and RB2 in Figure 32. For RB3, longitudinal CFRP reinforcement is added to the beams and increases their moment strength as well as that of the adjoining joint (see Figure 30). Despite the increase in strength, the beam springs of RB3 still yield, but they undergo smaller deformations than those of RB1 and RB2 and they do not experience strength degradation. Similar observations are also made for the other beams and at the other levels.

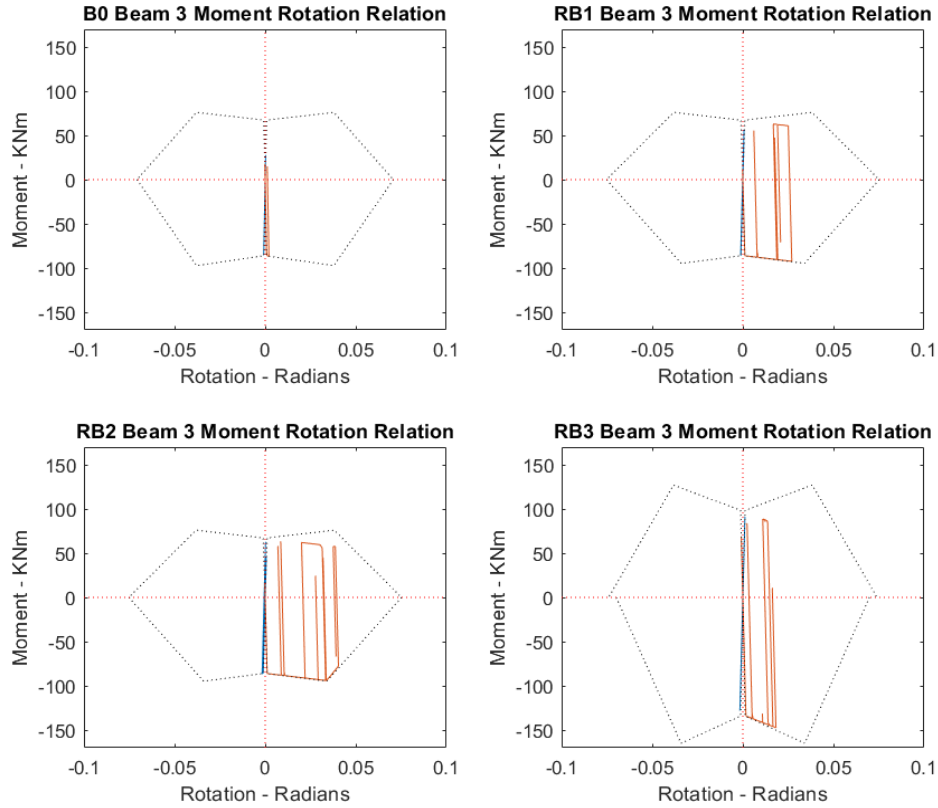


Figure 32: Moment-rotation response and backbone curve of the rotational springs of beam 3 on floor 8 in all models subjected to the same ground motion; the ground motion is scaled to $Sa(T)$ of 0.4g for RB0 and 1.1g for RB1, RB2 and RB3

In summary, most of the deformations at large ground motion intensities are concentrated at the joints. Thus the joints contribute the most to the large observed IDR values and to collapse, and are the critical elements to be reinforced. Large improvements in seismic collapse performance are achieved by increasing the strength and ductility of the joint springs. These factors in combination with the fact that the joint strength of the studied buildings is limited by beam strength, explain why RB1 and RB2 have similar performances and why RB3 has a better performance.

CHAPTER VII

SUMMARY, CONCLUSIONS AND RECOMMENDATIONS

A. Summary and Conclusions

Although Lebanon is in a region of moderate seismicity, many of the existing buildings were only designed to withstand gravity loading and are thus vulnerable to collapse in the event of large seismic events, posing a hazard to the lives of their occupants. The aim of this project is to examine the effectiveness of various retrofitting schemes on the seismic response of a representative 8-story gravity-load designed building that is typical of reinforced concrete structures built in Beirut in the 1970s to 1990s. These structures are characterized by wide beams, high aspect ratio columns, insufficient transverse reinforcement, unreinforced wide beam-narrow column joints, and lap splices located in potential plastic hinge regions. Three retrofitted versions of the 8-story building are designed and considered in this study. The seismic performance of the four buildings is evaluated following the FEMA P695 methodology [37]. Analytical models of the buildings are developed, non-linear pushover and incremental dynamic analyses are performed and collapse fragility functions calculated. The study aims to find out if the retrofitting methods considered are able to reduce to below 20% the probability of collapse in the event of an MCE ground motion intensity.

First, the design, modeling and seismic performance assessment of the unretrofitted structure, which was performed by Allabban [18], is reviewed and the main

structural deficiencies of the structure are noted. To address these deficiencies, two retrofitting methods are selected, concrete jacketing of the columns and adding CFRP strips to the beams, and three retrofitted buildings are designed. The first building (RB1) uses the minimum possible concrete jacket thickness with minimum steel reinforcement as per ACI 318 for all columns of the structure. In the second building (RB2), the concrete column jackets are designed to resist the seismic loads obtained from the equivalent lateral load procedure in ASCE 7[64]. The third building (RB3) utilizes concrete column jacketing identical to that of RB2, but CFRP longitudinal reinforcement is added to the beams. This CFRP reinforcement is designed based on the guidelines of ACI 440 [73] such that the beams can resist the flexural loads obtained from the equivalent lateral load procedure while still satisfying the strong column-weak beam requirement.

Next, 2D non-linear models of the exterior frames in the longitudinal direction of the retrofitted structures are developed in OpenSees. The lumped plasticity approach is used for modelling, whereby non-linear deformations are lumped at springs located at the element ends. The model developed by Ibarra et al.[47] and recalibrated versions [48]of the predictive relations proposed by Haselton et al. [41] are used to define the force-deformation relationships of the beam and column rotational springs (shear and axial springs are not used in the models of the retrofitted structures). To model the joints, the rigid link scissor approach developed by Alath and Kunnath [52] is used. This approach consists of rigid links representing the physical dimensions of the joint and connected to a rotational spring defined by a hysteretic model having a multi-linear backbone curve [52, 57]. The hysteretic model of the joint spring is typically calibrated using experimental

results, but it has not been calibrated to wide beam-narrow column joints, which are characteristic of the buildings assessed in this study. Therefore the hysteretic model is calibrated in this study to the experimental tests of Elsouiri and Harajli [74] on wide beam-narrow column joints.

Then the models of the retrofitted structures are used to perform both non-linear pushover analysis and multi-incremental dynamic analysis (MIDA), and the MIDA results are used to construct fragility curves for each building. The pushover analysis results show that the overstrength factor tends to increase as retrofits are added from B0 to RB1 to RB2 to RB3, and that the ductility capacity of the retrofitted structures is higher than of that of the unretrofitted one. The fragility analysis results show that RB1, RB2 and RB3 have a probability of collapse probabilities of 17.0%, 17.1% and 13.4% at the MCE ground motion intensity, respectively (considering only record to record uncertainty), compared to 87% for B0. Therefore, the retrofitting methods and designs considered in this study are able to reduce the collapse probability to below the FEMA P-695 [37] recommendation of 20%.

Additionally, the individual responses of the rotational springs are examined. In the models of all the retrofitted buildings, large deformations are concentrated at the joint springs and failure is found to propagate from the joint springs as well. The columns jackets in all the retrofitted buildings are extended through the slab and thus result in an increase in the joint area, shear strength, stiffness and ductility [32]. However, the beams in RB1 and RB2 are not retrofitted and they limit joint strength and thus seismic performance. This explains the relatively similar performances of RB1 and RB2 and the improved performance of RB3, in which the beams are strengthened. These findings inform us that

for the studied building, the effectiveness of column retrofitting on seismic performance can be improved by also retrofitting the beams. Additional improvement in seismic performance can probably be achieved if the joints can be further strengthened.

Although the performances of RB1 and RB2 are relatively similar, RB2 has a lower probability of collapse than RB1 at ground motion intensities below the MCE but a higher probability of collapse at higher ground motion intensities. This observation can be attributed to the fact that the columns of RB2 are larger columns than those of RB1 only at the bottom two floors. This can result in a whiplash effect in RB2, whereby the displacements and IDRs at the top floors are larger than those of RB1 at higher ground motion intensities, which results in a slight increase in the collapse probability of RB2.

B. Limitations and Recommendations for Future Work

During this project, several limitations and constraints were encountered. Addressing these limitations can provide avenues for future work and other projects. They are listed as follows:

- The OpenSees model only accounts for the heavy mass of the masonry infill walls, but not for their effect on structural stiffness. In moment resisting frames, infill walls may resist a small portion of the lateral forces when subjected to lower intensities of ground shaking. Additionally, concrete structures in the region commonly lack infill walls at the ground floor, which could lead to a soft story failure.

- Only the exterior frame in the longitudinal direction is modeled in this study. Models that are more elaborate could be developed and assessed in future work, such as a combined model of the exterior and interior frames, a model of the transverse direction or a 3-dimensional model. However, they may result in difficulties in convergence.
- The predictive relations developed to calculate the backbone parameters for the joint spring of wide beam-narrow column joints are based on a small set of experimental data. Additionally, these experimental tests involved newly cast joints, with both beams and columns designed according to seismic requirements. On the other hand, the joints of the studied buildings are originally unreinforced but are concrete jacketed along with the columns, and their adjoining beams are not seismically designed. Future work into this topic would involve additional experiments to better calibrate the joint model and better understand the effects of joint location, beam column orientation, and concrete jacketing on joint seismic response.
- The effect of the CFRP longitudinal reinforcement is assumed to only affect the moment strength parameters of the beam rotational springs. The CFRP transverse wraps, which are added only to anchor the beam longitudinal CFRP strips, are assumed in this study to have a negligible effect on beam deformation capacity. Nonetheless, these wraps do improve the beam's deformation capacity if only slightly. Future work could include experimental work and finite element modelling in order to better characterize the moment rotation response of beams with longitudinal and transverse CFRP.

- A relatively modest amount of IDA runs is used for this project due to computational limitations. Only 15 scale factors are examined for every ground motion up to a maximum $S_a(T_1; \zeta = 5\%)$ value of 1.5g. For some ground motions, the retrofitted building models do not collapse at this maximum value. An increase in the number of scale factors examined would lead to more precise results and possibly lower dispersion (β) values.
- Only two retrofitting methods are closely examined. Future work could examine the effect of additional retrofitting methods such as beam concrete jacketing or the addition of shear walls.
- This study is limited to a single 8-story building. Future work could examine different building heights and plan configurations. For example, the configuration studied does not include shear walls or concrete cores. Future work could involve their inclusion in different archetype configurations.
- This work focuses only on the hazard and damage analysis aspects of reinforced concrete structures. The fragility curves produced in this work form the basis of a probabilistic loss analysis which could be carried out to examine the cost to benefit ratio of the retrofitting of these structures.

BIBLIOGRAPHY

1. Huijjer, C., M. Harajli, and S. Sadek, *Re-evaluation and updating of the seismic hazard of Lebanon*. Journal of Seismology, 2015. **20**(1): p. 233-250.
2. Institution, L.S., *Protection from Earhquakes: General Rules NL-135*, in *NL-135*
- L.S. Institution, Editor. 2012: Lebanon.
3. Elias, A., et al., *Active thrusting offshore Mount Lebanon: Source of the tsunamigenic AD 551 Beirut-Tripoli earthquake*. Geology, 2007. **35**(8): p. 755-758.
4. Baradaran Shoraka, M., *Collapse assessment of concrete buildings: an application to non-ductile reinforced concrete moment frames*. 2013, University of British Columbia.
5. Porter, K., *Beginner's guide to fragility, vulnerability, and risk*. Encyclopedia of earthquake engineering, 2015: p. 235-260.
6. Galanis, P.H. and J.P. Moehle, *Development of collapse indicators for risk assessment of older-type reinforced concrete buildings*. Earthquake Spectra, 2015. **31**(4): p. 1991-2006.
7. A. Suwal, A.M., and A. Lepage. *Performance of a Nonductile RC Building for the FEMA P695 Far-Fault Ground Motion Data Set*. in *11th National Conference in Earthquake Engineering*. 2018. Los Angeles, CA: Earthquake Engineering Research Institute.
8. Vamvatsikos, D. and C.A. Cornell, *Incremental dynamic analysis*. Earthquake Engineering & Structural Dynamics, 2002. **31**(3): p. 491-514.
9. ASCE, *Seismic Evaluation and Retrofit of Existing Buildings*. Seismic Evaluation and Retrofit of Existing Buildings. 2017.
10. 369, A.C., *ACI 369. 1-17 Standard Requirements for Seismic Evaluation and Retrofit of Existing Concrete Buildings (ACI 369. 1-17) and Comment*. 2017: American Concrete Institute.
11. Sattar, S. and A.B. Liel, *Seismic Performance of Nonductile Reinforced Concrete Frames with Masonry Infill Walls—II: Collapse Assessment*. Earthquake Spectra, 2016. **32**(2): p. 819-842.
12. Liel, A.B., C.B. Haselton, and G.G. Deierlein, *Seismic collapse safety of reinforced concrete buildings. II: Comparative assessment of nonductile and ductile moment frames*. Journal of Structural Engineering, 2010. **137**(4): p. 492-502.
13. El-Khoury, N.R. and M.H. Harajli, *Seismic Risk Assessment of Existing Building Structures in Lebanon*. 1997.
14. Makhoul, N., et al., *Assessment of seismic damage to buildings in resilient Byblos City*. International journal of disaster risk reduction, 2016. **18**: p. 12-22.
15. TSIONIS, G. and M.N. FARDIS. *Seismic fragility curves for reinforced concrete buildings and bridges in Thessaloniki*. in *2nd European Conference on Earthquake Engineering and Seismology, Istanbul*. 2014.
16. Kirçil, M.S. and Z. Polat, *Fragility analysis of mid-rise R/C frame buildings*. Engineering Structures, 2006. **28**(9): p. 1335-1345.

17. Committee, J.A.C.I.-A.S.C.E., *352.IR-11: Guide for Design of Slab-Column Connections in Monolithic Concrete Structures*. 2012: Farmington Hills, MI : American Concrete Institute, .
18. Labban, A.A., *Seismic Collapse Assessment of Midrise reinforced Concrete Structures in Beirut*. 2018.
19. Shinozuka, M., et al., *Fragility curves of concrete bridges retrofitted by column jacketing*. *Earthquake Engineering and Engineering Vibration*, 2002. **1**(2): p. 195-205.
20. Harrington, C. and A. Liel, *QUANTIFYING IMPROVEMENTS IN SEISMIC PERFORMANCE POSSIBLE THROUGH RETROFIT OF RC FRAMES*. *Proceedings of the 11th National Conference in Earthquake Engineering*, 2018.
21. Liel, A.B. and G.G. Deierlein, *Cost-benefit evaluation of seismic risk mitigation alternatives for older concrete frame buildings*. *Earthquake Spectra*, 2013. **29**(4): p. 1391-1411.
22. Niroomandi, A., et al., *Seismic performance of ordinary RC frames retrofitted at joints by FRP sheets*. *Engineering Structures*, 2010. **32**(8): p. 2326-2336.
23. Ronagh, H.R. and A. Eslami, *Flexural retrofitting of RC buildings using GFRP/CFRP—A comparative study*. *Composites Part B: Engineering*, 2013. **46**: p. 188-196.
24. Antonopoulos, C.P. and T.C. Triantafillou, *Analysis of FRP-strengthened RC beam-column joints*. *Journal of composites for construction*, 2002. **6**(1): p. 41-51.
25. Harajli, M.H. and E.G. Hantouche, *Effect of active versus passive confinement on seismic response of wide RC columns with lap splices*. *Journal of Structural Engineering*, 2014. **141**(9): p. 04014221.
26. Priestley, M.N., et al., *Seismic design and retrofit of bridges*. 1996: John Wiley & Sons.
27. Buckle, I.G. and R.L. Mayes, *Seismic Isolation: History, Application, and Performance—A World View*. *Earthquake Spectra*, 1990. **6**(2): p. 161-201.
28. Mokha, A.S., et al., *Seismic isolation retrofit of large historic building*. *Journal of Structural Engineering*, 1996. **122**(3): p. 298-308.
29. Hany, N.F., E.G. Hantouche, and M.H. Harajli, *Generalized axial stress-strain response of rectangular columns confined using CFRP jackets and anchors*. *Journal of Composites for Construction*, 2016. **21**(1): p. 04016063.
30. Hassan, W. and A. Bilal. *SEISMIC RETROFIT OF SHEAR CRITICAL BEAM-COLUMN JOINTS IN EXISTING CONCRETE BUILDINGS*. in *National Conference on Earthquake Engineering Frontiers of Earthquake Engineering-10th, Alaska, US pp*. 2014.
31. Karayannis, C.G., C.E. Chalioris, and G.M. Sirkelis, *Local retrofit of exterior RC beam-column joints using thin RC jackets—An experimental study*. *Earthquake Engineering & Structural Dynamics*, 2008. **37**(5): p. 727-746.
32. Alcocer, S.M. and J.O. Jirsa, *Strength of reinforced concrete frame connections rehabilitated by jacketing*. *ACI structural journal*, 1993. **90**(3).
33. El-Amoury, T. and A. Ghobarah, *Seismic rehabilitation of beam-column joint using GFRP sheets*. *Engineering Structures*, 2002. **24**(11): p. 1397-1407.

34. Vega-Behar, P., et al., *Seismic risk assessment of as-built and retrofitted non-ductile reinforced concrete frames*.
35. Agency, F.E.M., *Multi-Hazard Loss Estimation Methodology: Hazus-MH 2.1, User Manual*. 2003: Washington D.C.
36. McKenna, F., G.L. Fenves, and M.H. Scott, *Open system for earthquake engineering simulation*. University of California, Berkeley, CA, 2000.
37. Council, A.T., *Quantification of building seismic performance factors*. 2009: US Department of Homeland Security, FEMA.
38. 318, A.C. and A.C.I.C. 318, *Building code requirements for structural concrete : (ACI 318-95) ; and commentary (ACI 318R-95)*. 1995: Farmington Hills, MI : American Concrete Institute, [1995] ©1995.
39. DeBock, D.J., et al., *Importance of seismic design accidental torsion requirements for building collapse capacity*. *Earthquake Engineering & Structural Dynamics*, 2014. **43**(6): p. 831-850.
40. Chopra, A.K., *Dynamics of Structures*. 2007: Pearson Education.
41. B. Haselton, C., et al., *Calibration of Model to Simulate Response of Reinforced Concrete Beam-Columns to Collapse*. *ACI Structural Journal*, 2016. **113**(6).
42. Haselton, C.B., A.B. Liel, and G.G. Deierlein, *Simulating structural collapse due to earthquakes: model idealization, model calibration, and numerical solution algorithms*. *Computational Methods in Structural Dynamics and Earthquake Engineering (COMPdyn)*, 2009.
43. Haselton, C.B., et al., *An assessment to benchmark the seismic performance of a code-conforming reinforced-concrete moment-frame building*. *Pacific Earthquake Engineering Research Center*, 2008(2007/1).
44. Panagiotakos, T.B. and M.N. Fardis, *Deformations of reinforced concrete members at yielding and ultimate*. *Structural Journal*, 2001. **98**(2): p. 135-148.
45. ASCE, *Seismic rehabilitation of existing buildings*. 2007, ASCE Reston, VA.
46. Sattar, S. and A.B. Liel, *Collapse indicators for existing nonductile concrete frame buildings with varying column and frame characteristics*. *Engineering Structures*, 2017. **152**: p. 188-201.
47. Ibarra, L.F., R.A. Medina, and H. Krawinkler, *Hysteretic models that incorporate strength and stiffness deterioration*. *Earthquake engineering & structural dynamics*, 2005. **34**(12): p. 1489-1511.
48. Galanis, P., *Probabilistic Methods to Identify Seismically Hazardous Older-Type Concrete Frame Buildings*. 2014, UC Berkeley.
49. Elwood, K.J., *Modelling failures in existing reinforced concrete columns*. *Canadian Journal of Civil Engineering*, 2004. **31**(5): p. 846-859.
50. Elwood, K.J. and J.P. Moehle, *Drift capacity of reinforced concrete columns with light transverse reinforcement*. *Earthquake Spectra*, 2005. **21**(1): p. 71-89.
51. Elwood, K.J., *Shake table tests and analytical studies on the gravity load collapse of reinforced concrete frames*. 2004.
52. Alath, S., *Modeling inelastic shear deformation in reinforced concrete beam-column joints*. 1995.

53. Celik, O.C. and B.R. Ellingwood, *Modeling Beam-Column Joints in Fragility Assessment of Gravity Load Designed Reinforced Concrete Frames*. Journal of Earthquake Engineering, 2008. **12**(3): p. 357-381.
54. Walker, S.G., *Seismic performance of existing reinforced concrete beam-column joints*. 2001, University of Washington.
55. Pantelides, C.P., et al., *Assessment of reinforced concrete building exterior joints with substandard details*. PEER report, 2002. **18**.
56. Beres, A., et al., *Implications of experiments on the seismic behavior of gravity load designed RC beam-to-column connections*. Earthquake Spectra, 1996. **12**(2): p. 185-198.
57. Lowes, L.N. and A. Altoontash, *Modeling Reinforced-Concrete Beam-Column Joints Subjected to Cyclic Loading*. Journal of Structural Engineering, 2003. **129**(12): p. 1686-1697.
58. De Risi, M.T., P. Ricci, and G. Verderame. *Influence of joint response in the assessment of seismic performance of existing reinforced concrete frames*. in *COMPDYN 2015, 5th ECCOMAS Thematic Conference on Computational Methods in Structural Dynamics and Earthquake Engineering*. 2015.
59. Park, S. and K. Mosalam, *Simulation of Reinforced Concrete Frames with Nonductile Beam-Column Joints*. Earthquake Spectra, 2013. **29**: p. 233-257.
60. Elsouri, A. and M. Harajli, *Interior RC wide beam-narrow column joints: Potential for improving seismic resistance*. Engineering structures, 2015. **99**: p. 42-55.
61. Elsouri, A. and M. Harajli, *Seismic response of exterior RC wide beam-narrow column joints: earthquake-resistant versus as-built joints*. Engineering Structures, 2013. **57**: p. 394-405.
62. Hoffman, G., et al., *Gravity-load-designed reinforced concrete buildings: Seismic evaluation of existing construction and detailing strategies for improved seismic resistance*. 1992.
63. ASCE, *Minimum Design Loads for Buildings and Other Structures*. Minimum Design Loads for Buildings and Other Structures. 2010.
64. American Society of Civil Engineers (ASCE), *Minimum design loads for buildings and other structures, ASCE/SEI 7-10*. 2010, ASCE/SEI 7-10.
65. Shome, N., et al., *Earthquakes, records, and nonlinear responses*. Earthquake Spectra, 1998. **14**(3): p. 469-500.
66. Ellingwood, B.R., O.C. Celik, and K. Kinali, *Fragility assessment of building structural systems in Mid-America*. Earthquake Engineering & Structural Dynamics, 2007. **36**(13): p. 1935-1952.
67. Vamvatsikos, D. and C.A. Cornell, *Applied incremental dynamic analysis*. Earthquake Spectra, 2004. **20**(2): p. 523-553.
68. Baradaran Shoraka, M., T. Yang, and K. Elwood, *Seismic loss estimation of non-ductile reinforced concrete buildings*. Earthquake Engineering & Structural Dynamics, 2013. **42**(2): p. 297-310.
69. Berry, M., M. Parrish, and M. Eberhard, *PEER Structural Performance Database, User's Manual (Version 1.0)*. University of California, Berkeley, 2004.
70. Baker, J.W., *Efficient analytical fragility function fitting using dynamic structural analysis*. Earthquake Spectra, 2015. **31**(1): p. 579-599.

71. Bousias, S.N., et al., *Strength, stiffness, and cyclic deformation capacity of concrete jacketed members*. ACI Structural Journal, 2007. **104**(5): p. 521.
72. Alsayed, S.H., et al., *Seismic response of FRP-upgraded exterior RC beam-column joints*. Journal of Composites for Construction, 2010. **14**(2): p. 195-208.
73. 440, A.C. and A.C.I.C. 440, *ACI Committee 440 - Guide for the Design and Construction of Externally Bonded FRP Systems for Strengthening Concrete Structures (2017)* 2017: American Concrete Institute.
74. Elsouri, A. and M. Harajli, *Behavior of Reinforced Concrete Wide Concealed-Beam/Narrow-Column Joints under Lateral Earthquake Loading*. Structural Journal, 2013. **110**: p. 205-215.